University of Groningen

Master thesis

Astronomy

The habitability of icy exomoons

Author:
Jesper N.K.Y. Tjoa

Supervisor:
Prof. Floris F.S. Van Der Tak
Dr. Michael "Migo" Müller

June 27, 2019

Abstract

We present surface illumination maps, tidal heating models and melting depth models for several icy Solar System moons and use these to discuss the potential *subsurface* habitability of exomoons. Small icy moons like Saturn's Enceladus may maintain oceans under their ice shells, heated by endogenic processes. Under the right circumstances, these environments might sustain extraterrestrial life. We investigate the influence of multiple orbital and physical characteristics of moons on the subsurface habitability of these bodies and model how the ice melting depth changes. Assuming a conduction only model, we derive an analytic expression for the melting depth dependent on seventeen physical and orbital parameters of a hypothetical moon. We find that small to mid-sized icy satellites (Enceladus up to Uranus' Titania) locked in an orbital resonance and in relatively close orbits to their host planet are best suited to sustaining a subsurface habitable environment, and may do so largely irrespective of their host's distance from the parent star: endogenic heating is the primary key to habitable success, either by tidal heating or radiogenic processes. We also find that the circumplanetary habitable edge as formulated by Heller and Barnes (2013) might be better described as a manifold criterion, since the melting depth depends on seventeen (more or less) free parameters. We conclude that habitable exomoons, given the right physical characteristics, may be found at any orbit beyond the planetary habitable zone, rendering the habitable zone for moons (in principle) arbitrarily large. As such, habitable exomoons may outnumber habitable exoplanets and may thus take precedence over exoplanets as potential sites of extraterrestrial life.

Acknowledgements

End of the road! And like any other, it wasn't walked alone. In no particular order beyond recollection:

I would like to thank my supervisors, Migo Müller and Floris van der Tak, for their invaluable assistance and commentary in times of need. While some aspects of this work were initially as alien (hah) to them as to me, they did their utmost best to drag me through and help me see the light. I especially thank them for their comprehensive comments on the actual writing and wording of this work, and which no doubt shaved off more than a few dozen sentences of dead weight. I would also like to thank Nick Oberg for helping out in any number of ways, from troubleshooting code to refining my methods to determining proper axis label sizes. And, of course, for the inspiring discussions and coffee breaks, whether they regard astronomy or something else entirely.

I would like to thank Teresa Steinke, Marc Rovira Navarro and Stéphanie Cazaux from TU Delft for taking the time to discuss the finer touches of tidal heating with me. Their input regarding volcanic heat loss and crustal tidal dissipation is much appreciated. A word of gratitude is also due to Bas Roelenga, who helped me out with setting up my own N-body code; while it wasn't used in the final results of this thesis, it was an important stepping stone towards the finish.

I would also like to thank the people of room 0265b for the fruitful discussions, the encouragement and the scientific & emotional support. Similarly, I would like to thank the people of Kapteyn at large, from bachelor students to professors, for educating me, for providing an inspiring scientific environment, and for always being there in tougher times. And special thanks to Pratika Dayal for being second reader – I hope I've given you no reason to regret it.

Contents

1 Introduction **4**
1.1 Moons . . . 4
1.1.1 Defining moons . . . 4
1.1.2 Moons of the Solar System . . . 4
1.1.3 Thermal conditions & energy budget . . . 5
1.2 Habitability . . . 6
1.2.1 Defining habitability . . . 6
1.2.2 Contributions to habitability . . . 6
1.3 Tidal heating . . . 7
1.3.1 Significance of tidal heating . . . 8
1.3.2 Tidal heating in the Solar System . . . 9
1.3.3 Approaches to tidal heating . . . 9
1.4 Aims . . . 10
1.4.1 Objects of interest . . . 10

2 Thermodynamics & energy budget **11**
2.1 Overview of processes . . . 11
2.2 Planet & star properties . . . 11
2.3 Moon properties . . . 11
2.4 Exogenic heating . . . 12
2.4.1 Direct stellar illumination . . . 13
2.4.2 Reflected stellar illumination . . . 14
2.4.3 Planetary thermal illumination . . . 15
2.5 Endogenic heating . . . 16
2.6 Tidal heating: fixed Q vs viscoelasticity . . . 17
2.6.1 Fixed Q models . . . 17
2.6.2 Viscoelastic models . . . 18
2.7 Cooling . . . 19

3 Approach **22**
3.1 Geometry . . . 22
3.2 Exogenic heating model . . . 22
3.3 Endogenic heating model . . . 22
3.3.1 Mass-quality factor trend . . . 23
3.3.2 Estimation of tidal parameters . . . 23
3.4 Melting depth model . . . 24
3.4.1 Derivation of melting depth expression . . . 24
3.4.2 Model dependencies . . . 27
3.4.3 Uncertainties . . . 29

4 Results **30**
4.1 Surface maps . . . 30
4.2 Tidal heating . . . 33
4.3 Melting depths . . . 33

5 Discussion **40**
5.1 Plausibility . . . 40
5.1.1 Exogenic heating . . . 40
5.1.2 Endogenic heating . . . 40
5.1.3 Melting depth model . . . 40
5.2 Effect of eclipses . . . 42
5.3 Importance of endogenic heating . . . 42
5.4 Circumplanetary habitable zone & tidal habitable “edge” . . . 45

5.5 Habitability & long-term stability . . . 46
5.5.1 Long-term stability of the environment . . . 46
5.5.2 Ocean habitability . . . 46
5.5.3 Implications for exomoons . . . 47
5.6 Model limitations . . . 47

6 Conclusions **49**
6.1 Implications for subsurface oceans & exomoon habitability . . . 49
6.2 Prospects . . . 50

A Geometry **51**
A.1 Surface landing coordinates . . . 51
A.2 Planetary eclipses . . . 54
A.3 Dusk, dawn & polar illumination . . . 56
A.4 Planetary phase . . . 58

1 Introduction

Earth's Moon has fascinated human civilization since time immemorial. Regardless, it was only with the Renaissance that the notion of worlds beyond Earth began to emerge (Bruno, Huygens). The discovery of the moons of Jupiter by Galilei (1610) and of Titan by Huygens (1656) gradually revealed that our moon was not as unique as previously thought. The eventual discovery of Uranus and Neptune – and of moons around them – as well as the discovery of many more satellites of Jupiter and Saturn showed that planets are well outnumbered by their satellites.

The discovery of exoplanets by Mayor and Queloz (1995) opened a new avenue for moon research. Sartoretti and Schneider (1999) first theorized about exomoon detection; later, Kipping (2009) suggested transit timing variations (TTVs) could provide a venue of exomoon detection. He also suggested that, assuming that exomoons are terrestrial (rocky and/or icy) – as they are in our Solar System – they might constitute more habitable environments than their planetary (and often gaseous) counterparts. Additionally, since moons outnumber planets in the Solar System, it is fair to assume that they do so around other stars also.

The first exomoon candidates emerged in the 2010s. Teachey and Kipping (2018) presented transit photometry-based evidence for a Neptune-sized exomoon in orbit around Kepler-1625b. However, subsequent papers claimed this moon transit might rather be explained as an artifact of the data reduction process (Kreidberg et al., 2019): hence, the hunt for the first confirmed exomoon is still ongoing.

Regardless of their detection, the question of exomoon habitability has arisen in recent years. Heller and Barnes (2013) analysed the habitability of exomoons as constrained by their energy budgets and found that the circumstellar habitable zone for moons extends further out than for planets. This thesis intends to further investigate under what circumstances (exo)moons may sustain habitable environments.

1.1 Moons

1.1.1 Defining moons

This section discusses the status quo regarding the study of moons, and by extension, exomoons. First, let us define what a moon *is*. For the purposes of this work, we define a moon to be any body which conforms to all of the following conditions:

1. It is gravitationally bound to a substellar parent body/binary more massive than itself, i.e. it orbits a more massive parent;
2. Its parent orbits a star/stellar remnant or is gravitationally unbound;
3. It is not artificial.

Condition 1 includes all conventional satellites in the Solar System, including such disputable moons as Pluto's Charon (the Pluto-Charon barycenter lies well outside Pluto). Condition 2 ensures moons of rogue planets and pulsar planet moons are also included in the definition, but excludes hypothetical moons of moons (henceforth dubbed *grandmoons*). Condition 3 excludes all human (and alien) spacecraft.

A brief consideration of this definition shows that for this work 'moon' is not a physical, but a dynamical classification. While other works might classify two Earth-mass objects orbiting their common barycenter as a double planet, this work would name the lesser of these two the moon, *without* invalidating the planetary status of either.

1.1.2 Moons of the Solar System

Before investigating exomoons, let us discuss what we know of the moons in our Solar System. It is not known whether the local population is representative of satellite systems in general, but to date, they are all the moons we know. Of the almost 200 moons in our Solar System, at least 19 are gravitationally rounded, with sizes varying from tens of kilometers to planet-sized, like Jupiter's Ganymede. Dry, rocky moons like our Luna exist but are not typical: icy moons like Jupiter's Europa & Ganymede and Saturn's Enceladus show that moons can be covered in icy shells and may sustain subsurface oceans (even our Luna has recently been shown to hold polar water ice deposits; see Li et al. (2018)). Both regular

volcanism (Jupiter's Io) and cryovolcanism (Neptune's Triton, Enceladus; see section 1.3 for details) have been discovered on moons (Morabito et al., 1979; Soderblom et al., 1990; Porco et al., 2006): the ejecta may provide us with insights into the moons' internal structure. Titan sustains a unique hydrology (fluid cycle) of liquid methane and ethane flowing across a surface of water ice, concealed by a thick atmosphere of hydrocarbons and nitrogen haze (Stofan et al., 2007). This goes to show that the satellites of our Solar System are as diverse, if not more so, than its planetary population.

In total, the surfaces of all but three (Luna, Io, Titan) major moons are dominated by water ice. It is this type of moon – rounded, with an icy shell and a mantle/core composed of ice and/or (molten) silicates – on which we will focus our attention. Known members of this type are:

- The Galilean moons Europa, Ganymede and Callisto;
- The Saturnian moons Mimas, Enceladus, Tethys, Dione, Rhea and Iapetus;
- The Uranian moons Miranda, Ariel, Umbriel, Titania and Oberon;
- The Neptunian moon Triton;
- The Plutonian moon Charon.

All these moons but Triton are regular, i.e. orbit in the same direction as their parent planet rotates: these are almost always moons which formed with the planet. Irregular moons like Triton orbit retrogade (opposite to the rotation of their host) with respect to the planet and are thought to have been captured later on by their hosts (Rufu and Canup, 2017), but save Triton none of them are large enough to be gravitationally rounded. Hence, our main focus lies with the regular population.

1.1.3 Thermal conditions & energy budget

Exomoon thermal conditions are expected to vary widely, as they do for moons in our own Solar System. Exomoon distance to the star may vary almost as much as exoplanets'; an inner limit exists where the orbital region of stability around the planet becomes smaller than the Roche limit, where tidal shear tears the moon apart. Otherwise, exomoon semi-major axes around their host planets are limited by the Roche limit (for nominally fluid bodies, generally around $\sim 2.5R_p$) and Hill orbital stability criteria (i.e. $a_{moon} < 0.5R_H$; the Hill sphere of radius R_H of a planet is where the planet's gravitational pull dominates over the star's (Markellos and Roy, 1981)). For larger, regular bodies, eccentric orbits or orbits inclined relative to the axial tilt of the host planet tend to be circularised and flattened (relative to the planet's equator) on relatively short timescales through tidal damping (Heller and Barnes, 2013). However, if multiple moons become locked in a mean motion resonance (where a superior body completes a small integer number of orbits for every larger small integer number of orbits of an inferior body), eccentricity may be forced, thus preserving the possibility for tidal heating (see sections 1.3 and 2.6 (Hussmann and Spohn, 2004)).

Titan proves that atmospheres are possible on massive moons, although the Galilean moons show it need not be common. Heller et al. (2015) proposed the Grand Tack (the inward migration of Jupiter and Saturn until becoming caught in a 2:3 orbital resonance, subsequently migrating outward again) as the origin of this dichotomy, posing that the Galilean satellites formed prior to Jupiter and Saturn's rapid inward migration and lost any primordial atmospheres to the young Sun's intense XUV radiation. Conversely, Saturn, which accreted at a lower rate, only obtained Titan after locking in mean motion resonance with Jupiter and migrating outward again, sparing Titan the XUV.

Contrary to planets, tidal heating (heating of a body's interior by tidal forces of a more massive neighbour; for a detailed treatment, see sections 1.3 (qualitative) and 2.6 (quantitative)) can be an important source of heat for a moon. The main contributions to the energy budget are, in no particular order, stellar illumination & reflected stellar illumination by the planet (unless the host planet is rogue, i.e. not gravitationally bound to a star), tidal heating and planetary thermal emission. Note that in this list, stellar and planetary illumination are those registered at the top of, if present, the atmosphere: one of sufficient opacity will no doubt change surface circumstances (Heller and Barnes, 2013). Illumination at any point on the surface scales with distance to and elevation of the source; tidal heating scales with the moon's semi-major axis, but other important parameters are its eccentricity and composition (Dobos and Turner, 2015). Since it determines the temperature on and below the surface of the moon,

a treatment of exomoons' energy budgets is at the heart of this thesis, and is detailed quantitatively in Chapter 2.

1.2 Habitability

1.2.1 Defining habitability

Since all biochemistry currently observed in nature requires liquid water to function, our conditions must reflect this; let us thus define what we mean by habitable. For exoplanets, the habitable zone is defined as the region where stellar illumination is sufficiently strong to allow for liquid water on the surface, without provoking a runaway greenhouse effect (where the planet fails to radiate away all the incoming heat and thus warms up catastrophically; Venus is in such a state). Hence, habitability is a temperature criterion, and as such primarily dependent on the luminosity of the host star, the distance from this star to the planet and the planet's albedo (see Kaltenegger et al. (2002) for a review of planetary habitability). In the absence of an atmosphere to provide pressure, the water would sublimate and escape into space; however, if the planet is massive enough to maintain an atmosphere, surface bodies of water may exist. For the purposes of this work, this situation is labeled as *surface habitability,* and must conform to the following criteria:

1. The planet's surface temperature is typically between the melting and boiling points of water;
2. The planet is massive enough to maintain an (appreciable, not trace) atmosphere, preventing the volatile water from sublimating and escaping into space.

A moon in the circumstellar habitable zone, if massive enough, might well be surface habitable. However, the moons in our Solar System are both airless (except Titan) and less massive than planets. While they have plenty of water ice, they are therefore *not* surface habitable. However, a body of water does not need to be situated on the surface to be hospitable to a wide array of life forms. Earth's deepest oceans are active habitats: plenty of organisms thrive in caves, underground lakes, near hydrothermal vents (geochemically active, chimney-like structures on the ocean floor expelling a gaseous soup which serves as nutrition to certain microbes; see Martin et al. (2008) for a review) or in other extreme locations. Hence, if liquid water is present *below* the surface, this may too constitute a habitable environment; in the absence of an atmosphere, a solid crust/shell must then prevent the liquid water from escaping. We label this situation *subsurface habitability,* and it must conform to the following criteria:

1. The planet's surface temperature is, on average, below the sublimation point of water ice ($\sim$150 K);
2. Sufficient internal heat allows a global shell/pockets of liquid water to exist underneath the frozen surface.

Following these two definitions, Earth is the only object known to be surface habitable, while objects like Enceladus, Europa or Ganymede may be subsurface habitable. Since this thesis treats icy, airless moons, habitability means **subsurface** habitability unless otherwise specified. Subsurface habitability is easier to attain than its surface counterpart: the amount of energy needed is lower (no high surface temperature to sustain), and an atmosphere is not required, lowering mass constraints.

1.2.2 Contributions to habitability

Since internal heat is required to sustain subsurface water, tidal heating (sections 1.3 and 2.6) introduces a major component to the energy budget and may render an otherwise frozen satellite habitable – or turn an otherwise habitable one into first a runaway greenhouse, then an inhospitable Io-analogue (Heller and Barnes, 2013). Heller (2012) investigated the influence of orbital conditions and tidal heating on exomoon habitability, finding that a low inclination relative to the ecliptic and/or low semi-major axis can introduce a major reduction in stellar illumination through frequent planetary eclipses. Especially in the case of low semi-major axis, this loss can be countered by tidal heating, but gravitational perturbations by neighbouring moons – or in the case of a low-mass star, the nearby star and/or neighbouring planets – may induce disastrous eccentricities, turning the moon into a volcanic wasteland. This introduces a

"habitable edge" exclusion zone around the planet, where the moon would undergo a runaway greenhouse effect, rendering surface conditions inhospitable to life as we know it (studies into a *subsurface* habitable edge have not yet been conducted; it is our hope to find one in this thesis, if it exists). This *edge* differs from the circumstellar habitable *zone* in that the zone has both a lower and an upper limit; the circumplanetary edge only describes a minimum semi-major axis below which surface habitability is thought impossible, since a moon might be surface habitable at any distance from its host planet if stellar illumination allows (Heller and Barnes, 2013). These findings were confirmed by Zollinger et al. (2017), who concluded that M-dwarfs with masses below $0.2M_\odot$ cannot host habitable exomoons: since the habitable zone of these stars is very small as a consequence of their low luminosity, the host planet would have to orbit close in, resulting in a very small Hill sphere and thus very small moon semi-major axes. The star's deleterious influence might continue to affect the habitable zone up to $0.5M_\odot$; subsequent eccentricity forcing by the star would see the exomoon tidally roasted.

Heller and Barnes (2013) continued investigating exomoon habitability in the context of the energy budget. They found that tidal heating may drive plate tectonics, enhancing surface habitability, but again stressed the importance of maintaining a low eccentricity and/or sizeable semi-major axis not to let the moon lapse into a runaway greenhouse state (when the incoming flux exceeds what the body can radiate away, some 300 W/m^2 in Earth's case). They also found that for optimal surface habitability, exomoon mass would need to be above $0.25M_\oplus$ to drive (with increasing mass) a magnetic field, an atmosphere and plate tectonics. Forgan and Yotov (2014) and subsequently Forgan and Dobos (2016) studied the effect of eclipses on the ice-albedo feedback mechanism (where the high albedo of surface ices drives an additional temperature decline) and found that if the orbits of moon and planet are close to coplanar, this mechanism may drive the moon into a snowball state that it finds hard to escape. However, if one wishes to create a subsurface habitable environment, snowball states are acceptable as long as internal heat is sufficient to sustain an ocean layer. Also, Lammer et al. (2014) studied exomoon atmospheres and found that those with masses below $0.5M_\oplus$ cannot maintain their atmospheres for long during the early days of their system: XUV radiation from the young star would see the moons desiccated, evolving into either Mars-like habitats or airless bodies like Callisto. This agrees with the findings of Heller et al. (2015) regarding the Galilean moons, which while of comparable mass with Titan lack anything beyond trace atmospheres.

There is another way in which tidal – or other internal – heating contributes to habitability. The aforementioned hydrothermal vents are a consequence of geological activity: since they unite biochemistry (microbial colonies) and geochemistry (expulsion of mineral/gaseous soup), they have been suggested as catalysts of abiogenesis (appearance of life from lifeless building blocks) on Earth. The first life forms on Earth could have emerged here – they would have been autotrophs, meaning that they produce their own nutrients from inorganic compounds found in the surroundings of such vents (Martin et al., 2008). The geological activity (at least on Earth) required to sustain these environments is driven by the dissipation of internal energy; tidal heating may induce similar situations in the subsurface oceans on exomoons, further improving habitability.

Summarized, for habitation by carbon-based lifeforms like Earth's, water must be present in liquid form either on or below the surface. However, surface habitability has been extensively studied; subsurface habitability, conversely, has garnered less attention (although several papers exist about specifically several Solar System icy moons, see for instance Hammond et al. (2018)). This is where we hope to contribute.

1.3 Tidal heating

Tidal heating presents a major influence on exomoon habitability, and one generally not present on exoplanet habitability (generally, since in M-dwarf systems like TRAPPIST-1 the scales *do* allow for tidal interactions: see Dobos et al. (2019) for a recent review). The fact that it deposits heat *at depth* rather than on the surface (as illumination mechanisms do) is why it is so important, since it directly interacts with the body's interior – which is where the oceans we are interested in are located. Additionally, thermal conduction of internal heat out of the body is relatively inefficient, which means that the internally deposited tidal heat can be retained over long timescales.

Tidal *forces* arise when two massive bodies orbit one another: their mutual gravities pull on one another, causing both objects (if sufficiently deformable) to become deformed. This force also gives rise to ocean tides on Earth. Tidal *heating* or *heat dissipation* is the resulting phenomenon from sufficiently

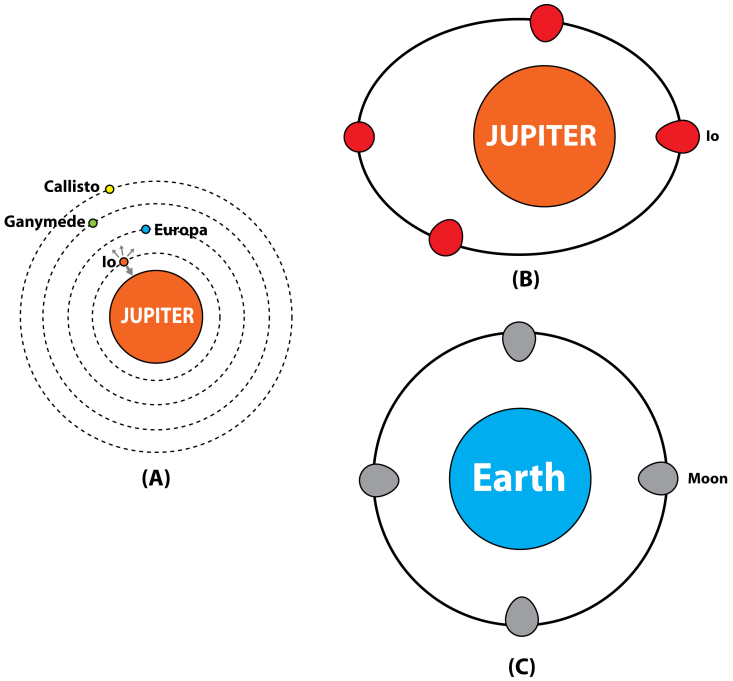

Figure 1: A schematic view of tidal forces deforming moons. Taken from Wikipedia, May 2019.

powerful tidal forces on a secondary body in a non-circular orbit around a more massive primary body. If the secondary's orbit were perfectly circular, the gravitational pull exerted by the primary on the secondary would be constant over an orbit, permanently deforming the secondary into an oblate spheroid, with its longest axis directed towards the primary (see Figure 1, panel C). However, if an eccentricity is introduced, the primary's gravitational pull on the secondary will vary since the secondary's distance to the primary changes over its orbit. This varying pull causes the secondary's material to undergo deformation and relaxation over its orbit, dissipating tidal heat (Figure 1, panel B) in its interior. This heat is then conducted towards and radiated away from the surface. Similar to kneading dough, this heat dissipation is maximal if the secondary's material is viscous and elastic: if the body is completely rigid, it cannot be deformed, while if it is completely fluid, it will not relax to its original shape (Segatz et al., 1988).

Since this tidal energy comes at the expense of orbital energy, the secondary will suffer orbital damping, circularising its orbit and slowing its rotation rate over time – this will eventually render the secondary "tidally locked", i.e. always presenting the same face to the primary (a prime example of this is our own moon Luna, although all round satellites in our Solar System are in fact tidally locked). As eccentricity decreases, tidal heating decreases, until eventually the secondary no longer experiences appreciable tidal forces (Jackson et al., 2008). To maintain tidal heating on longer timescales, a mechanism is required to 'force' an eccentricity: mean motion resonances can be a solution here, as they are in the Jovian satellite system. The periodic gravitational tugs experienced by the inferior partner in a small integer resonance (2:1, 3:1, 3:2 etc.) boost its eccentricity sufficiently to counteract the orbital damping.

1.3.1 Significance of tidal heating

As a consequence of tidal heating, melting of subsurface layers (be it silicates to magma or ice to water) and thus motion underneath the crust may see moons experience either regular volcanism (rocky moons) or cryovolcanism (icy moons). Both processes are similar: a temperature gradient over the fluid subsurface layers leads to convective flows, putting stress on the crust. These fluids are eventually expelled at weakened sites in the crust, creating a volcano (or, specifically for cryovolcanism, a geyser). If the crust is icy, and the fluid being expelled is water, we speak of cryovolcanism rather than regular volcanism (Spencer et al., 2009). This process thus provides a secondary outlet of internal heat (both

tidal and otherwise generated), next to conductive and radiative heat loss through the crust.

Tidal heating is also important to us since it presents a key deviation of exomoon habitability from exoplanet habitability. Exoplanetary systems, except for compact M-dwarf systems (again, see Dobos et al. (2019)), are generally too large to allow for significant tidal effects; the magnitude of tidal heating scales inversely and strongly with the distance between the bodies ($\dot{E}_{tidal} \propto a^{-7.5}$, with a the semi-major axis of the secondary body; see section 2.5 for a detailed treatment), and thus cannot take place over large distances. Satellite systems, conversely, are relatively small compared to the sizes of the bodies involved and thus have greater chance to be tidally active.

An important characteristic of tidal heating is pointed out by Henning et al. (2009), who write that *"dominance over insolation* (solar irradiation) *is unnecessary for Io-like supertidal properties"*. Although the tidal heat flux might be an order of magnitude lower than stellar or even planetary illumination, it can fundamentally change the interior structure of the moon by virtue of where it is dissipated. Exogenic flux must penetrate into the moon through the surface, whereas tidal heat is dissipated internally and thus directly influences the moon's core and mantle. In addition, it provides (if the moon is resonance locked or otherwise of eccentricity ensured) a constant source of heating, rather than the variable exogenic flux. And since it is dissipated internally, it has a direct influence on the presence of internal, subsurface oceans.

1.3.2 Tidal heating in the Solar System

Prominent local examples of forced eccentricity configurations are the Io-Europa-Ganymede resonance (4:2:1), Enceladus-Dione (2:1) and Pluto-Neptune (3:2 – many KBO's are in fact resonant with Neptune, but because of the distances involved there is no appreciable tidal heating), although several other Uranian and Saturnian satellites may have been in mean motion resonance in the past (Tittemore and Wisdom, 1990). The first two generate appreciable levels of tidal heating; Earth and Luna also exert tidal forces on one another, but because the two are relatively far apart, the effects remain limited to ocean tides (water is of course far more deformable than the silicates composing Earth's crust).

The two most studied cases of tidal heating are Io (by Jupiter) and Enceladus (by Saturn). The amount of tidal stress received by Io, in combination with its large mass, may have led to (partial) melting of its rocky interior, thus providing the viscous & elastic substance most effective at tidal heating (Moore, 2003); Io might harbour a subsurface magma ocean (Khurana et al., 2011). Enceladus, on the other hand, is too small to sustain an interior of molten silicates[1], but its high heat flux (particularly through its "tiger stripes" on its active south polar terrain Porco et al. (2006)) imply that its interior must be substantially deformable. The current prevailing hypothesis predicts Enceladus to have a porous, spongiform core/mantle, allowing the water of its presumed subsurface ocean to efficiently transport the internally dissipated tidal heat upward, maintaining its liquidity. The spongiform core would also render the core more susceptible to tidal heat dissipation (Nimmo et al., 2018).

The subsurface ocean is believed to owe its existence to tidal heating; it has been shown to be theoretically possible and there is empirical evidence to support it, such as Enceladus' geological activity: as a consequence of its tidal heating, Enceladus also displays vigorous cryovolcanism on its active south pole, feeding Saturn's E-ring with plumes of fine, icy particles (Porco et al., 2006). In addition, the recent discovery of molecular hydrogen in these plumes suggests that hydrothermal processes are occurring in Enceladus' ocean to replenish this volatile, and hint at the presence of hydrothermal vents. The chemical energy these provide would further increase Enceladus' habitability (Waite et al., 2017).

1.3.3 Approaches to tidal heating

Two model approaches are commonly used to compute tidal heating: fixed Q and viscoelastic models. Fixed Q models assume that the body is uniform in composition – they lump the entire object's tidal response into two terms: the tidal quality factor Q, which describes the body's spring response to being kneaded, and the second order Love number k_2, which describes physical characteristics like density and rigidity. However, if a body is sufficiently non-homogeneous (i.e. molten interior, differentiation, all things found in high-mass moons like Europa), this treatment becomes precarious. Conversely, viscoelastic models describe the body in a more detailed fashion, assuming that it has a convective, viscous interior

[1] In this thesis, a "molten interior" means a mantle and core consisting of molten *silicates;* a subsurface ocean is *not* what is meant by "molten interior".

where tidal energy is dissipated, and a crust which does not participate but conducts and radiates away the internally generated heat. Key parameters are the mantle viscosity η and the mantle shear modulus S. These depend on the mantle temperature, which in turn depends on the amount of tidal heat being generated, thus allowing one to model the interaction between mantle characteristics and tidal response of the body. A more detailed, quantitative approach of both models can be found in section 2.6; in this thesis, we use a fixed Q description.

1.4 Aims

Summarized, the habitability of moons seems to be dependent on both their physical characteristics (mass, composition, water fraction), orbital parameters and effects (semi-major axis, eccentricity, distance to star, tidal heating) and star or host planet properties (stellar luminosity and stability; planet mass and albedo). This work will focus on the energy budget and the influence of different heat sources on (exo)moon subsurface habitability. We will determine under what circumstances exomoons can successfully host subsurface oceans. From this, we will attempt to determine where one could reasonably expect to find habitable exomoons. We hypothesize that the circumstellar habitable zone for exomoons extends further out than for planets due to additional heating by the planet & tidal effects.

1.4.1 Objects of interest

Given our aims, we can narrow down our selection of interesting moons by introducing a mass cut: because of our fixed Q tidal heating approach, we are limited to small to mid-sized icy moons. Known examples are the rounded moons of Saturn save Titan, the rounded moons of Uranus, and Charon. These bodies have masses ranging from 10^{19} to several times 10^{21} kg, with densities varying between 1 and 2 g/cm^3. This indicates a composition primarily of water ice, with varying fractions of silicates and, possibly, metals. Since they had to form beyond the snow line – the distance from the star below which water ice sublimates, and also beyond where giant planets form – all known icy moons except Charon orbit giant planets; hence, we also assume the moons' hosts to be gaseous, with mass between Neptune and several Jupiter masses (thus excluding Charon from our selection).

While Jupiter's Galilean moons (save Io), Saturn's largest moon Titan and Neptune's Triton are all sizeable and host large quantities of water (Titan's atmosphere provides an additional point of interest with regards to exomoon habitability), they are not well fit to serve as potential objects of study for the purposes of this work. Their masses ($> 10^{22}$ kg) and densities (> 2 g/cm^3) set them well apart from the lesser icy satellites, and they are massive enough to sustain a molten interior. This complicates tidal heating models, rendering our fixed-Q approach an insufficiently detailed approximation. Once a molten interior manifests, viscoelastic models of its mantle convection (section 2.6) must be employed. A reference table of the moons in our Solar System to which our model applies can be found in Chapter 2 (Table 3), where we will discuss the unifying physical characteristics of these moons in greater detail.

We will first discuss the physical processes involved in icy moon habitability (Chapter 2). Subsequently, we will present our particular approach to determine exomoon energy budgets and ice melting depths (Chapter 3). We will then present our results (Chapter 4), our discussion (Chapter 5) and conclusions (Chapter 6) regarding the habitability of icy moons.

2 Thermodynamics & energy budget

This chapter discusses the thermodynamical framework of our exomoon energy budget model. The model's geometry as well as the setup of its code are discussed in Chapter 3 and Appendix A.

2.1 Overview of processes

The physics under consideration is mostly thermodynamics and radiative transfer. We require a treatment of radiation propagation for those heating processes involving illumination, as well as for radiative cooling. Additionally, we need to understand thermal conduction and convection to describe the propagation of internal heat, and a treatment for tidal heating. This introduces a variety of different quantities: to avoid ambiguities, Tables 1 and 2 list the different symbols used in this thesis.

symbol	value	units	name
c	2.99792×10^{8}	m s^{-1}	Speed of light
G	6.67408×10^{-11}	m^{3} kg^{-1} s^{-2}	Gravitational constant
σ	5.67037×10^{-8}	W m^{-2} K^{-4}	Stefan-Boltzmann constant
$\dot{E}_{ac,rg,\oplus}$	2×10^{13}	W	Earth's radiogenic heat production

Table 1: The recurring constants used in this thesis.

2.2 Planet & star properties

We make several assumptions about possible host planets. First, since the host planet, given the type of moon we are interested in, is likely to be a gas giant and thus shrouded in diffusely scattering clouds, we assume it is a Lambertian, i.e. diffuse reflector. This means that incoming radiation is scattered in all directions, independent of incident angle, where the outgoing radiation at some angle is given by

$$F_r = F_i \cos\theta \tag{1}$$

wherein F_r is the reflected flux, F_i the incident flux to some area and θ the angle between the surface normal and outgoing radiation.

Second, we assume the planet to be roughly isothermal between its day and night sides. Since the giant planets in our Solar System rotate rapidly as compared to the terrestrial worlds (close to 24 hours for Earth and Mars, 243 Earth days for Venus; as compared to about 10 hours for Jupiter and Saturn, 17 for Uranus and 16 for Neptune), this distributes the incoming solar radiation evenly across the surface. The internally generated heat is emitted homogeneously either way, so the total thermal emission of the planet is assumed to be roughly the same for the entire surface.

2.3 Moon properties

Since the fixed Q approach we use to model tidal heating cannot model a molten interior with sufficient detail, we avoid such interiors by limiting ourselves to small to mid-sized moons (Mimas up to Titania). We also limit ourselves to icy moons (with densities between $\sim$1 and $\sim$2 g/cm^3), since we are interested in habitability, which depends on the presence of liquid water. These moons possess a largely homogeneous interior, surrounded by an icy shell and (possibly) an ocean of liquid water at the interface of core/mantle and crust. Their internally dissipated heat is assumed to be lost solely through conduction towards and radiation from the surface, so *no* volcanism. Their composition is primarily water ice, mixed with silicates, possibly metals and some mass fraction of salts and ammonia. We also assume the moons to be tidally locked to their host planet, and to be covered in a finely grained layer of dust called regolith (just like Luna) where heat transport is dominated by radiative rather than conductive processes. A reference table of relevant Solar System moons follows (Table 3).

symbol	conventional units	quantity
L	W, $L_\odot$	Luminosity
P	W	Radiative power
$\dot{E}$	W	Internal heat generation
F	W m^{-2}	Flux
T	K	Temperature
α	n/a	Bond albedo
ϵ	n/a	Emissivity
R	m, $R_\oplus$, R_{Jup}, $R_\odot$	Radius
M	kg, $M_\oplus$, M_{Jup}, $M_\odot$	Mass
ρ	g cm^{-3}	Density
g	m s^{-2}	Surface gravity
r_x	m, AU	Distance from x
d_{xy}	m, AU	Distance from x to y
a	m, AU	Semi-major axis (SMA)
ω	radians s^{-1}, degrees s^{-1}	Orbital frequency
e	n/a	Orbital eccentricity
i	radians, degrees	Orbital inclination
ε	radians, degrees	Orbital phase
χ	n/a	Phase function
δ	radians, degrees	Elevation
f_{vis}	n/a	Visibility fraction
f_v	n/a	Volume fraction
f_m	n/a	Mass fraction
x_{exc}	n/a	Thermal flux excess
Φ	n/a	Tidal efficiency factor
Q	n/a	Tidal quality factor
k_2	n/a	Second order Love number
μ	Pa	Rigidity
S	Pa	Shear modulus
η	Pa s	Viscosity
D	m	Depth/shell thickness
k	W m^{-1}K^{-1}	Thermal conductivity
K	W m^{-1}	Integrated thermal conductivity

Table 2: The different variables used in this thesis.

Host	Moon	M (10^{20} kg)	R_m (km)	ρ (g cm^{-3})	a (10^3 km)	a (R_p)	e
Saturn	Mimas	0.37	198.2	1.15	185.40	3.2	0.0202
	Enceladus	1.08	252.1	1.61	237.95	4.1	0.0047
	Tethys	6.17	531.1	0.98	294.62	5.1	0.0001
	Dione	10.95	561.4	1.48	377.40	6.5	0.0022
	Rhea	23.07	763.8	1.24	527.11	9.1	0.0013
	Iapetus	18.06	734.5	1.09	3560.82	61.2	0.0286
Uranus	Miranda	0.66	235.8	1.20	129.39	5.1	0.0013
	Ariel	13.53	578.9	1.59	191.02	7.5	0.0012
	Umbriel	11.72	584.7	1.39	266.30	10.5	0.0039
	Titania	35.27	788.4	1.72	435.91	17.2	0.0011
	Oberon	30.14	761.4	1.63	583.52	23.0	0.0014

Table 3: Solar System icy moons relevant to this research. Data retrieved from Wikipedia, May 2019.

2.4 Exogenic heating

There are three main exogenic heating processes:

- *Direct stellar illumination:* thermal (primarily optical & UV) radiation emitted by the star which directly strikes the moon's surface.
- *Reflected stellar illumination:* thermal (primarily optical & UV) radiation emitted by the star which first reflects off the moon's host planet before reaching the moon.
- *Planetary thermal illumination:* thermal (primarily infrared) radiation emitted by the host planet which directly strikes the moon's surface.

We will now describe these processes one by one. In the following treatment, the subscript q shall denote any point on the moon's surface, $*$ denotes the star, p denotes the planet and c denotes the moon as a whole.

2.4.1 Direct stellar illumination

Stars emit thermal radiation in all directions. Their total luminosity L_* scales with their temperature T_* and radius R_* via the Stefan-Boltzmann law of blackbody radiation:

$$L_* = 4\pi R_*^2 \sigma_B T_*^4$$

Since the radiation flux F_* falls of quadratically with distance, the stellar flux received at some distance d is equal to

$$F_*(d) = \frac{L_*}{4\pi d^2} \tag{2}$$

The amount of illumination absorbed by some surface element on the moon's surface q is also dependent on the surface's Bond albedo (how dark the surface is, and thus how much radiation it absorbs), how large a fraction of the face of the star is visible and the elevation of the star in the moon's sky:

$$F_*(d_{*q}) = \begin{cases} \dfrac{L_*\,(1-\alpha_q)}{4\pi d_{*q}^2} f_{*,vis} \sin\delta_*, & \delta_p > 0 \\ 0, & \delta_p < 0 \end{cases} \tag{3}$$

wherein d_{*q} is the distance from the star to q, α_q is the surface Bond albedo at q, $f_{*,vis}$ is the visible fraction of the star and δ_* its elevation in the sky at q. The factor $f_{*,vis}$ is a consequence of possible eclipses by the host planet (which, in close orbits, can have noticeable effects, at least for surface habitability – see Forgan and Dobos (2016)) and situations where the star is partially occluded by the horizon. It is, for any arbitrary source x, given by:

$$f_{x,vis} = f_{x,ecl} \cdot f_{x,hoc} \tag{4}$$

wherein $f_{x,ecl}$ is the eclipse component, and $f_{x,hoc}$ the horizon occlusion component. The computation of both components can be found in the appendix regarding our model's geometrical approach, under subsections A.2 and A.3; δ is computed in subsection A.1 (the computations of elevation for both star and planet are identical).

Averaged over the moon's year, Heller and Barnes (2013) found the average absorbed stellar flux to the entire moon to be

$$\bar{F}_* = \frac{L_*\,(1-\alpha_c)}{16\pi a_p^2 \sqrt{1-e_p^2}}$$

wherein α_c is the average Bond albedo of the moon (subscript c standing for child, i.e. child body of the parent planet p), a_p is the semi-major axis of the host planet's orbit and e_p is that host planet's orbital eccentricity. This thesis introduces an additional modifier to account for effects of possible eclipses:

$$\bar{F}_* = \frac{L_* (1-\alpha_c)}{16\pi a_p^2 \sqrt{1-e_p^2}} \bar{f}_{*,vis} \tag{5}$$

wherein $\bar{f}_{*,vis}$, the average visibility fraction, is given by

$$\bar{f}_{*,vis} = 1 - \frac{R_p}{2\pi a_c} |\cos i_c| \tag{6}$$

wherein R_p is the planet's radius, a_c the moon's semi-major axis around the planet and i_c the moon's orbit's inclination relative to the planet's orbital plane – so the moon's inclination relative to the planet's equator *plus* the planet's own axial tilt. This was found by first computing how large a fraction of its orbit the moon spends in the planet's shadow (assuming small eccentricities i.e. < 0.1, this equals $\sim R_p/2\pi a_c$), and then multiplying it with the cosine of its inclination to find the average over one orbit.

2.4.2 Reflected stellar illumination

Assuming the host planet has a nonzero Bond albedo, it also reflects stellar illumination onto the moon. Following Equation 2, the flux received by the planet's face is

$$F_*(d_{*p}) = \frac{L_*}{4\pi d_{*p}^2}$$

wherein d_{*p} is the distance from the star to the planet p. Since the planet is projected over a disk as seen from the star, the total received power equals

$$P_*(d_{*p}) = \frac{L_*}{4\pi d_{*p}^2} \cdot \pi R_p^2 = \frac{L_* R_p^2}{4 d_{*p}^2}$$

We do not take into account possible blocked illumination by the moon (or any other satellites), as this represents only a negligible fraction of the total illumination by the star. As stated in section 2.2, we assume the planet to be a Lambertian, i.e. diffuse reflector due to its gaseous envelope. Hence, the total reflected power equals

$$P_{r,total} = P_*(d_{*p}) \cdot \alpha_p = \frac{L_* R_p^2 \alpha_p}{4 d_{*p}^2}$$

wherein α_p is the average Bond albedo of the reflecting planet. The amount of power then visible from the moon is dependent on the moon's phase ε_c via the phase function of a spherical object:

$$\chi(\varepsilon_c) = \frac{1}{\pi} (\sin \varepsilon_c + (\pi - \varepsilon_c) \cos \varepsilon_c) \tag{7}$$

wherein the phase function $\chi(\varepsilon_c)$ represents the visibility fraction of the total reflected illumination at the moon's phase ε_c (where $\varepsilon = 0$ means that the moon is directly in between star and host planet; so seen from the planet, this would mean new moon). Hence, we find that

$$P_{r,vis} = P_{r,total} \cdot \chi(\varepsilon_c) = \frac{L_* R_p^2 \alpha_p}{4\pi d_{*p}^2} (\sin \varepsilon_c + (\pi - \varepsilon_c) \cos \varepsilon_c)$$

Finally, since we are at distance d_{pq} from our host planet, we divide the radiation *not* by $4\pi d_{pq}^2$ – since the radiation is not homogeneously emitted over a sphere – but by d_{pq}^2. And since the radiation must

also be absorbed by the moon's surface, we add albedo, elevation and visibility modifiers analogously to our stellar flux description (section 2.4.1, obtaining

$$F_r(d_{pq}) = \begin{cases} \frac{L_*}{4\pi d_{*p}^2} \frac{R_p^2 \alpha_p (1-\alpha_c)}{d_{pq}^2} (\sin\varepsilon_c + (\pi - \varepsilon_c)\cos\varepsilon_c) f_{p,vis} \sin\delta_p, & \delta_p > 0 \\ 0, & \delta_p < 0 \end{cases} \tag{8}$$

wherein δ_p is the elevation of the planet in the moon sky at q and $f_{p,vis}$ the visibility fraction of the planet, both computed as outlined in appendix A; as opposed to $f_{*,vis}$ in Equation 3, $f_{p,vis}$ only describes occlusion of the planet behind the horizon at q. It is possible for the planet to be (partially) occluded by a fellow moon, but we consider these incidences minor enough to be neglected.

We have split the fraction in two components to clearly indicate the different implications: the first describes illumination of the host planet by the star, while the second describes reflection by the planet and illumination of the target moon. Averaged over the year, here Heller and Barnes (2013) found for the average absorbed reflected flux that

$$\bar{F}_r = \frac{L_* (1-\alpha_c)}{16\pi a_p^2 \sqrt{1-e_p^2}} \frac{\pi R_p^2 \alpha_p}{2a_c^2} \tag{9}$$

wherein a_c is the semi-major axis of the moon around its host planet.

2.4.3 Planetary thermal illumination

The final contribution to the exogenic energy budget comes from the planet itself. A planet emits blackbody radiation corresponding to its effective temperature:

$$L_p = 4\pi R_p \sigma_B T_{p,eff}^4$$

Since planets of themselves produce relatively little heat, the effective temperature $T_{p,eff}$ is primarily dependent on the stellar luminosity and distance via

$$T_{p,eff} = \sqrt[4]{\frac{L_* (1-\alpha_p)}{16\pi\sigma_B d_{*p}^2}}$$

However, since all giant planets in our Solar System have been found to emit more radiation than they receive from the Sun – because of such processes as Kelvin-Helmholtz heating, where the planet contracts under gravity and thus generates heat – we modify this by a flux excess factor x_{exc}:

$$T_{p,eff} = \sqrt[4]{\frac{L_* (1-\alpha_p)}{16\pi\sigma_B d_{*p}^2} \cdot x_{exc}}$$

This flux excess factor varies from close to unity (as in Uranus' case) to above 2.5 (as for Saturn). Hence, the final expression for a planet's thermal luminosity becomes

$$L_p = 4\pi R_p^2 \sigma_B \cdot \frac{L_* (1-\alpha_p)}{16\pi\sigma_B d_{*p}^2} \cdot x_{exc} = \frac{L_* R_p^2 (1-\alpha_p)}{4d_{*p}^2} \cdot x_{exc} \tag{10}$$

Since the giant planets in our Solar System are not tidally locked and, in fact, rotate quickly when compared to the terrestrial worlds, we assume the heat from stellar illumination to be evenly distributed across the surface, as stated in section 2.2. Hence, the planet emits the same amount of thermal radiation in all directions, and thus the planetary thermal flux absorbed by the moon is equal to, after introducing visibility, albedo and elevation modifiers analogously to our stellar flux description (section 2.4.1):

$$F_p(d_{pq}) = \frac{L_p\,(1-\alpha_q)}{4\pi d_{pq}^2} \cdot f_{p,vis} \sin\delta_p$$

Or, rather (by filling in L_p and realizing that for $\delta_p < 0$ the planet is invisible):

$$F_p(d_{pq}) = \begin{cases} \dfrac{L_* R_p^2\,(1-\alpha_p)\,(1-\alpha_q)}{16\pi d_{*p}^2 d_{pq}^2} \cdot x_{exc} \cdot f_{p,vis} \sin\delta_p, & \delta_p > 0 \\ 0, & \delta_p < 0 \end{cases} \tag{11}$$

This is much the same as Equation 3, but like in Equation 8, the factor $f_{p,vis}$ only describes horizon occlusion. Since we assume the planet's surface temperature to be the same everywhere, we can integrate over the entire year and the moon's surface to obtain

$$\bar{F}_p = \frac{L_* R_p^2\,(1-\alpha_p)\,(1-\alpha_c)}{32\pi a_p^2 a_c^2 \sqrt{1-e_p^2}} \cdot x_{exc} \tag{12}$$

for the average absorbed planetary thermal flux. Hence, our final expression for the average absorbed exogenic flux incident on some particular surface element on a given exomoon becomes

$$\begin{aligned} \bar{F}_{exo} &= \bar{F}_* + \bar{F}_r + \bar{F}_p \\ &= \frac{L_*\,(1-\alpha_c)}{16\pi a_p^2 \sqrt{1-e_p^2}} \bar{f}_{*,vis} + \frac{L_*\,(1-\alpha_c)}{16\pi a_p^2 \sqrt{1-e_p^2}} \frac{\pi R_p^2 \alpha_p}{2a_c^2} + \frac{L_* R_p^2\,(1-\alpha_p)\,(1-\alpha_c)}{32\pi a_p^2 a_c^2 \sqrt{1-e_p^2}} \cdot x_{exc} \end{aligned}$$

Which can ultimately be shown to reduce to

$$\bar{F}_{exo} = \frac{L_*\,(1-\alpha_c)}{16\pi a_p^2 \sqrt{1-e_p^2}} \left[\bar{f}_{*,vis} + \frac{\pi R_p^2 \alpha_p}{2a_c^2} + \frac{R_p^2\,(1-\alpha_p)}{2a_c^2} x_{exc} \right] \tag{13}$$

2.5 Endogenic heating

Endogenic heat dissipation takes three main forms:

- *Residual accretion heating:* during moon formation, material clumps together faster than the heat can be radiated away, trapping it in the body's core.
- *Radiogenic heating:* radioactive elements in the moon's interior decay over large timescales, providing a steadily declining background level of internal heat generation. Isotopes involved in radiogenic heating are Aluminum-26 and Iron-60 (during the body's infancy), Potassium-40 and various isotopes of Uranium and Thorium (Mousis et al., 2017; Sahijpal and Bhatia, 2015).
- *Tidal heating:* varying tidal forces induced by the moon's host planet deform and relax it, generating tidal heat at the expense of orbital energy.

For both residual accretion heating and radiogenic heating, since they are fairly constant over small (millions of years, assuming formation to be long ago) timescales, a simple recipe is adopted:

$$\dot{E}_{ac,rg} = \dot{E}_{ac,rg,\oplus} \cdot \frac{M_c}{M_\oplus} \tag{14}$$

wherein $\dot{E}_{ac,rg,\oplus}$ is the total internally generated heat of Earth (about 20 TW, as found by Jellinek and Jackson (2015)), and M_c and $M_\oplus$ are the masses of the object under consideration and Earth

respectively. Hence, we scale Earth's internal heat production to the moon. Since these processes generally only provide background levels of heat – particularly at the scale of most small, icy moons – this approximation is reasonable. This treatment is in decent agreement with the value found by Czechowski (2004) for Enceladus: $3.25 \cdot 10^{-12}$ W/kg versus $3.33 \cdot 10^{-12}$ W/kg via Equation 14.

Conversely, tidal heating can reach appreciable levels on exomoons. The equation describing the total amount of tidal heat dissipated in a satellite per second, given a roughly circular orbit, is given by

$$\dot{E}_{tidal} = \Phi \cdot \frac{21G^{1.5}}{2} \cdot \frac{M_p^{2.5} R_c^5 e_c^2}{a_c^{7.5}} \tag{15}$$

As stated in e.g. Henning et al. (2009), and wherein M_p is the mass of the parent, and R_s, e_s and a_s are the radius, orbital eccentricity and semi-major axis of the child body, respectively. These quantities are all readily observable; the main unknown is Φ, the tidal efficiency factor, which describes how efficiently tidal heat is dissipated throughout the body. Multiple methods exist to compute it: it can be determined from the motion of the body's satellites, or inferred from the observed heat. Based on Enceladus' observed heat flux, it has been empirically determined for Enceladus to be $0.0026 < \Phi < 0.0127$, but this leaves a lot to interpretation as to what this means for the moon's interior (Nimmo et al., 2018). As such, this value cannot simply be taken as typical for icy exomoons.

Regardless, the total endogenic heat generation is equal to

$$\dot{E}_{endo} = \dot{E}_{tidal} + \dot{E}_{ac,rg} \tag{16}$$

And the combined endogenic flux passing through any particular surface element of a given exomoon is given by

$$\bar{F}_{endo} = \frac{\dot{E}_{endo}}{4\pi R_c^2} = \Phi \cdot \frac{21G^{1.5}}{8\pi} \cdot \frac{M_p^{2.5} R_c^3 e_c^2}{a_c^{7.5}} + \dot{E}_{ac,rg,\oplus} \cdot \frac{M_c/M_\oplus}{4\pi R_c^2} \tag{17}$$

Because we assume the exomoon to be roughly symmetrical, the heat flux is the same irrespective of longitude or latitude. This is not necessarily true, as for instance Enceladus radiates more heat through the tiger stripes in its south polar region (Nimmo et al., 2018), but we are interested in obtaining an average impression of exomoon habitability. Hence, we neglect possible crustal asymmetry.

2.6 Tidal heating: fixed Q vs viscoelasticity

The amount of tidal heating is dependent on the tidal efficiency factor Φ. Many methods exist to determine this parameter, prime among which are the empirical fixed Q approach (which we use) and the more detailed viscoelastic models, particularly the Maxwell model (discussion will follow).

2.6.1 Fixed Q models

In fixed Q models, the tidal efficiency factor is given by

$$\Phi = \frac{k_2}{Q} f_{v,t} \tag{18}$$

wherein Q is an empirical tidal quality factor, describing the body's spring response to deformation, $f_{v,t}$ is the volume fraction of the satellite partaking in tidal heating and k_2 is the second order Love number. Q can be thought of as describing the lag between a tidal force and the moon's response: high Q means a large lag, while low Q means the body responds quickly to deformation. The Love number is a dimensionless parameter describing the rigidity of a planetary body and its mechanical properties, and is given by

$$k_2 = \frac{3/2}{1 + \frac{19\mu}{2\rho g R}} \tag{19}$$

wherein μ is the rigidity of the body, ρ its density, g its surface gravity and R its radius. However, while ρ, g and R can be observed or directly measured, and μ can be reasonably estimated if one knows the composition of the target body, Q is essentially a free parameter. Since it depends on both external characteristics, composition and internal structure of the body under consideration, it is difficult to make an informed estimate as to what it would be given a moon of some characteristics. We know Q of some Solar System bodies, but only by reverse engineering the tidal heating equations – i.e., we observed some tidal flux, filled in the other parameters and solved the equation for Q – or by studying orbits around the body in question (Lainey, 2016). In addition, fixed Q assumes the body to be of uniform composition, which is often not the case: once a moon receives enough endogenic heating (through tides or radiogenic sources), melting of its mantle and subsequent differentiation (sinking of heavier elements to the core) will occur, which is difficult to model with a fixed-Q approach. The minimum energy production to initiate this process depends on the moon's mass and composition, but current models indicate the Galilean moons (save Callisto) plus some Saturnian moons have undergone differentiation at some point in their pasts (McKinnon, 1997).

2.6.2 Viscoelastic models

Conversely, viscoelastic models allow the user to make more informed parameter picks for tidal heating. It models the satellite as having a viscoelastic mantle (note: this approach is thus primarily useful if the object *has* a mantle to begin with) taking up some fraction of its volume, so its tidal efficiency factor becomes

$$\Phi = -Im(k_2) f_{v,t} \tag{20}$$

wherein $f_{v,t}$ is now the volume fraction of the satellite taken up by the viscoelastic mantle, and $Im(k_2)$ is the imaginary component of the second order Love number, in a Maxwell model given by

$$Im(k_2) = \frac{-57\eta\omega}{4\rho g R \left[1 + \left(1 + \frac{19S}{2\rho g R}\right)^2 \frac{\eta^2\omega^2}{S^2}\right]} \tag{21}$$

wherein ω is the orbital frequency, η the mantle's viscosity (how sticky the mantle is) and S the mantle's shear modulus (how easily layers of the mantle can move past one another). Note that this equation holds for a Maxwell model: different viscoelastic models exist, each with different descriptions of $Im(k_2)$. The Maxwell model specifically regards the mantle's behaviour as spring-like; it has an instantaneous, elastic response, then slowly, viscously yields to the deformation.

Since it takes viscosity and other mantle parameters dependent on temperature as input for the tidal heating process, viscoelastic models allow for feedback between heating and these mantle parameters. If the mantle heats enough, it will start to melt, passing first the solidus temperature as it slowly turns into a crystal lattice with trapped liquid pockets. Viscosity and shear drop as the temperature increases: the more liquid the mantle is, the more easily it moves and the less sticky it becomes (see Figure 2). Eventually, it passes a point where it has become sufficiently liquid (the breakdown temperature) that the crystal lattice breaks down, turning the mantle into a suspension of crystal grains; at this point, tidal heating efficiency drops rapidly. Finally, above the liquidus temperature, the mantle is assumed to be fully liquid and as such inefficient at tidal heating. As such, viscoelastic models tend towards an equilibrium, where the mantle is partially molten but still sticky, close to the breakdown temperature, where tidal heating is most efficient (Moore, 2003).

However, since our target moons are small to mid-sized, their interiors are unlikely to undergo differentiation or melting. Enceladus is thought to have an undifferentiated, porous core, allowing for efficient heat transfer between the ocean flowing through these pores and the tidally heated, sponge-like core (Nimmo et al., 2018), but is unlikely to have a mantle. The other icy moons of Saturn (apart from, possibly, Rhea) and the moons of Uranus (apart from, probably, Titania and, possibly, Oberon) are thought to have similar undifferentiated internal structures, and if at all they possess a mantle it is unlikely to have undergone extensive enough melting to necessitate a viscoelastic approach (Hussmann et al., 2006). For more recent, detailed discussions of various tidal heating approaches, see Dobos and Turner (2015) and Renaud and Henning (2018).

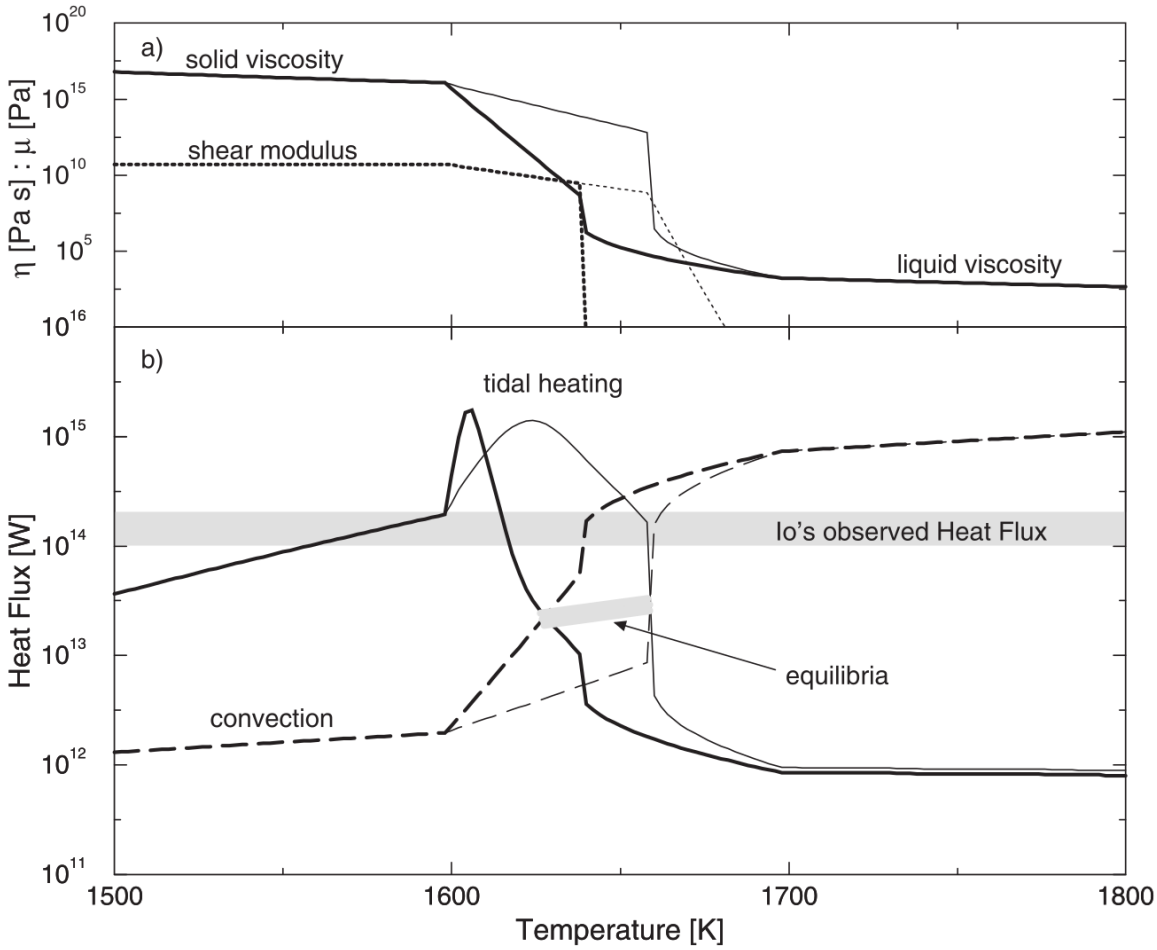

Figure 2: *Top panel:* mantle viscosity and shear modulus with changing mantle temperature given two different viscoelastic rheologies (model of internal structure and dynamics) for Io. Note that here, μ denotes the shear modulus, *not* the rigidity. *Bottom panel:* Io's tidal heat production (solid lines) and convective heat loss (dashed lines) for two different rheologies at different mantle temperatures. Note the equilibrium between heat production and convective loss around the breakdown temperature (around 1630 K for the thick line, around 1660 K for the thin line). In both panels, the thick line assumes a strong dependence of viscosity on the mantle melt fraction, while the thin line assumes a weaker dependence. Taken from Moore (2003).

2.7 Cooling

Exomoon cooling, in the absence of an atmosphere and assuming a solid crust with at most a small fraction participating in cryovolcanism (Enceladus' tiger stripes, for example), occurs only through conduction and radiation. Hence, the thermal conductivity and thus the insulation provided by the crust play a major role in maintaining habitability on an icy moon. For a certain surface temperature T_{surf} and moon emissivity ϵ_c:

$$F_{cool} = \epsilon_c \sigma_B T_{surf}^4 \tag{22}$$

Since radiative cooling is notoriously inefficient, under the right conditions (i.e. large surface area, low emissivity, low surface temperature), an icy moon can, in the absence of additional endogenic heat influx, hold on to its internal heat on million year timescales (Nimmo et al., 2018).

To maintain equilibrium with its surroundings, the heat flux into a surface element must equal the flux *out* of that same surface. That is, if the heat flux in is higher than the flux out, the temperature will increase; and vice versa, if the heat flux out is higher, it will cool down. Hence:

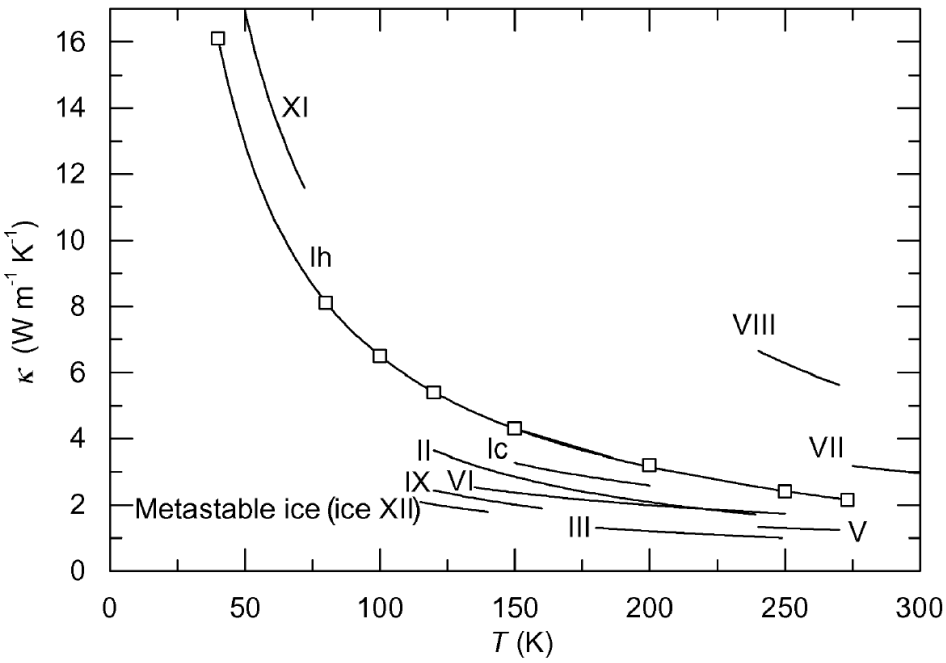

Figure 3: Changing thermal conductivity with changing temperature and crystalline structure of ice. Our primary concern is the curve of ice Ih, i.e. regular hexagonal ice. Taken from Andersson and Inaba (2005).

$$F_{cool} = F_{total}$$
$$\rightarrow T_{surf} = \sqrt[4]{\frac{F_{total}}{\epsilon_c \sigma_B}}$$

Since the only way for the internal heat to escape is through the surface, the total flux per surface element is the sum of the exo- and endogenic contributions, so

$$T_{surf} = \sqrt[4]{\frac{\bar{F}_{exo} + \bar{F}_{endo}}{\epsilon_c \sigma_B}} \tag{23}$$

This is the starting point of our melting depth model (as detailed in subsection 3.4). The endogenic flux is conducted through the crust: for conduction, the flux F through a layer of thickness D of *constant* thermal conductivity k given a temperature difference ΔT is

$$F = k\frac{\Delta T}{D}$$

Which can be rewritten for the temperature difference to become

$$\Delta T = \frac{D \cdot F}{k} \tag{24}$$

At some depth D_l below the surface, the temperature eventually becomes high enough to sustain liquid water; this depth is the melting depth. It is our primary interest, since it tells us whether or not a moon can sustain a subsurface ocean: if D_l is less than the suspected thickness of the moon's ice crust, a subsurface ocean is possible.

The thermal conductivity k is taken to be that of water ice Ih – this is the regular, hexagonal crystal

structure of water ice, and also the most abundant type of ice found on Earth and in the Solar System. Other, more exotic crystal configurations exist, but they manifest only under extreme circumstances not relevant to this thesis (Bland et al., 2012). Ice Ih's thermal conductivity changes with temperature T via the relation found by Andersson and Inaba (2005) (see also Figure 3):

$$k(T) = \frac{632}{T} + 0.32 - 0.00197T \tag{25}$$

However, it must be noted that this relation holds for *pure* water ice; when one introduces a fraction of ammonia (NH_3, as is thought to be the case for most icy moons forming in the outer Solar System (Hammond et al., 2018)), salts, clathrate hydrates (ice crystal lattices wherein small guest molecules like CH_4 are trapped; these are thought to occur in the outer Solar System (Lunine and Stevenson, 1985)) and/or other impurities, this would probably lead to changes in its coefficients, if not overall form. Research into those changes does not seem to exist; we only considered the effects of ammonia, since its effects on water ice melting temperature (and thus the melting depth D_l) have been studied in literature.

Another note must be made of our assumption that cryovolcanism is limited. Cryovolcanism represents a convective cooling mechanism, which releases heat from the moon's interior via the expulsion of hot gas and vapor. Since convection is known to be a more efficient cooling mechanism than conduction, if a large part of the moon's surface partakes in volcanic activity (like Io's case, although Io suffers from regular volcanism), this process can no longer be neglected. We will revisit the implications hereof in Chapter 5.

3 Approach

This chapter discusses our own approach to analysing the potential habitability of exomoons. Unless stated otherwise, the following treatment is our own. All model codes were written in Python.

3.1 Geometry

To determine the amount of exogenic heat received by any point on the moon's surface, we must know the positions of moon, host planet and host star relative to one another. We have to account for eclipses of the star, the phase of the planet's stellar reflection and the elevation of the (extended) illumination sources in the moon's sky. The simulations in this thesis used the N-body code *Rebound*[2] (Rein and Liu, 2012) to compute motions and positions of star, planet and moon: this yielded Cartesian coordinates (x, y, z) and velocities (v_x, v_y, v_z) of the bodies in a stationary rest frame. We then defined a moon-dependent frame of reference in which the x'-axis points towards the host planet, the z'-axis is perpendicular to the moon's orbital plane around the planet, and the y'-axis is perpendicular to the x', z'-plane. Since the moon is tidally locked, the x'-axis will always point through the same site on the moon's surface; this is the subplanetary point. We use this point to define a geographic coordinate system for the moon's surface in which the equator (where the moon intersects with the x', y'-plane) is defined as 0 latitude (φ), and the subplanetary point on the equator has longitude (θ) 0. Appendix A discusses in detail how we then computed their elevations, eclipses, occlusions and phases at any given time, and at any given point on the moon's surface.

3.2 Exogenic heating model

For our modelling of the exogenic contribution to the moon's energy budget, we ran *Rebound* for a single planetary orbit. Via the treatment outlined in appendix A and Equations 3, 8 and 11, we then computed the elevations of host star and host in the moon's sky for a grid of landing sites on the surface (every 10 degrees of longitude and latitude) and determined the incident radiation to those sites. We calculated the radiation incident to the top of the atmosphere: if there is (close to) none, this radiation directly strikes the surface. However, the presence of an atmosphere can strongly reduce the amount of light actually reaching the surface – Earth's atmosphere, for instance, is opaque to UV and large portions of the infrared. Since the moons we consider are in general not massive enough to possess more than a trace atmosphere, we did not take into account atmospheric effects.

We computed all three radiation contributions separately and plotted their illumination curves over the course of the moon's orbit around its host, and the host's orbit around the star. We then summed the contributions, combined all these grid points into a 2d surface map and plotted the motion of the illumination pattern across the moon's surface over one full planetary year. As fiducial models we elected Enceladus and Titania: their details can be found in Table 5. We benchmarked our illumination model to Heller and Barnes (2013), whose equations we also used to compute the year-averaged exogenic flux in the melting depth model (section 3.4).

3.3 Endogenic heating model

We adopted a fixed-Q approach for tidal heating (see section 2.5). We used Equation 14 to model the internal heat generated by radiogenic and residual heating processes, and Equation 15 for tidal heat with Equation 18 for the tidal efficiency factor Φ. We then varied the moon's rigidity μ between at most 100 GPa (a highly rigid, metallic/silicate body) and at least 100 MPa (a highly porous, easily deformable body of water and ice), and the tidal quality factor Q from 1 to 1000 (the range in which all terrestrial bodies in the Solar System fall). It should be noted that both Q and μ are poorly coupled to readily observable physical characteristics of a body, which is why these tidal parameters were given a broad range.

[2] can be downloaded freely at `http://github.com/hannorein/rebound`

	Enceladus	Io
host planet	Saturn	Jupiter
M_p (10^{26} kg)	5.68	18.98
M_c (10^{20} kg)	1.08	893.20
R_c (10^3 m)	252.1	1821.6
ρ_c (g cm^{-3})	1.61	3.53
g_c (m s^{-2})	0.113	1.796
Φ_c	0.005	0.015
μ_c (10^9 Pa)	$\sim$1	$\sim$5
Q_c	$\sim$2	$\sim$40
$f_{v,t}$	0.8	0.8
a_c (10^6 m)	237.95	421.70
e_c	0.0047	0.0041
$\dot{E}_{obs}$ (10^{12} W)	0.004-0.016	100-200

Table 4: The relevant fiducial parameters for endogenic heating. Note that 1) the densities are average densities, i.e. presuming a homogeneous body; 2) the rigidities μ are estimates based on their presumed composition and typical values given by Henning et al. (2009); 3) the tidal quality factors Q are deduced from the trend given by Equation 26 (data from Lainey (2016)); and 4) both the rigidities and tidal quality factors are poorly constrained. Data taken from Wikipedia, May 2019.

3.3.1 Mass-quality factor trend

To obtain estimates for the tidal quality factor Q, we investigated possible relations between Q and more directly observable satellite properties. From least squares fitting the tidal efficiency data of Lainey (2016), we found indications of a trend between Q and mass (Figure 4), wherein the Q factor scales with the mass of a terrestrial body via

$$Q \approx 10^{-8.83} \cdot M^{0.45} \tag{26}$$

With M the mass of the body in kg, and Q the corresponding tidal quality factor. Note however that this trend is based on only three data points, and that it is purely empirical: we did not expect this based on theory. Q measurements of (for instance) Earth diverge widely: it has been measured as low as 32 (Yoder, 1995) and as high as 280 by Lainey (2016), the latter of which we used in Figure 4.

3.3.2 Estimation of tidal parameters

Since the tidal heat flux is properly constrained for only two bodies in our Solar System, we used them as fiducial models: Enceladus and Io. While Io is far from a potentially habitable environment, it is the most studied case of tidal heating (even though it is likely to sustain a molten interior, and as such better described by viscoelastic models – see sections 1.3 & 2.6). Based on Equation 26, the expected Q value for Enceladus would be approximately 2; for Io, it would be around 40 (for our other fiducial models – see section 3.4.2 – we predict Q for both Oberon and Titania around 7, for Rhea around 6). The full fiducial models are given in Table 4. The values for μ are estimates based on both the observed heat flux of both bodies, their masses and their presumed composition as per Henning et al. (2009), who found around 90 GPa for undamaged rocky material, 8 GPa for Io's rigidity, and 4 GPa for an icy body. Since both Enceladus and Io are thought to be partially molten (albeit applying for the former to the mantle, and for the latter to the ocean) and Enceladus is thought to be porous – increasing the efficiency of tidal heat dissipation from core to ocean to crust – we adjust their rigidities to be 1 and 5 GPa, respectively. The values for $f_{v,t}$ result from two considerations: one, because of its low density, Enceladus is thought to have a porous interior, implying that the entire body but for the crust and ocean (at most some 20% of its volume) partakes in tidal heating; and two, while Io's crust takes up less volume than Enceladus', it is thought to have a massive core (Moore, 2003). If that core is fully rigid, its contribution to tidal heating would be negligible, hence we too for Io set the tidally active fraction to

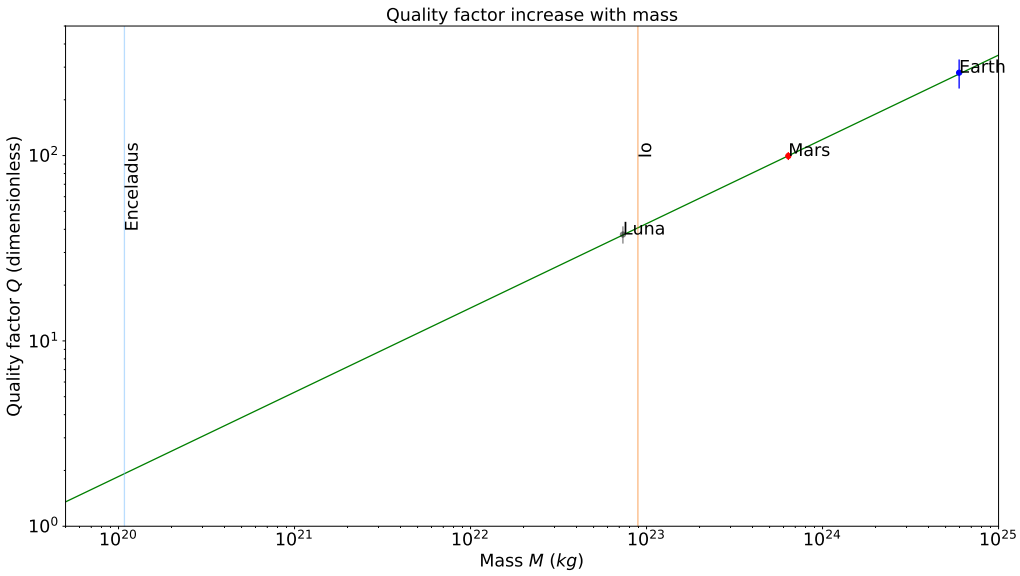

Figure 4: Masses of those worlds with determined Q values versus those Q values, plus the masses of Io and Enceladus. Note the clear trend (green), but also note we have only three data points – and none of those in Enceladus' mass range. Data for Luna, Mars and Earth taken from Lainey (2016).

0.8. We took our observed heat fluxes from Nimmo et al. (2018) for Enceladus, and from Moore (2003) for Io.

3.4 Melting depth model

Our melting depth model computes the depth at which ice begins to melt due to increasing temperatures. It is a purely conductive approach: we do not consider the heat lost through convective processes (volcanism/cryovolcanism or tectonic activity). We assume the crust has two layers: the thicker, solid ice shelf below, and a finely grained layer of dust and icy particles of very low thermal conductivity on top – this substance is called regolith. Our algorithm first computes the surface temperature (Equation 23) as induced by some endogenic flux and some exogenic flux (computed via the equations derived by Heller and Barnes (2013)), then the temperature below the insulating regolith layer D_{rego}, and then the depth below D_{rego} at which the temperature reaches the melting point (also called the liquidus temperature) of water for some given mass fraction of ammonia (NH_3). We consider the fraction of ammonia as it strongly influences the liquidus temperature (Leliwa-Kopystyński et al., 2002; Hammond et al., 2018). Our method eventually yielded an analytic expression for the melting depth D_l, assuming conduction only.

3.4.1 Derivation of melting depth expression

Recall from section 2.7 that the surface temperature is given by Equation 23. If this surface temperature exceeds 150 K (the snow line: see Armitage et al. (2016)), we assume the water ice on the surface to have been sublimated and the moon desiccated; if not, we compute the temperature underneath the insulating regolith layer D_{rego}, using Equation 24 to calculate the temperature gradient over the regolith:

$$T_{rego} = T_{surf} + \Delta T_{rego} = T_{surf} + \frac{D_{rego} \cdot \dot{E}_{endo}}{4\pi \left(R_c - D_{rego}\right)^2 k_{rego}} \tag{27}$$

wherein k_{rego} is the thermal conductivity of the porous regolith layer; since this layer consists of finely grained material (shattered ice, snow, dust), the majority of its volume is vacuum (in the absence

of an atmosphere) and heat transport is therefore dominated by radiative processes. Since these are very inefficient, the value of k_{rego} is taken to be between 0.0001 and 0.001 W/mK (based on Yu and Fa (2016), who determined Lunar regolith properties).

Subsequently, we compute the temperature at some depth D into the solid ice shell. Recall that the thermal conductivity of ice is given by Equation 25, as found by Andersson and Inaba (2005). Let us then subdivide the ice shell in layers of thickness ΔD, each with a slightly higher temperature than the one above, and thus a slightly different thermal conductivity. Suppose the temperature in layer n is T_n; assuming the ice shell to form a small fraction of the moon's radius, following Equation 24, the temperature in layer $n+1$ at depth D_{n+1} must then be

$$T(D_{n+1}) = T(D_n) + \Delta T(D_{n+1}) = T(D_n) + \frac{\Delta D \cdot \dot{E}_{endo}}{4\pi \left(R_c - D_{n+1}\right)^2 k(T(D_{n+1}))} \tag{28}$$

wherein D_n is the depth of layer n. We divide $\dot{E}_{endo}$ by the surface area of each layer separately, since, as the surface area shrinks, the amount of heat escaping per surface area must go up. Doing this iteratively, we obtain (by setting $T_{rego} = T_0$)

$$T(D_N) = T_{rego} + \sum_{n=1}^{N} \frac{\Delta D \cdot \dot{E}_{endo}}{4\pi \left(R_c - D_n\right)^2 k(T(D_n))} \tag{29}$$

If ΔD tends to zero, this becomes the following integral:

$$T(D) = T_{rego} + \int_{D_{rego}}^{D} \frac{\dot{E}_{endo}}{4\pi \left(R_c - D'\right)^2 k(T(D'))} dD' \tag{30}$$

Where the superscript $'$ is added to distinguish between the actual target depth D and the integration variable D'. This integral cannot be immediately solved, since k is dependent on T, which is dependent on D in an unknown way. Hence, on both sides, we take the derivative with respect to D:

$$\frac{dT}{dD} = \frac{\dot{E}_{endo}}{4\pi \left(R_c - D\right)^2 k(T)}$$
$$\rightarrow k(T)dT = \frac{\dot{E}_{endo}}{4\pi} \left(R_c - D\right)^{-2} dD$$

Let us define the constant factor $\dot{E}_{endo}/4\pi = X$. Next, to find the melting depth, we integrate on both sides from T_{rego}, D_{rego} to T_l, D_l (l for liquid):

$$\int_{T_{rego}}^{T_l} k(T)dT = X \int_{D_{rego}}^{D_l} \left(R_c - D\right)^{-2} dD$$

Filling in Equation 25 on the left, we find that

$$\int_{T_{rego}}^{T_l} k(T)dT = \left[632 \ln T + 0.38T - 0.00985T^2\right]_{T_{rego}}^{T_l} = K(T) \tag{31}$$

Let us define the function $632 \ln T + 0.38T - 0.00985T^2 = K(T)$, the integrated conductivity. Then integrating the right side gives

$$X \int_{D_{rego}}^{D_l} \left(R_c - D\right)^{-2} dD = X \left[\left(R_c - D\right)^{-1}\right]_{D_{rego}}^{D_l}$$

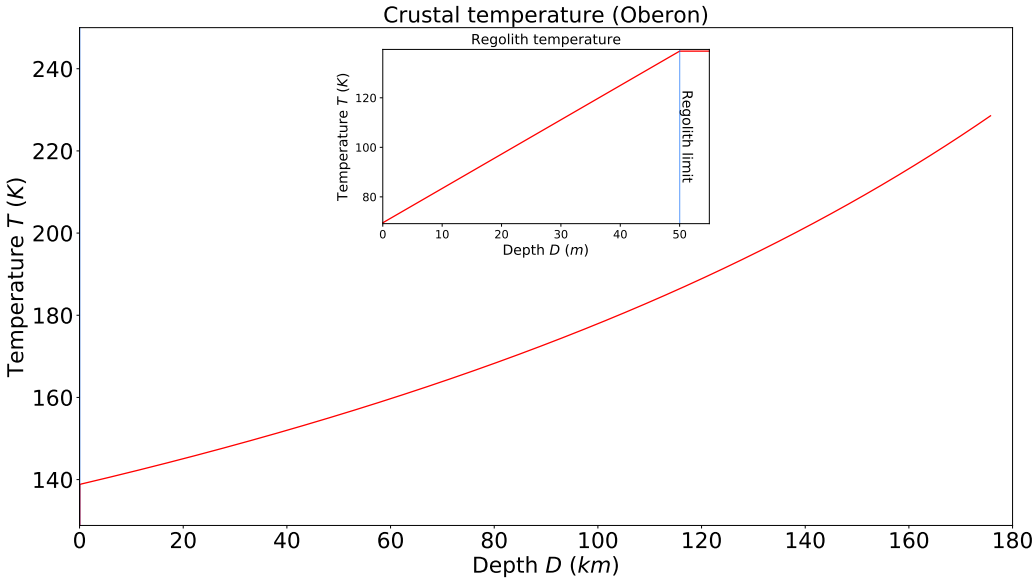

Figure 5: An example of a crustal temperature curve for our fiducial Oberon model, with inset regolith temperature curve. This plot was not used in our final results, but serves to illustrate the increasing temperature with depth, and the increasing rate of temperature increase with depth due to a changing conductivity. Note its sudden terminus around 175 km; this is the melting point of its ice crust, lowered considerably due to added ammonia.

So we find that

$$K(T_l) - K(T_{rego}) = X\left(R_c - D_l\right)^{-1} - X\left(R_c - D_{rego}\right)^{-1}$$

Which we can solve for D_l, thus (after resubstituting X) finally yielding

$$D_l = R_c - \left[4\pi \dot{E}_{endo}^{-1}\left(K(T_l) - K(T_{rego})\right) + \left(R_c - D_{rego}\right)^{-1}\right]^{-1} \tag{32}$$

Which is our analytic expression for the melting depth. Given some input fiducial model, this equation can thus directly determine the melting depth, and as such explore the parameter space within which any exomoon may exist. This is an important result, since Equation 32 holds for different expressions for $k(T)$ and associated $K(T)$ – hence, if the shape of $k(T)$ is in future experiments more precisely determined, Equation 32 can be easily updated.

Our default value for the liquidus temperature T_l is 273.15 K. However, as mentioned previously, icy moons may possess sufficient ammonia to influence both the functional shape of the conductivity and the liquidus temperature (Hammond et al., 2018). It must be noted that, according to Hammond et al. (2018), the ammonia preferentially ends up at the bottom of the ice shelf (where the ice is partially molten) and in the subsurface ocean, so the shape of the ice crust's conductivity is not expected to change much. Hence, we did not take possible changes to $k(T)$ into account, but we *did* adjust the melting temperature dependent on the mass fraction of ammonia f_{m,NH_3}. Since Leliwa-Kopystyński et al. (2002) found that the liquidus temperature reaches a minimum at 176.2 K for 32.6% ammonia, we used the following linear interpolation between 0 and 32.6% ammonia:

$$T_l(f_{m,NH_3}) = \frac{176.2 - 273.15}{0.326} \cdot f_{m,NH_3} + 273.15 \tag{33}$$

In reality, Dodson-Robinson et al. (2009) found the ammonia fraction in the protosolar nebula to be at most around 15%, so we adopted that as the maximum used value. We set a maximum melting

depth of 30% of the moon's radius based on estimates by Hussmann et al. (2006). We also assume a minimum melting depth of 100 m underneath the regolith layer. The finely grained regolith has to rest on something; since this radiative processes-dominated regolith layer can take any value between ~ 1 m (as for our own moon, see Yu and Fa (2016)) and several tens of meters (as we assume to be the case for Enceladus, due to its own cryovolcanic ejecta precipitating back onto the surface), we selected 100 m of ice as a stable limit. If the melting depth is smaller than 100 m, we assume the moon to be desiccated – or at best, covered in a relatively thin icy coating – since without an ice shell, the volatile water will quickly escape into space. If the melting depth is larger than $0.3R_c$, we assume the moon is frozen solid.

3.4.2 Model dependencies

Our model is in total dependent upon seventeen parameters. These are, plus their (simplified) implications:

- The stellar luminosity L_*: the brighter the star, the higher the moon's surface temperature.
- The planet's mass M_p: the more massive the planet, the stronger the tidal forces.
- The planet's semi-major axis a_p: the further from the star, the lower the moon's surface temperature.
- The planet's eccentricity e_p: the more eccentric the planet's orbit, the more variable the moon's surface temperature.
- The planet's Bond albedo α_p: the darker the planet, the less reflection hits the moon.
- The planet's emissivity ϵ_p: the lower the emissivity, the less planetary emission hits the moon.
- The planet's flux excess x_{exc}: the lower the flux excess, the lower the planet's thermal flux.
- The moon's mass M_c: the more massive the moon, the stronger the tidal forces.
- The moon's density ρ_c: the denser the moon, the weaker the tidal forces.
- The moon's semi-major axis a_c: the further from the planet, the weaker the tidal forces.
- The moon's eccentricity e_c: the higher the eccentricity, the stronger the tidal forces.
- The moon's inclination i_c: the higher the inclination, the less planetary eclipses.
- The moon's Bond albedo α_c: the darker the moon, the higher the surface temperature.
- The moon's emissivity ϵ_c: the lower the emissivity, the longer the moon takes to cool.
- The moon's regolith thickness D_{rego}: the thicker the regolith blanket, the warmer the moon's interior.
- The moon's tidal efficiency factor Φ_c: the higher the tidal efficiency, the stronger the tidal heating.
- The moon's ammonia mass fraction f_{m,NH_3}: the higher the ammonia content, the lower the melting point of ice.

Exogenic heating processes also depend on the radius of the planet, but gas giant density and radius were found by Chen and Kipping (2017) to scale with mass; hence, we used planet mass as a proxy for planet radius. This relation is given by

$$\log_{10}\left(\frac{R}{R_\oplus}\right) = \begin{cases} 0.3756 + 0.589 \cdot \log_{10}\left(\frac{M}{M_\oplus}\right), & 2.04M_\oplus \leq M \leq 0.414M_{Jup} \\ 83.6663 - 0.044 \cdot \log_{10}\left(\frac{M}{M_\oplus}\right), & 0.414M_{Jup} \leq M \leq 0.0800M_\odot \end{cases} \tag{34}$$

Of the seventeen model parameters, twelve strongly influence the melting depth, with the moon's orbital inclination and emissivity, and the planet's albedo, emissivity and flux excess being of only minor influence. The planet's eccentricity only begins to strongly influence the melting depth for values greater than 0.1, which renders acquisition of an extensive satellite system unlikely a priori. In addition, such high eccentricities do not occur in the Solar System (apart from Mercury, where general relativistic effects play a role, or KBOs like Pluto). Icy moon densities vary only between about 1 and 2 g cm^{-3}, a range which does not introduce large changes in our results. Icy moon albedo, while varying widely from moon to moon, influences how far beyond the snow line it can maintain its icy shell and not so much its melting depth. The tidal efficiency and ammonia mass fraction are not well constrained. Hence, we used only the fiducial values per moon for these parameters, reducing our model to the following seven variables: L_*, M_p, a_p, M_c, a_c, e_c and D_{rego}. We then varied two parameters at a time within reasonable ranges, plotting all seven parameters against one another and computing the corresponding melting depths in terms of the moon's radius. These ranges – plus corresponding scientific questions and physical comparisons & justification for the limits – are:

- $10^{-2}L_\odot \leq L_* \leq 10^2 L_\odot$: can subsurface oceans exist on icy exomoons around different stellar types? The range stretches from the faintest M dwarfs to B stars. This covers essentially the entire main sequence save O stars, which are so luminous and live so briefly that planet formation, let alone the development of life, is unlikely, hence our exclusion of them.

- $10^{25}kg \leq M_p \leq 10^{28}$ kg: can subsurface oceans exist on icy exomoons around more massive gas giants, or worlds smaller than Neptune? The range stretches from roughly 2 Earth to 10 Jupiter masses. 2 Earth masses is the "Neptunian world" cutoff described by Chen and Kipping (2017), above which planets acquire extensive gaseous envelopes; 10 Jupiter masses is near the canonical cutoff point for brown dwarfs as described by Spiegel et al. (2011).

- $1AU \leq a_p \leq 10^2$ AU: how does the melting depth depend on stellar proximity, and thus stellar illumination? The range stretches from the Solar habitable zone to roughly twice the distance of the Kuiper Belt. Inward the habitable zone, habitability is impossible a priori; beyond the upper limit, stellar illumination plays little role, hence further distance from the star makes very little difference.

- $10^{19}kg \leq M_c \leq 10^{22}$ kg: can subsurface oceans exist on less/more massive exomoons? The range stretches from 0.1 Enceladus to roughly 3 Titania masses. 0.1 Enceladus masses is close to the mass of Mimas, the smallest gravitationally rounded body in the Solar System; above several Titania masses, we enter the regime of the Galilean moons, which possess the molten interiors our model does not apply to.

- $10^8 m \leq a_c \leq 10^9$ m: is there a circumplanetary, subsurface habitable edge or zone, and if so, where is it located? The range stretches from roughly 2 Saturn radii to about the semi-major axis of Titan. The lower limit is close to the fluid Roche limit; beyond the upper limit, tidal heating no longer plays an appreciable role, hence further distance from the planet makes very little difference.

- $10^{-4} \leq e_c \leq 10^{-1}$: how dependent is the melting depth on eccentricity – are eccentricities critical to maintaining a subsurface ocean? The range stretches from essentially circular to half the eccentricity of Mercury ($\sim$0.2). Most regular moon orbits have eccentricities around 10^{-2}; however, in hypothetical systems with more eccentricity pumping (by either mean motion resonance with neighbouring moons or, in M dwarf systems, the nearby star/planets) this might still go up, hence our upper limit of 10^{-1}.

- $1 \leq D_{rego} m \leq 10^2$ m: how does the melting depth depend on surface isolation – can subsurface oceans exist if the solid, icy crust is directly exposed? The range stretches from Lunar levels to 100 times that. Above 100 m, we assume gravity compresses the regolith to a solid crust; we considered less than 1 m of finely grained material unlikely.

We used as fiducial models those small to mid-sized icy Solar System moons most likely to harbor subsurface oceans, but (presumably) without a molten interior: Enceladus, Rhea, Titania and Oberon. Table 5 lists all relevant host planet and moon parameters; in all fiducial models, the host star is equal to the Sun, i.e. mass 1 $M_\odot$, radius 1 $R_\odot$ and luminosity 1 $L_\odot$.

	Saturn	Uranus
M_p ($M_\oplus$)	95.159	14.536
R_p (10^6 m)	58.232	25.362
α_p	0.342	0.3
$x_{p,exc}$	2.5	1.1
a_p (AU)	9.5826	19.2184
e_p	0.0565	0.0464
i_p (deg)	2.485	0.773

	Enceladus	Rhea	Titania	Oberon
host planet	Saturn	Saturn	Uranus	Uranus
M_c (10^{20} kg)	1.08	23.06	35.27	30.14
ρ_c (g cm^{-3})	1.61	1.24	1.72	1.63
α_c	0.81	0.70	0.17	0.14
ϵ_c	0.95	0.90	0.60	0.60
Φ_c	0.005	0.009	0.010	0.010
D_{rego} (m)	20	50	50	50
f_{m,NH_3}	0.00	0.10	0.15	0.15
a_c (10^6 m)	237.95	527.11	435.91	583.52
e_c	0.0047	0.0013	0.0011	0.0014
i_c (deg)	26.74	27.08	98.11	97.83

Table 5: The planets (left) and moons (right) used as fiducial models. Note that 1) the densities are average densities, i.e. presuming an homogeneous body; 2) the emissivities are average estimates; 3) the inclinations listed here are equal to the inclinations of the moons relative to their parents' equators *plus* the axial tilts of those parent bodies; and 4) the values for $x_{p,exc}$ are also estimates. Data taken from Wikipedia, 2019.

3.4.3 Uncertainties

The three least certain fiducial parameters are the tidal efficiency factor Φ_c, the regolith cover thickness D_{rego} and the ammonia mass fraction f_{m,NH_3}. Only for Enceladus has $\Phi_c = k_2/Q$ been decently constrained: Nimmo et al. (2018) found that $0.0026 \leq \Phi_c \leq 0.0127$, so we picked as fixed value $\Phi_c = 0.005$. Nimmo et al. (2018) cites $\Phi_c \approx 0.015$ for Io, implying increasing Φ with increasing mass and SMA; since Rhea, Titania and Oberon are considerably more massive than Enceladus, but also (since they are further from their hosts, allowing for less tidal heating and thus less partial melting of the interior) presumably less deformable than Enceladus or Io, we picked $\Phi_c = 0.01$ for the other three moons.

The regolith cover thickness is unknown for any body beyond our own moon (less than 1 m, see (Yu and Fa, 2016)), but we can make an informed estimate. Since Enceladus' tidally induced cryovolcanism creates the icy E Ring around Saturn (Kempf et al., 2018), this material is scooped back up by Enceladus' leading hemisphere (recall that since the moon is tidally locked, one side continually leads in its orbit), and also by those of Rhea, Tethys, Dione and Mimas, which all orbit within the extensive E Ring. In addition, since these moons are all less massive than Luna, their gravity compresses the porous regolith less. Hence, we expect the regolith cover on Rhea to be far thicker than that on our own moon: we adopt 50 m. The Uranian system is thought to have a similar, more tidally active past (primarily due to Miranda and Ariel, see Desch et al. (2007)), so we also assume 50 m for Titania and Oberon. Conversely, Enceladus is still tidally active and shows signs of recent resurfacing (Nimmo et al., 2018), so here we assume the regolith cover to be thinner; since the surface is so young, regolith has not yet had the time to pile up, so we assume 20 m.

Finally, the ammonia mass fraction is known to be larger in the outer Solar System, where conditions allowed for the condensation of ammonia ices into the accreting moons. More generally, f_{m,NH_3} goes up as temperature (and thus, illumination) goes down. Additionally, suggestions of Enceladus' recent in situ formation as opposed to from Saturn's circumplanetary disk 4.5 Gyr ago (Truong et al., 2019; Glein et al., 2018) makes it unlikely to possess extensive ammonia deposits. Hence, we have adopted a no ammonia model for Enceladus, 10% for Rhea as it is further from Saturn and, possibly, indigenous to the Saturnian system, and 15% for Titania and Oberon since they are further from the Sun.

4 Results

We now present our results. We provide an analysis of our illumination curves, surface maps, endogenic heating models and melting depth models. We will discuss our results in greater detail in Chapter 5, where we also compare with literature findings.

4.1 Surface maps

We investigated how surface illumination changes over the course of a moon day/planetary year, producing illumination curves for a regular grid of surface sites for two of our four fiducial moons: Enceladus and Titania. Several examples are shown for Enceladus during equinox in Figure 6, and for Titania during its northern summer solstice in Figure 7. Our moon coordinate system was defined by setting the equator as 0 latitude, and the subplanetary point (on the equator, with the planet directly at zenith) as

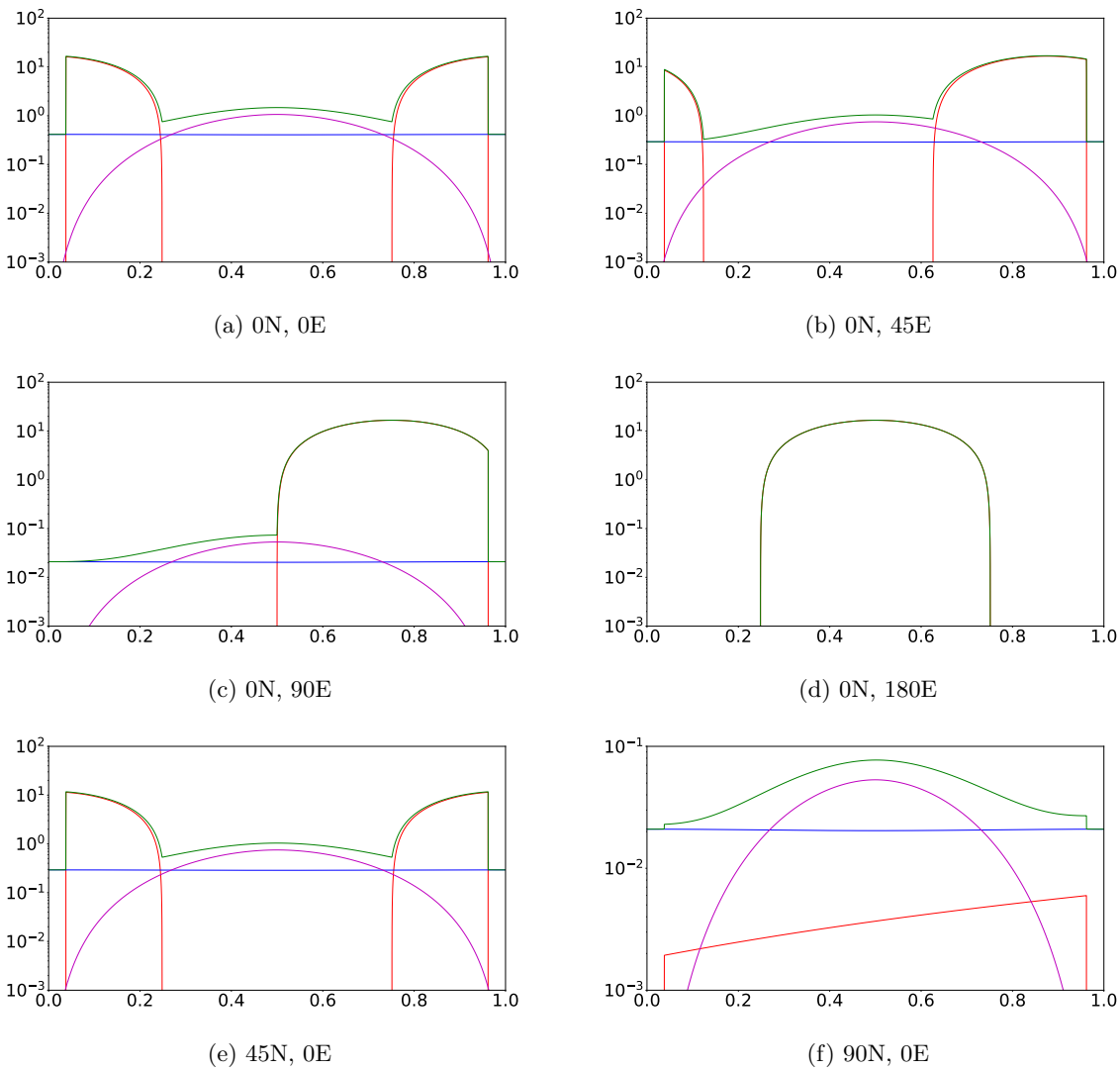

Figure 6: Illumination curves for landing sites on Enceladus during equinox. The x-axis shows time in Enceladian days (i.e. orbits around Saturn); the y-axis shows illumination in W/m^2. Red is the direct stellar contribution, magenta the planetary reflected stellar contribution, blue the planetary thermal contribution, and green the sum, so the total illumination. We do not show examples of the southern hemisphere since the pattern is symmetrical during equinox. Note the eclipses at the start and end of all panels save *d:* there, the planetary contributions are too weak to show at this scale, so the stellar contribution appears to overlap with the total illumination.

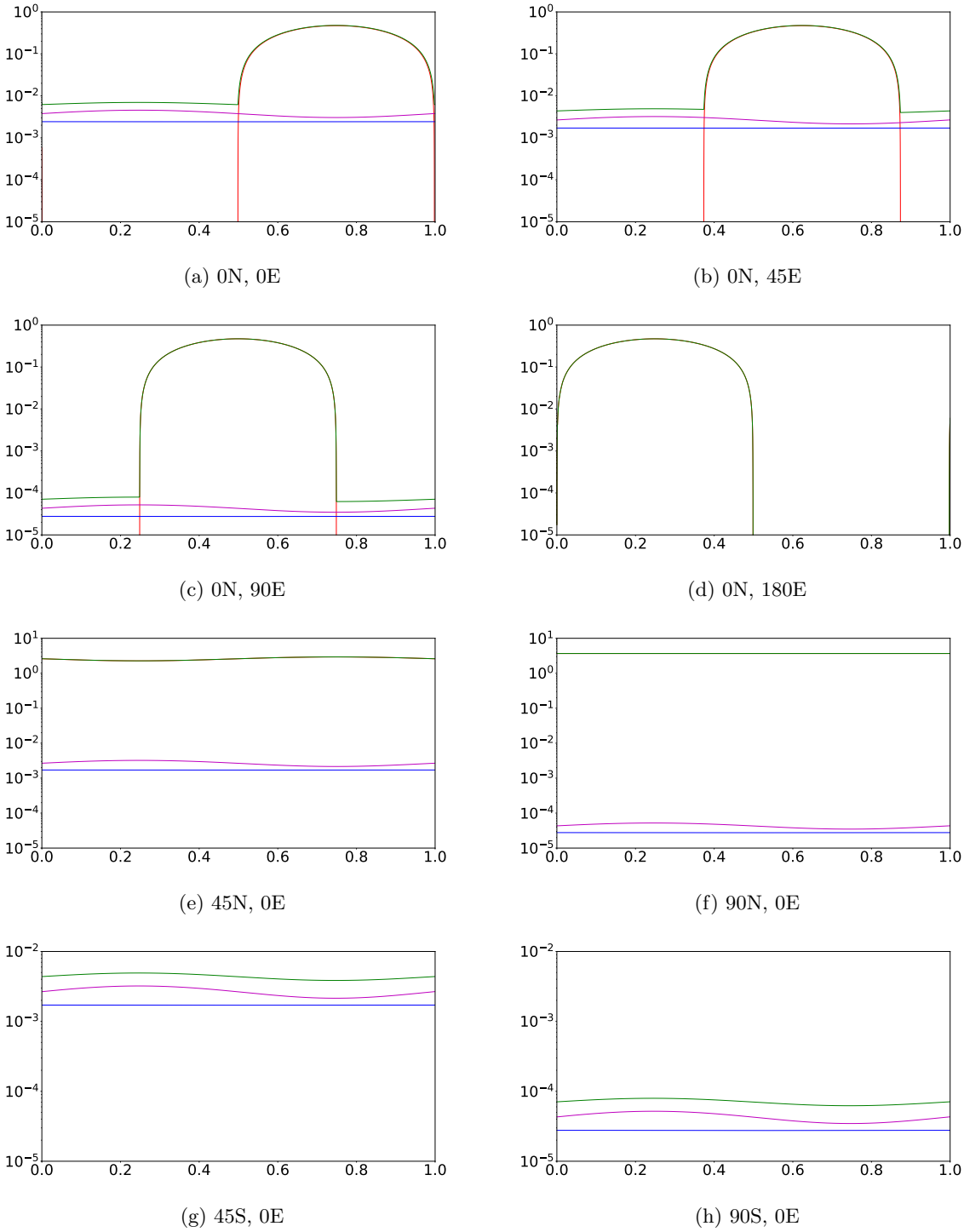

Figure 7: As Figure 6, but for Titania during northern summer solstice. The x-axis shows time in Titanian days (i.e. orbits around Uranus); the y-axis shows illumination in W/m^2. Curve colours have the same meaning as in Figure 6. Here, there *is* a striking asymmetry between the northern and southern hemispheres, owing to Uranus' extreme axial tilt. No light reaches Titania's south pole; conversely, only sunlight strikes its north pole. Note also the complete lack of eclipsing by Uranus, which only happens during equinoxes. Note also that in panel *d*, the planetary contributions are too weak to show at this scale, so the stellar contribution appears to overlap with the total illumination. Similarly, in panels *e* and *f*, the stellar contribution is so dominant it again appears to overlap with the total illumination.

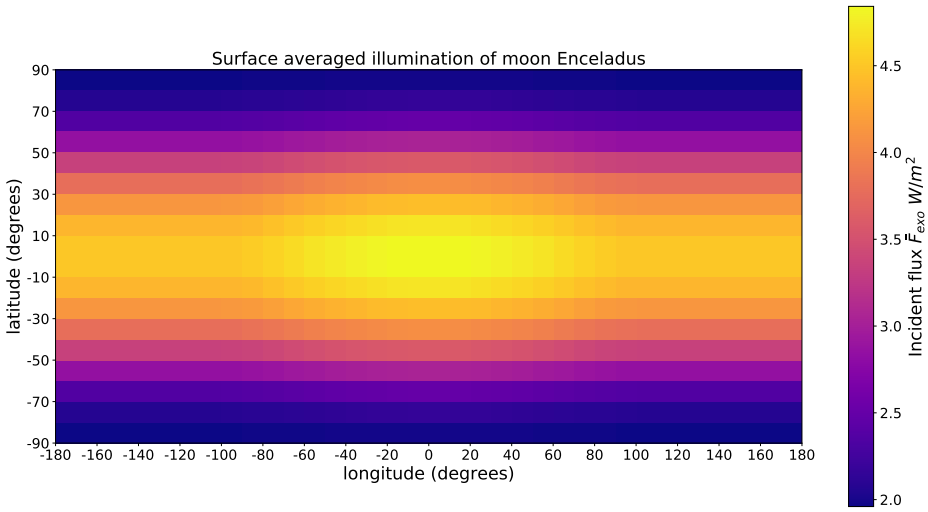

Figure 8: The yearly averaged surface illumination map for Enceladus. Note the planetary thermal/reflected flux bump on top of the solar pattern at the subplanetary point (at 0,0).

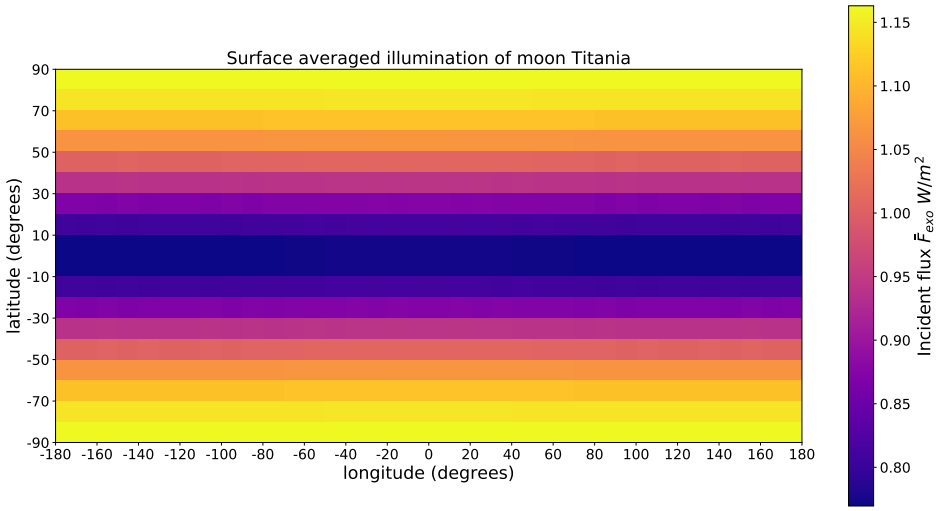

Figure 9: The yearly averaged surface illumination map for Titania. The planetary thermal/reflected flux bump at the subplanetary point (at 0,0) is invisible due to Uranus' extremely low thermal output; the stellar illumination is concentrated on the poles. This is caused by Uranus' extreme axial tilt, rendering both Uranian and Titanian days at the poles a full Uranian year long.

0 longitude.

From these illumination curves we computed yearly averaged surface illumination maps: see Figures 8 and 9. Note, in both cases, the planetary thermal/reflected flux bump at their respective subplanetary points – a consequence of their tidal locking. In both fiducial cases, the stellar illumination on average does not exceed 5 W/m^2: for Enceladus, it at any time reaches at most around 15 W/m^2; for Titania, around 3 W/m^2. Compared to Earth's solar flux at the top of the atmosphere ($\sim$400 W/m^2 on average around the equator, $\sim$1400 W/m^2 at most at any given time), the influence of exogenic heating on exomoon surface conditions is small, and thus we expect its influence on the moon's internal state to be small as well.

While close-in moons are regularly eclipsed by their host planet, already for Enceladus, despite being close enough to Saturn to be eclipsed frequently, we do not register an expected decrease in received flux to the subplanetary point: this is due to Saturn's own axial tilt (26.73 degrees), and as its moons' orbital plane is tilted likewise, Enceladus is lifted out of Saturn's shadow for most of the year. This situation is found more extremely on Titania, where Uranus' extreme axial tilt (97.77 degrees) alternatingly puts one hemisphere of the moon in sunlight for half a Uranian year. During a single orbit of Titania around Uranus at either solstice, one hemisphere is constantly in sunlight; conversely, during the equinoxes, any point on the equator is illuminated for only half a Titanian orbit, and experiences peak illumination only briefly. Hence, the average stellar illumination is not evenly distributed across its surface, instead being concentrated around the poles.

We did not map Rhea and Oberon since, as they are the same distance from the sun and in the same orbital plane as their siblings, their surface illumination patterns would look nearly identical: the primary difference would be the planetary thermal/reflected flux bump at the subplanetary point. For both Rhea and Oberon, it is expected to be lower due to their larger semi-major axes. Note that these maps show the *incident* flux to the moons' surfaces, not the *absorbed* flux: this can be up to half a order of magnitude lower, owing to high surface albedo (of Enceladus and Rhea; Titania and Oberon's dark surfaces absorb about 80% of incoming radiation).

Additionally, we created time lapses which show the tracking of stellar illumination across the moons' surfaces over the course of a planetary year, as well as over the course of a single day at equinox (Enceladus) and at northern summer solstice (Titania). Finally, we produced a time-zoomed lapse of Enceladus emerging from Saturn's eclipse. All lapses can be found on `www.astro.rug.nl/~tjoa/science.php`. Note that in our lapses, the flux at the fringe of the stellar illumination bump seems to vary; this is an artifact of the finite resolution of our algorithm. Also, in all cases, *t0* indicates the starting moment of the simulation: for Enceladus this is the exact moment of the equinox, in Saturn's shadow; for Titania's year lapse it is also the equinox, in Uranus' shadow; and for its day lapse, it is the northern summer solstice (though due to Uranus' extreme axial tilt, i.e. flipped on its side, the exact orientation of Titania relative to Uranus at that moment hardly matters).

4.2 Tidal heating

Figures 10 and 11 show the tidal quality factor versus the dissipated tidal heat for 5 different rigidities for Enceladus and Io, the two most studied cases of tidal heating within our Solar System. We varied the Q factor from 1 to 1000 (a range containing all terrestrial worlds with determined tidal factors); rigidity μ was varied from 100 MPa to 10 GPa for Enceladus, and from 1 to 100 GPa for Io. Based on the trend of Equation 26 we predicted a Q value of Enceladus around 2, and based on its internal structure a rigidity around 1, corresponding to porous, partially molten icy material: Figure 10 shows that this assumption is reasonable.

Conversely, for Io we predicted a Q of around 40, and a rigidity of about 5 (based on Henning et al. (2009)): however, in Figure 11 we observe a marked departure from our assumptions. If we assume the Q value to be correct, the rigidity must be lower than expected ($<$ 1 GPa); if we assume μ to hold, the Q-mass trend described by Equation 26 must be violated and Io's Q must be between 10 and 20. Possible reasons for this discrepancy will be discussed in Chapter 5.

4.3 Melting depths

Figures 12, 13, 14 and 15 show the melting depth plot grids for Enceladus, Rhea, Titania and Oberon respectively in terms of their radii. All parameters have been plotted logarithmically. To reiterate, the

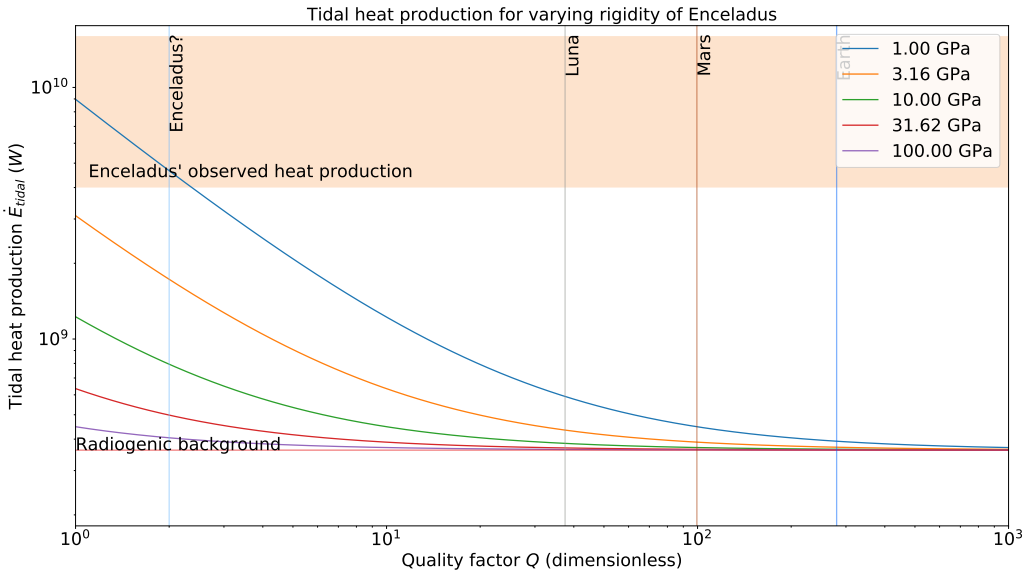

Figure 10: Different tidal heating models for Enceladus: Q and μ are varied and compared to the observed tidal output. Note the radiogenic background, which is over an order of magnitude lower than the observed heat production.

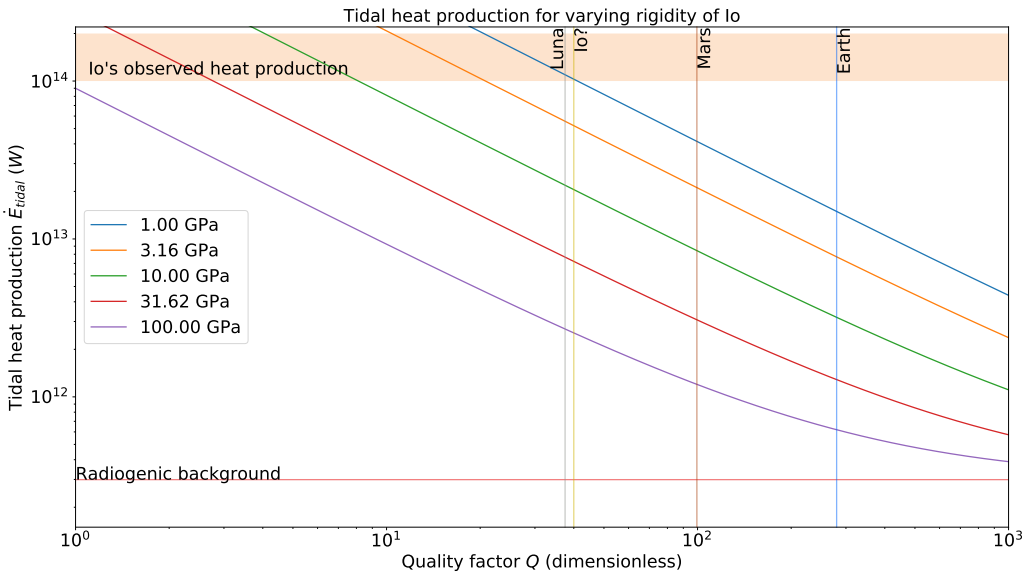

Figure 11: As Figure 10, but for the case of Io. Note the marked disagreement between our anticipated Q value (~ 40) and rigidity (~ 5 GPa): at least one of our assumptions must be flawed to match observations.

parameter ranges in all plots are:

- $10^{-2}L_{\odot} \leq L_{*} \leq 10^{2}L_{\odot}$;
- $10^{25}kg \leq M_p \leq 10^{28}$ kg;
- $1AU \leq a_p \leq 10^2$ AU;
- $10^{19}kg \leq M_c \leq 10^{22}$ kg;
- $10^{8}m \leq a_c \leq 10^{9}$ m;
- $10^{-4} \leq e_c \leq 10^{-1}$;
- $1m \leq D_{rego} \leq 10^2$ m.

Justification for these ranges can be found in section 3.4.2. The gradient region indicates the regime where an ocean might exist between 100 m and 30% of the moon's radius. Red regions indicate the surface temperature is above the ice sublimation temperature (i.e. 150 K); dark grey regions indicate a melting depth greater than $0.3R_c$; and light grey regions indicate a melting depth less than 100 m, or where the temperature underneath the regolith cover is above the melting temperature. Note that for the Uranian moons, the red regions extend notably further out from their host star: while Titania and Oberon are as icy as Rhea and Enceladus, their surfaces are covered in dark regolith ($\alpha_{Titania} = 0.17$, $\alpha_{Oberon} = 0.14$) which absorbs the exogenic flux more effectively than Enceladus' and Rhea's ice/snow cover. We will now discuss each fiducial moon separately.

In agreement with the current understanding of Enceladus' internal structure Nimmo et al. (2018), our model predicts a subsurface ocean to be present 3.6 km below the crust. Additionally, from those plots with the host semi-major axis, we may deduce that irrespective of solar illumination, if its other parameters remain fixed, Enceladus could maintain a subsurface ocean at any distance from its host star. This is presumably the result of tidal heating by Saturn. It must be noted that firstly, our model assumes a radially symmetric moon, and secondly, it does not take into account cryovolcanic activity: it is purely conductive. Current models of Enceladus invoke an asymmetric structure, where the south polar crust is considerably thinner (as thin as 2 km vs ∼25 km for the rest of the moon, see Glein et al. (2018)). Additionally, cryovolcanism has been detected on the south pole as well (Nimmo et al., 2018). We will further compare our results with literature findings in Chapter 5.

Conversely, Rhea, despite its size, seems unable to maintain an ocean above 30% of its radius. As it receives the same solar flux as Enceladus (thermal and reflective planetary contributions are small), its lack of ocean is presumably due to weaker tidal forces from Saturn. It is either not massive enough, not close enough to Saturn or not eccentric enough to maintain sufficient levels of internal heat.

The Uranian moons respond more intensely to exogenic heating due to their dark surfaces: were Uranus closer than ∼4 AU to the Sun, their ice crusts would sublimate. They are able to sustain oceans, though, albeit at considerably greater depth than Enceladus' – below 150 km, or over 20% of their radii. Additionally, we see that there is no upper limit to their semi-major axes, nor a lower limit on their eccentricities: Titania and Oberon would be able to maintain their oceans regardless, presumably owing to their high mass, thick crusts, dark surfaces and high ammonia fractions, which reduces the melting temperature of ice by several tens of K. Since Titania and Oberon show no lower limit on eccentricity, this indicates radiogenic and/or formation heat alone may be sufficient to sustain their subsurface oceans.

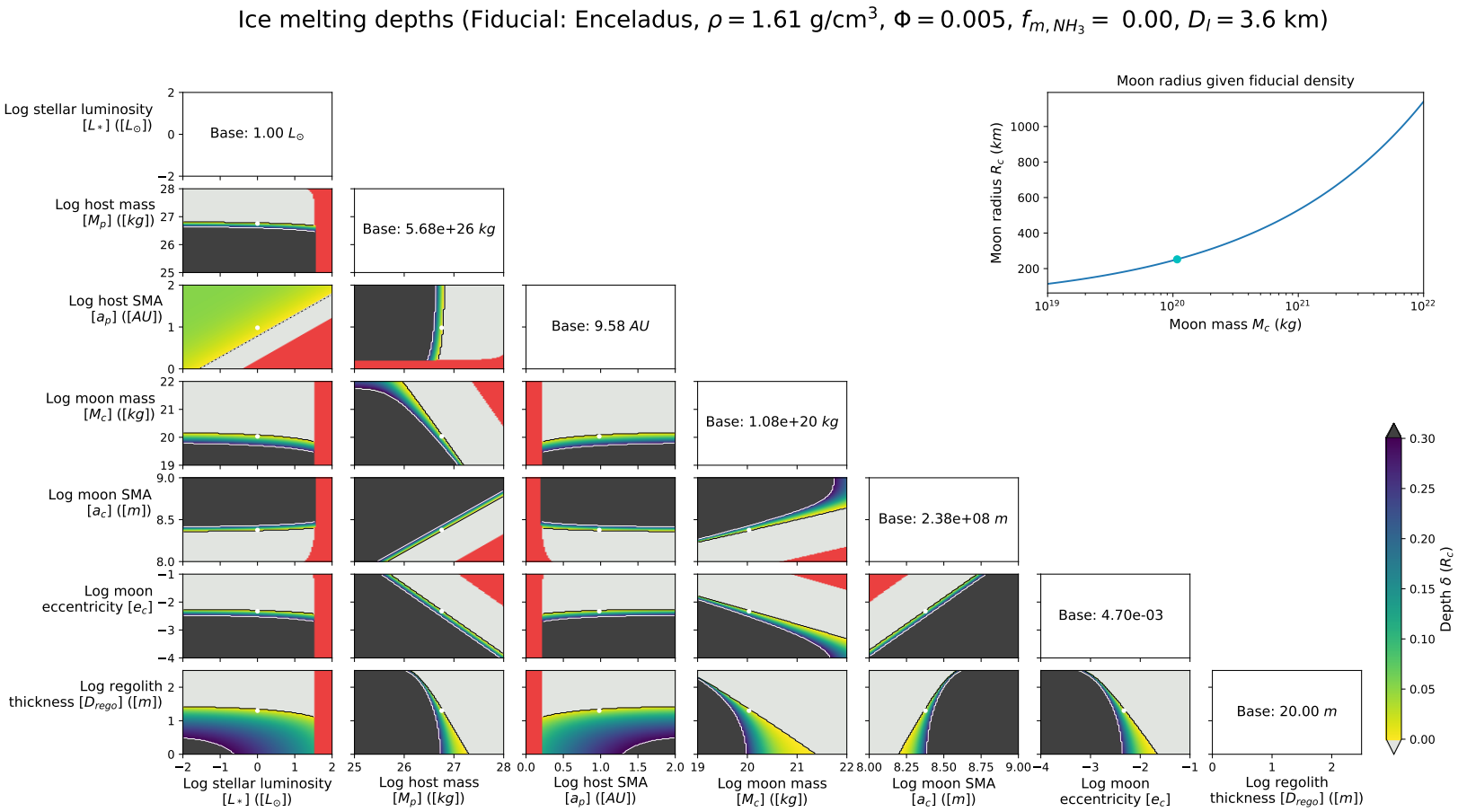

Figure 12: Melting depth parameter grid for Enceladus.

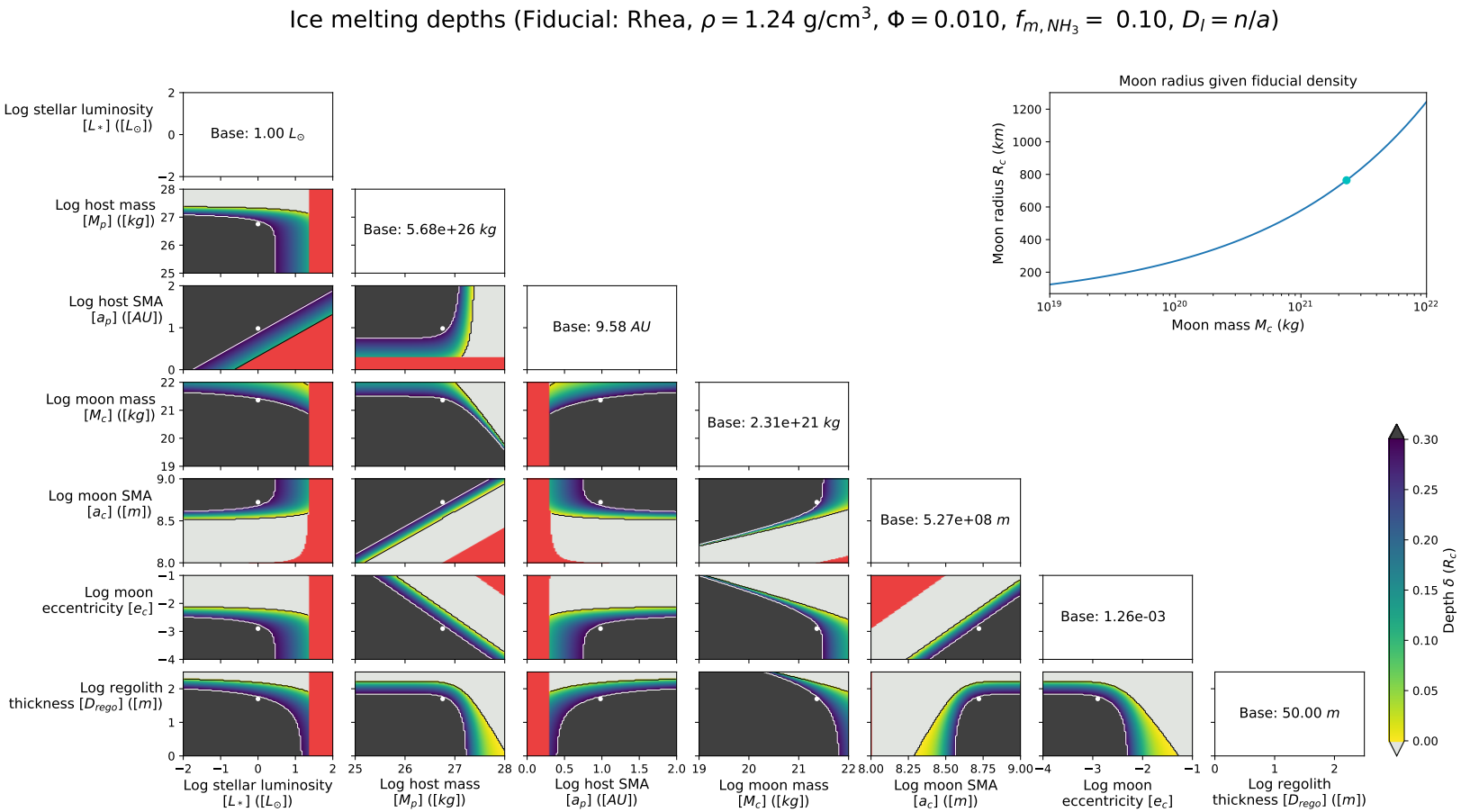

Figure 13: As previous figure, but for Rhea.

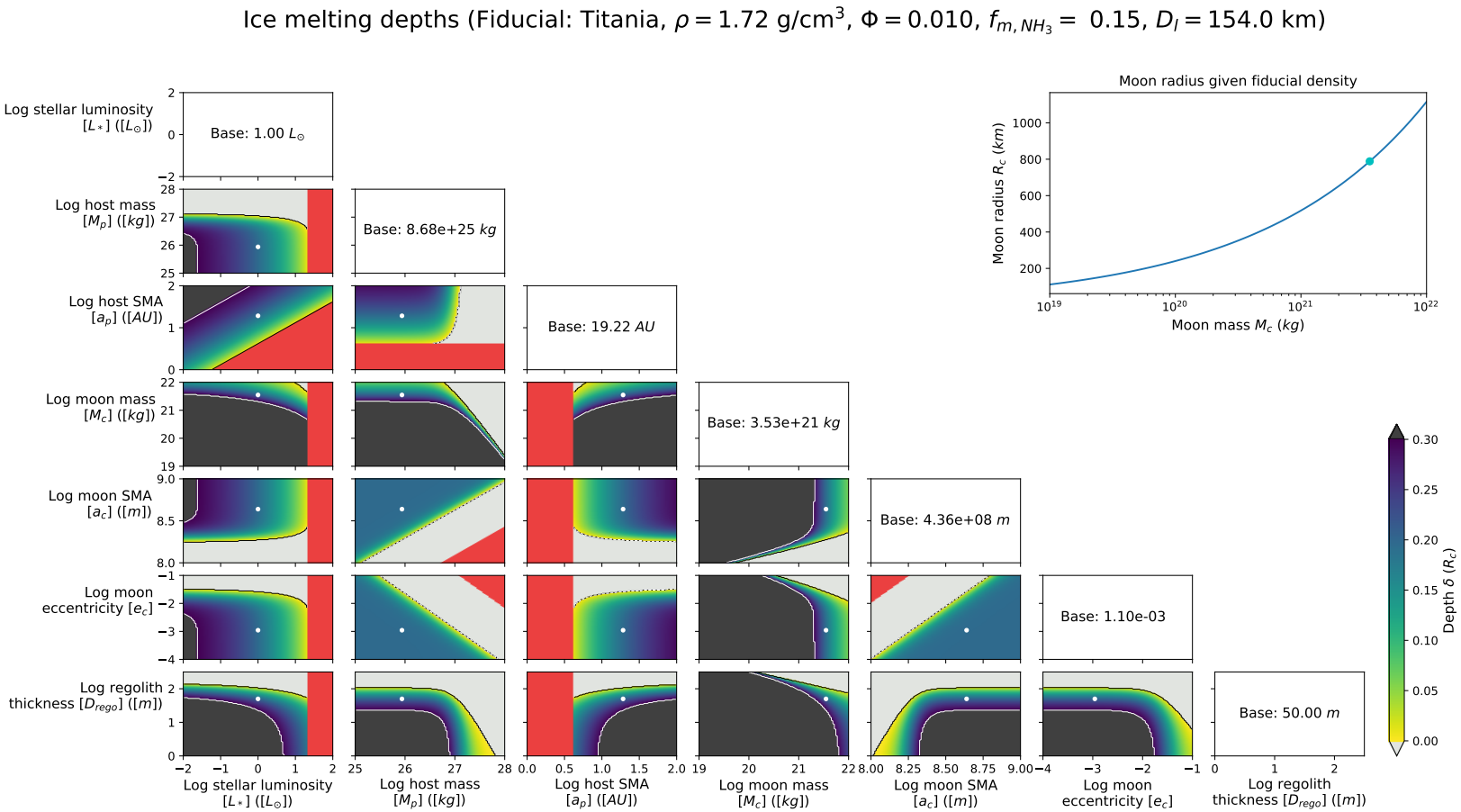

Figure 14: As previous figure, but for Titania.

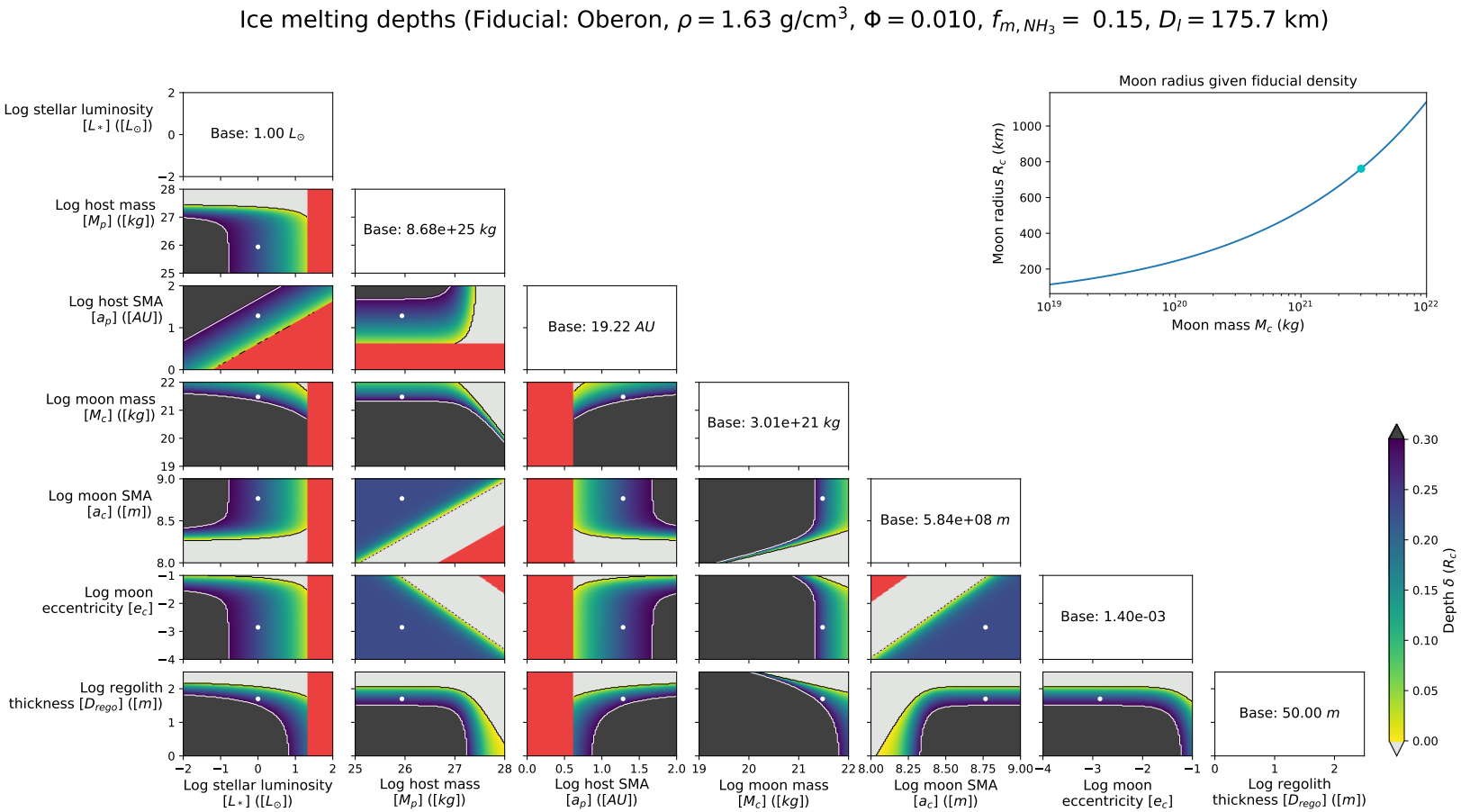

Figure 15: As previous figure, but for Oberon.

5 Discussion

5.1 Plausibility

5.1.1 Exogenic heating

Our exogenic heating results are similar to Heller and Barnes (2013). Since we used their equations to determine the surface averaged illumination maps, this is unsurprising; however, whereas they assume a temperature difference between the day and night sides of up to 100 K, we propose an isothermal planet, justified by giant planets' rapid rotation and atmospheric heat circulation. Though this does not strongly influence our results – planetary thermal emission is consistently the weakest component of the illumination budget – it could significantly affect surface illumination at large semi-major axis, where stellar illumination is comparable with planetary thermal emission generated by the planet's internal processes. Regardless, we find similar illumination patterns to Heller and Barnes (2013).

5.1.2 Endogenic heating

The results produced by our analysis of endogenic heating on Enceladus agree with our hypothesised values. Based on the mass trend deduced from the data of Lainey (2016) (Equation 26), we predicted a Q around 2 for Enceladus for a rigidity around 1 GPa, matching our results (Figure 10). However, Porco et al. (2006) assume a Q of 20 for Enceladus, an order of magnitude beyond our assumption. Meyer and Wisdom (2007) expand on this, studying the eccentricity evolution of Enceladus and its mean motion resonance with Dione for a given Q value. They find that for $Q = 100$, Enceladus' eccentricity equilibrium state approaches its current value, meaning that the resonance's evolution is complete; for $Q = 20$, the equilibrium eccentricity for Enceladus in its mean motion resonance with Dione is 0.014, implying that it is still evolving deeper into the resonance. Since we assumed $Q = 2$, it is likely that our Enceladus would continue to evolve far deeper into resonance, potentially desiccating it in due time. The discrepancy between our prediction for Q and theirs is due to different methods: they draw their value from orbital evolution, while we do so from an empirical mass trend. Since Lainey (2016) themselves do not point it out as significant either, our assumption that this trend is in any way meaningful might be flawed – as pointed out previously, Q-values for Earth vary widely and thus this trend is by no means definitive.

A higher Q means a lower tidal efficiency factor Φ and thus less tidal heating; hence, if Enceladus' Q is indeed larger and no other parameters change, it is more likely to be frozen. However, since Enceladus' Φ was observationally constrained to $0.0026 \leq \Phi_c \leq 0.0127$ by Nimmo et al. (2018), if Q were to be larger, k_2 and thus the rigidity μ would have to change to maintain the same Φ.

5.1.3 Melting depth model

Conversely, our melting models agree with literature: Enceladus is indeed thought to sustain a subsurface ocean, at a depth anywhere between 10 and 30 km (Nimmo et al., 2018). Our estimate is optimistic at 3.6 km, but it must be pointed out that our model is purely conductive: we did not consider the effects of cryovolcanism. Active volcanism on Enceladus may serve as an additional pathway to release excess internal heat, thus lowering the overall internal temperature and leading to a thicker ice crust.

A paradox emerges, though, when one compares the melting model results for Enceladus with its near twin Mimas. Both moons are close to Saturn; in mean motion resonance with a more massive companion; of low mass and radius; and, judging by their densities, composed almost entirely of water ice. Yet, for reasons not well understood, Mimas is a geologically dead body, while Enceladus is active. Running our melting depth model on Mimas yields the same result: Figure 16 clearly shows that Mimas' ices should have long molten and escaped into space. That they have not poses a problem, but solving this paradox is beyond the scope of this thesis. A possible resolution is explored by Czechowski (2004), who posits that Enceladus and Mimas are in different tidal states, with Enceladus occupying the excited level, and Mimas the basic, low-energy state.

Titania and Oberon are both not known to be active, but in their cases our overall knowledge regarding possible subsurface oceans is very limited. Hussmann et al. (2006) studied subsurface oceans in the outer Solar System: they found ice shell thicknesses well in excess of 200 km. It is important to note that their approach assumed the thermal conductivity of ice assumes a single, fixed value: 3.3 W/mK. However, the

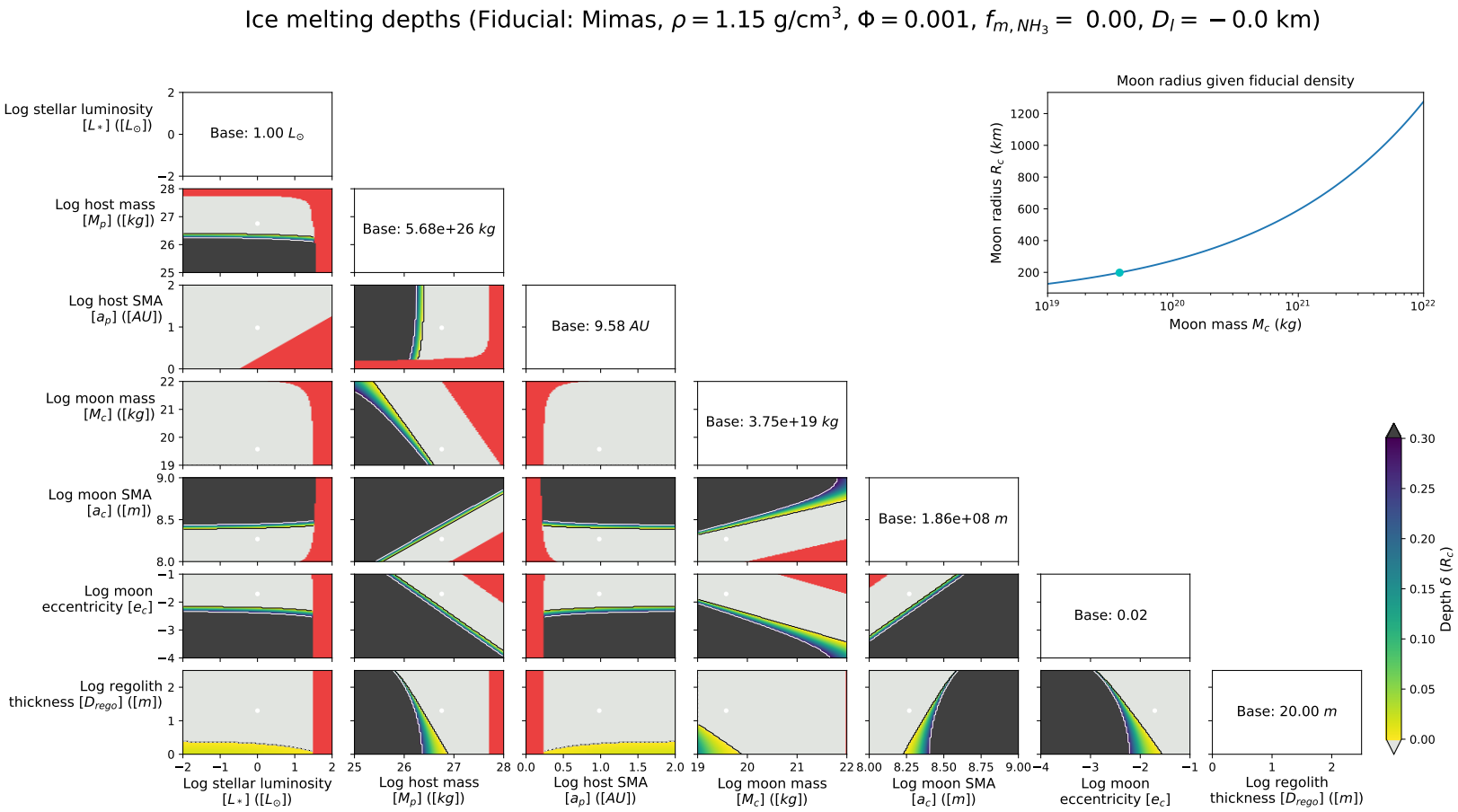

Figure 16: Melting depths parameter grid for Mimas. Note the fact that according to our model, Mimas should long have molten.

conductivity of ice is known to change with temperature (Andersson and Inaba, 2005); we implemented this gradient throughout the ice shells. k then goes as high as 10 W/mK around 75 K (approximate surface temperature at Saturn's SMA), which could well explain the discrepancy between our results and Hussmann et al. (2006). It is also critical to note that they assumed lower ammonia mixing ratios than we did, both in Rhea as in Oberon and Titania: our optimistic fractions of 10-15% contrast starkly with their 0.5 to 5%, contributing to our thinner ice crust. Strangely, however, their result for Rhea is considerably more positive than is ours: they predict an ocean at 400 km depth, while our Rhea remained solid. Reevaluation of the Rhea system with different ammonia fractions, tidal efficiency factors and regolith thickness might result in different predictions. In future studies these three unknowns should be well considered, since they can drastically alter results: we elected conservative values for Φ and D_{rego}, but it is well possible to melt or freeze one's otherwise habitable moon by tweaking these parameters (see Figure 17 for a desiccated Rhea, and Figure 18 for a frozen Enceladus).

Regardless of our differences with Hussmann et al. (2006) and Nimmo et al. (2018), our melting depth results are not inherently unreasonable. They may be better constrained by additional study of the tidal and surface conditions of our fiducial moons. It may also be beneficial to future research if the thermal behaviour of ice under vacuum conditions is studied more extensively, and if the ammonia fraction of outer Solar System icy moons is thoroughly mapped.

5.2 Effect of eclipses

Forgan and Yotov (2014) and Forgan and Dobos (2016) found that repeated eclipses may harm an exomoon's habitability by detracting from the moon's surface illumination. This (up to 8%) flux drop per orbit could drive the moon into a snowball state from which it cannot easily escape. However, our research indicates that this possibly detrimental effect may be averted by the introduction of an inclination to the moon's orbit. Enceladus, while relatively close to Saturn ($\sim 4R_{Sat}$), does not show a lack of illumination to its subplanetary point. Since its orbital plane is inclined relative to Saturn's own orbit around the Sun, except for brief periods around the equinoxes, it is lifted out of Saturn's shadow more often than not. A similar process occurs for Titania, which is raised even more dramatically from Uranus' shadow. A quick inspection of the timelapse of a single Enceladean day at equinox (hosted on `www.astro.rug.nl/~tjoa/science.php`) shows that – in situations where inclination does not affect a moon's ability to escape its host planet's shadow – eclipses may still occur and occlude the sun for well over an hour a day, but this would only occur for brief periods twice a year.

It should be noted that Forgan and Dobos (2016) were interested in eclipses' effects on *surface* habitability, and sought to remedy their effects by introducing the carbonate-silicate cycle. While this indeed may serve as a counter to eclipses putting moons in snowball states, the problem ceases to exist when an icy moon is what one is looking for. Since this thesis aims at *subsurface* habitability, it is unimportant whether or not the surface is covered by a kilometers thick ice shelf – what matters is whether internal conditions allow for a subsurface ocean. Exogenic fluxes to our Solar System's icy moons are low when compared to Earth's, and from our melting depth models for particularly the Uranian moons, it follows that stellar illumination is hardly a prerequisite to creating subsurface habitable conditions. Hence, we conclude that while eclipses may affect surface habitability conditions, they are not a primary concern for subsurface habitability.

5.3 Importance of endogenic heating

All four fiducial moons rely on some amount of endogenic heating to maintain their subsurface oceans. In Titania's and Oberon's cases, this is almost exclusively radiogenic and residual formation heat; Enceladus relies on tidal heating, while Rhea employs a combination of both. In all cases, the influence of exogenic heat is small (particularly on the Uranian satellites); stellar distance and thus flux are of small influence on the subsurface habitability of an icy moon beyond defining an inner limit (the snow line). This is critical, because it implies that subsurface oceans can be sustained regardless of distance to the star – in other words, the circumstellar subsurface habitable zone for moons may extend up to the very edge of the stellar system. This is a significant finding, since it greatly expands the circumstellar range where life-sustaining habitats may be found: if one only considers terrestrial planets as habitats, one's area of search is just the habitable zone, whereas if one includes icy moons (and, possibly, surface habitable terrestrial exomoons too), potentially habitable environments could be found all across an exoplanetary

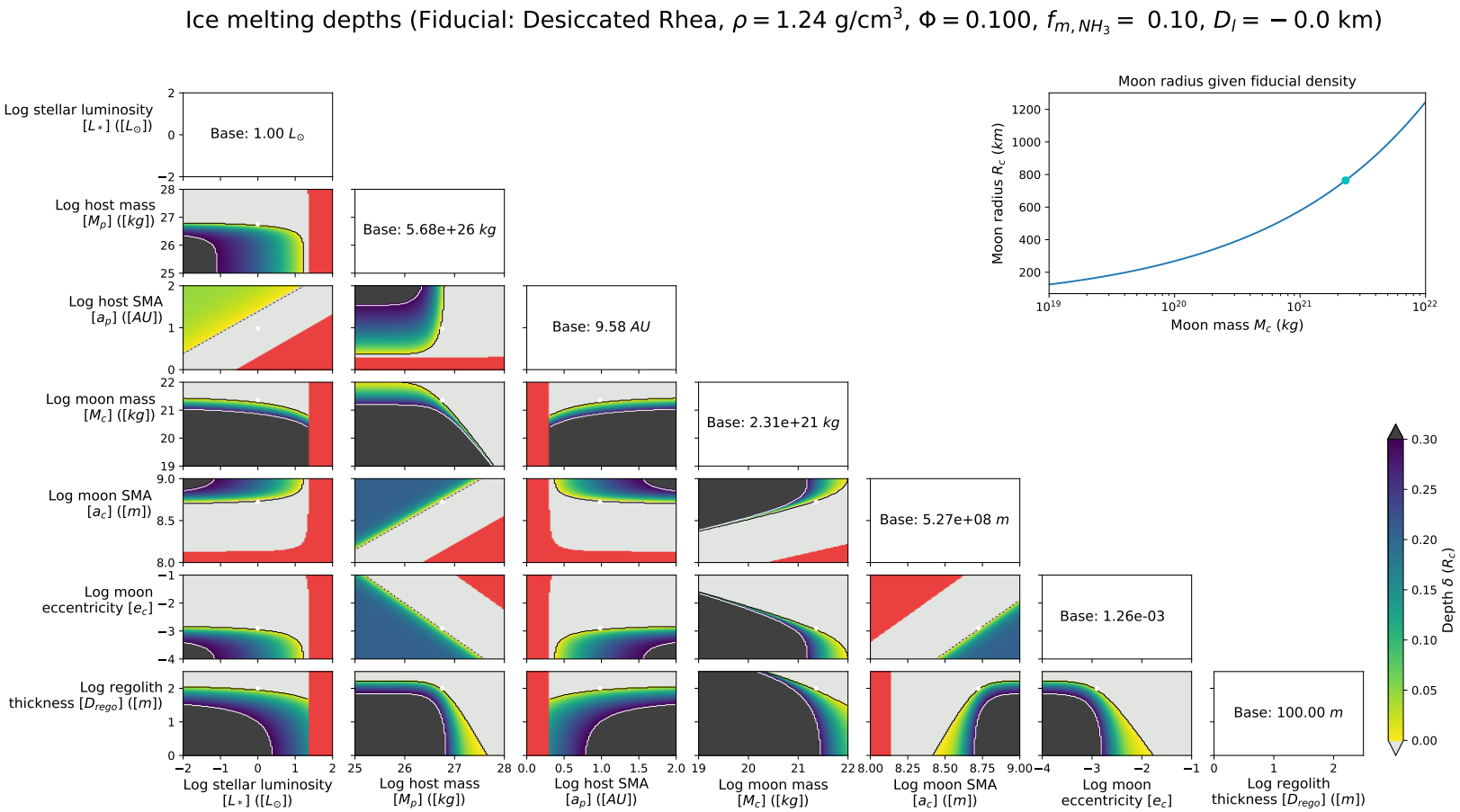

Figure 17: As Figure 16, but for a hypothetical desiccated Rhea. A tenfold increase of the tidal efficiency factor and a doubling of the regolith layer, while extreme and probably unphysical, can transform even frozen Rhea into a desiccated rock.

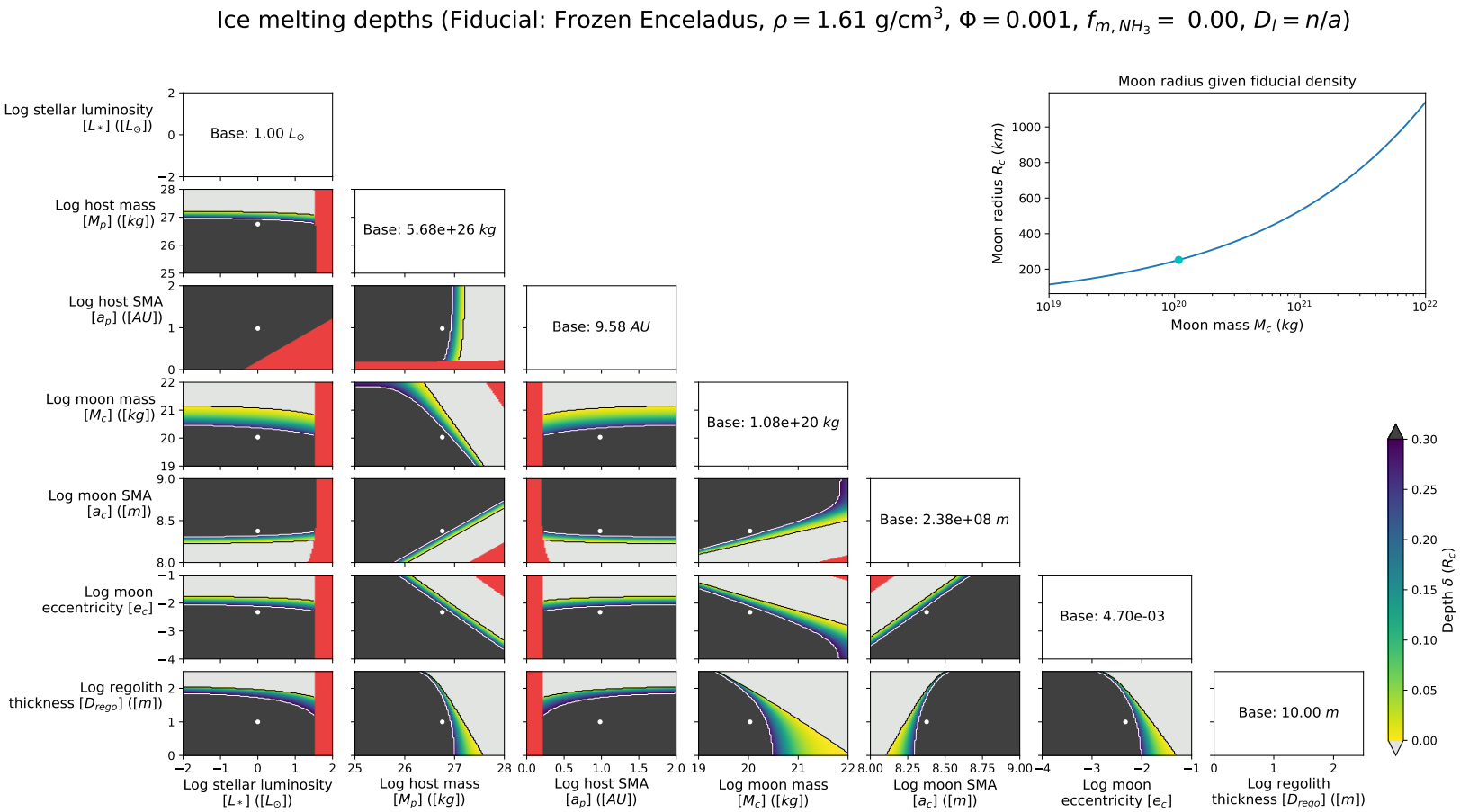

Figure 18: As Figure 16, but for a hypothetical frozen Enceladus. Dividing the tidal efficiency factor by 5 and halving the regolith blanket makes Enceladus cool dramatically, turning it into a solid ice ball.

system, and indeed our own Solar System as well.

Several notes must be made. Such an "indefinite" (in the sense that it is not limited within the stellar system itself) extent of the habitable zone assumes that the satellite under scrutiny has enough internal heat to sustain subsurface liquid water. Secondly, if the satellite is small (like Enceladus), tidal forces become the only viable source of internal heat: any radiogenic heat will dissipate on relatively short timescales. Since internal heating scales with volume (so with R^3) and radiative cooling with surface area (so with R^2), halving the radius of a moon would leave its cooling reduced by a factor 4, but its heating by a factor 8. Thirdly, the moon habitable zoon is eventually truncated at large distance from the host star; not due to lack of internal heat, but due to lack of material to form planets and moons from. Lastly, while the circumstellar subsurface habitable zone may extend "indefinitely" *outward*, exogenic processes do define an *inward* bound, namely the point at which the induced surface temperature on the moon exceeds the sublimation point of water ice (around 150 K). In parallel to Heller and Barnes (2013), we could thus call the snow line a circumstellar subsurface habitable edge, although it also depends on the moon's albedo and the amount of light reflected and thermally radiated by the planet.

5.4 Circumplanetary habitable zone & tidal habitable "edge"

The circumplanetary habitable zone depends on more factors than the circumstellar habitable zone. At least seven factors strongly influence whether a moon can be subsurface habitable; however, the melting depth in total depends on seventeen more or less free parameters. As discussed in section 5.1, the tidal efficiency factor, ammonia mass fraction and regolith thickness present three major unknowns which are all poorly constrained. Regardless, there are some limits we can impose on the circumplanetary habitable zone.

Firstly, there are dynamical constraints. Both the Roche limit (generally at $\sim 2.5R_p$) and Hill sphere (at distance R_H) limit exomoon orbits, although truly dynamically stable orbits cannot exceed $0.5R_H$. For the Roche limit, we mean the liquid Roche limit, since moons are large enough to be treated as deformable objects under the regime of hydrodynamics (Dobos et al., 2017); all major icy moons of the Solar System orbit well beyond that. However, the tidal habitable edge forms another inner limit: this is the closest orbit a moon can be on without undergoing such tidal heating that it turns into a runaway greenhouse, and eventually an Io-analogue (see section 1.2 for a more extensive description of the difference between the circumstellar habitable zone and the circumplanetary habitable edge, and also Heller and Barnes (2013) and Forgan and Dobos (2016) for in-depth analyses). While it is often stated in terms of only moon semi-major axis, our melting depth plot grids show that the habitable edge (the black lines in Figures 12 to 18) is described by more parameters than just that. The moon's eccentricity, mass, density, regolith cover, tidal efficiency factor and ammonia fraction all influence where this edge is located in terms of planetary radii.

However, it must be pointed out that the habitable edge was described for surface habitability. In our subsurface case, a habitable edge still exists, but ours does not need to be in agreement with literature seeking to define the surface habitable edge. Since it is such a manifold condition, it may in our case be more prudent to speak not of a habitable edge, but of a maximum melting criterion: a maximum amount of internal melting allowed before we consider the moon desiccated. Per our model, we find this criterion is satisfied whenever the melting depth as computed by Equation 32 is larger than 100 m + D_{rego}:

$$R_c - \left[4\pi \dot{E}_{endo}^{-1} \left(K(T_l) - K(T_{rego})\right) + \left(R_c - D_{rego}\right)^{-1}\right]^{-1} \geq 100 + D_{rego} \tag{35}$$

wherein all symbols take the meanings listed in Table 2. This 100 m limit imposed on the ice crust's thickness is fairly arbitrary, but the equation's form is a direct consequence of our model setup, so its shape does not change regardless of where its boundaries are. Similarly, we can define an upper edge – a minimum melting criterion – by arbitrarily picking a fraction of the moon's radius consisting of ice, and thus meltable into an ocean. In our case of 30%, we then find:

$$R_c - \left[4\pi \dot{E}_{endo}^{-1} \left(K(T_l) - K(T_{rego})\right) + \left(R_c - D_{rego}\right)^{-1}\right]^{-1} \leq 0.3R_c \tag{36}$$

5.5 Habitability & long-term stability

As discussed in the previous section, the subsurface circumplanetary habitable zone can be limited by Equations 35 and 36. This only dictates the possibility of liquid water, and follows from a simplified approach (no cryovolcanism, no viscoelastic tides). We will now discuss other concerns regarding habitability.

5.5.1 Long-term stability of the environment

Perhaps the primary condition for the appearance of life is not liquid water, nor nutrients, but the long-term stability of the environment. The emergence of the first carbon-based life on Earth (prokaryotes – unicellular organisms without a membrane-bound nucleus, and some of the simplest organisms known) from a primordial, amino acid-soup required at least millions, at most half a billion years; similar timescales may be needed throughout the universe, regardless of biochemistry. It then took another two billion years of evolution for eukaryotes (organisms with a membrane-bound nucleus and organelles – this includes all multicellular organisms) to appear; metazoan life (animals and other more complex lifeforms) only appeared 700 million years ago, and thus over 3 billion years since abiogenesis (Schwieterman et al. (2019); regardless, today most life on Earth is still in prokaryotes, i.e. Bacteria and Archaea). It is worth noting that while Earth did have an atmosphere 3.8 billion years ago (around the time of the first prokaryotes), it was markedly different from today: it contained no molecular oxygen, which appeared only after the great oxygenation event around 2.3-2 billion years ago (Schidlowski, 2001; Holland, 2002), around the appearance of the first eukaryotes. Still, that leaves a window of almost 2 billion years of relative environmental stability for life to emerge and take its first steps up the evolutionary ladder.

However, on small, icy exomoons, in the absence of an atmosphere and without strong insolation as a primary source of heat, the environment may be subject to change on timescales of millions rather than billions of years. Expecting tidal heating to supply the heat required to keep the ocean liquid is risky: the amount of tidal heat produced is coupled to the moon's orbital characteristics, and those may evolve over time. Driscoll and Barnes (2015) studied the tidal evolution of planetary orbits in M dwarf systems – which are essentially upscaled versions of the Jovian system – and found that the closer in a planet orbits, independent of initial eccentricity, the sooner will their orbits circularize. For a planet with a 0.01 AU semi-major axis (approximately the semi-major axis of Titan around Saturn), an orbit with an initial eccentricity of 0.5 will, after intense tidal heat dissipation, circularize within 1 million years. In a satellite system without major exogenic heating contributions, once the orbit is circularized, tidal heating drops to zero and the moon is frozen solid. This can be remedied by artificially pumping the eccentricity through mean motion resonance – as happens for Io and Enceladus – but those too are not always stable: the moons of Uranus are thought to have been in multiple resonances, but are no longer (Tittemore and Wisdom, 1990).

In summary, tidal heating is *not* a stable source of heat per se, and in absence of its contribution, at least small moons like Enceladus would be unable to maintain their internal ocean (see Figure 12; near zero eccentricity, the moon freezes solid). Larger, more distant moons like Titania and Oberon are massive enough to maintain liquidity even at very small eccentricities (see the eccentricity plots in Figures 14 and 15), but their radiogenic background heating is also considerably higher; their considerable ammonia fractions, thick mantles and regolith blankets also aid to keep them warm. Adding to that the possibility that Enceladus and the other icy Saturnian moons formed as little as 100 Myr ago (Ćuk et al., 2016), we must conclude that while such environments could be habitable *now*, they need not be, or have been for long. It may therefore be prudent to distinguish between transient habitable worlds, which through tidal effects are only habitable for a geologically brief interlude, and permanently habitable worlds like Earth, which maintain that status on billion year timescales.

5.5.2 Ocean habitability

While we treat our subsurface oceans a priori as habitable, they need not necessarily be hospitable to Earth life or, for that matter, any carbon-based lifeform. While we raised the ammonia mass fraction of our moons up to 15%, this may render the ocean toxic to all but the most hardy of organisms. In the model constructed by Hammond et al. (2018), ammonia was found to concentrate in the subsurface ocean, so while the mass fraction of ammonia over the entire moon might be as low as 5%, it might reach up to 30% in the ocean itself (Hussmann et al., 2006). Ip et al. (2001) state that ammonia concentrations

as low as < 1 mg/L might already be toxic, which is far less than 30%. Perhaps locally evolved lifeforms possess a way of metabolizing ammonia, but to many Earthly life forms, Titania's ocean would not constitute a viable habitat.

While internal heat might keep the ocean liquid, the question remains how life forms would thrive in such an environment. There is no sunlight, rendering photosynthesis as we know it impossible. Perhaps hydrothermal vents provide a solution, spewing nutrients (minerals, acids) into the ocean as well as providing a warm environment that might exacerbate biological and metabolic processes (warmer locales, in general, are more hospitable to microbial life than are colder environments). Similar environments are thought to have hosted the first life on Earth (Dodd et al., 2017), and are still host to a wide array of autotrophic organisms (Martin et al., 2008). Certainly on geologically active Enceladus, or any tidally heated exomoon, it is possible that autotrophic lifeforms could thrive underneath its ice shell, assuming the presence of hydrothermal vents (Taubner et al., 2018); and since Cassini detected molecular hydrogen in Enceladus' plumes, this strongly hints at their presence (Waite et al., 2017).

5.5.3 Implications for exomoons

Finally, we must reflect on what our models tell us about exomoons. Our fiducial moons are all Solar System moons, since we simply have no alternatives. However, our aim was to determine the habitability of exomoons under different environmental circumstances. We believe that our approach is general enough that it may be applied successfully to any set of fiducial values – our findings are snapshots of the full, seventeen-dimensional parameter space describing subsurface habitability within which any moon can be placed. We could continue sampling this space at arbitrary points to obtain a more complete picture; however, Equation 32 tells us what we need to know about how initial moon observables relate to the melting depth, and can be applied to both Solar System moons and exomoons alike. We therefore regard Equation 32 as the main result of this thesis: if, in the future, the properties of some exomoon become known, we can use Equation 32 to investigate whether that particular exomoon could sustain a subsurface ocean.

5.6 Model limitations

This work does not study long-term evolution of exomoon systems. Our models provide a momentary snapshot of an icy moon, but do not tell us much about its state in several million years, or several million years ago. Its eccentricity could change, it could move away from or towards its host planet (with profound effects on tidal heating, particularly if the maximum melting criterion is trespassed), or be destroyed entirely. This limits our ability to draw definitive conclusions regarding the habitability of such environments on anything but transient timescales. Such developments should be studied in further research.

Secondly, our fixed-Q approach to tidal heating is a simplified model which has in accuracy been superseded by viscoelastic models (section 2.6; see also Moore (2003), Henning et al. (2009), Dobos and Turner (2015)). While specifically the (still simplified) Maxwell model has found much literature use, more convoluted yet more accurate and detailed models exist (Andrade, Sundberg-Cooper – see Renaud and Henning (2018) for in depth treatments). Key to any viscoelastic treatment is that it models the reciprocal coupling between tidal heating and mantle conditions – i.e. how the mantle temperature changes as a function of tidal heat dissipated, and vice versa – thus allowing for a molten interior; not implementing this limited our model to moons small enough to maintain a uniform, non-molten interior. Viscoelastic tides would not strongly affect our predictions for heat dissipation in the regime of small moons like Enceladus, which lack a molten interior.

Thirdly, we are limited by our limited knowledge of several key ingredients of our melting depth model. For a detailed discussion, see sections 3.4 and 5.4; for more accurate predictions on what exomoons might look like, we must first properly determine the tidal coefficients of our fiducial moons (Q & μ) and determine how they scale with readily observable characteristics. In addition, it may be prudent to carry out studies into the regolith cover of icy moons, its thickness and composition.

Fourthly, we did not take into account the effects of asymmetrical structure and – though this applies only to geologically active exomoons – cryovolcanism. Both phenomena occur on Enceladus, with the icy envelope presumably shifted relative to its core (Nimmo et al., 2018), and active geysers on its south pole. These two phenomena may also influence each other: an asymmetric shell on a tidally active

exomoon may result in a crust so thin in certain regions that cryovolcanic activity there follows. This cryvolcanic activity, dependent on its intensity, may then considerably alter the outgoing energy balance of the exomoon, letting a relatively larger fraction of heat escape through highly efficient convection, rather than slow conduction through the crust. This may thicken the crust in turn, perhaps precipitating a cycle between geological activity and stagnancy, but such processes are beyond the scope of this thesis: our model is purely conductive. In a private discussion on June 20th, 2019, T. Steinke and M. Rovira Navarro from TU Delft indicated that up to 90% of Io's internal heat may be dissipated via volcanic processes; while Enceladus has far less internal heating than Io, the amount of heat lost via convection may thus still be appreciable and should be considered in future approaches.

Fifthly, this work does not consider tidal heat dissipation in the moon's ocean or ice crust. We assume all tidal heat to be dissipated in the (rocky/porous) core and mantle – from where it is first convected by the ocean and then conducted by the crust towards the surface – while this is not necessarily the case. Appreciable amounts of tidal heat can still be dissipated in the ocean; Tyler (2009) states that Enceladus' entire excess heat flux may be explained by tidal dissipation in its ocean alone, rather than its core. For moons with a thick ice crust, like Oberon and Titania, tidal heat dissipated in the crust may also play a role.

Finally, due to its setup, our model cannot be applied to hypothetical moons of moons. With the tentative detection of a Neptune-mass moon at Kepler-1625b (Kipping, 2009), questions quickly arose whether it could have satellites in turn (Kollmeier and Raymond, 2019); if Kepler-1625b I does exist, and if it *does* possess grandmoons, this thesis will unfortunately be unable to model them. While the existence of grandmoons might seem unlikely, it is not something we should rule out a priori. It might in the future provide an interesting new avenue of research – once we attain a firm understanding of exomoons, and their potential habitability, first.

6 Conclusions

6.1 Implications for subsurface oceans & exomoon habitability

The habitability of exomoons as we defined it (section 1.2) depends on whether liquid water can exist below the surface. Subsurface oceans analogous to what is believed to exist on Enceladus (and other Solar System moons) may thus provide a habitat for extraterrestrial life. We have found that beyond the snow line, these oceans may exist largely irrespective to distance from the host star, rendering the exomoon subsurface habitable zone arbitrarily large. Since (in our Solar System) there are more moons than planets, habitable planets may be vastly outnumbered by habitable moons. Moons have several heat sources planets lack, making them less dependent on stellar illumination: tides from their host planet – assuming the moon's eccentricity is nonzero, forced by for instance an orbital resonance with a fellow moon – may dissipate ample heat in a moon's interior to sustain a subsurface ocean (see sections 1.3 and 2.6 for detailed explanations of tidal heating).

We have studied under which conditions subsurface oceans can exist. To this end, assuming conductive heat transfer through the moon's ice shell only, we derived an analytic expression for the melting depth – Equation 32 – which is dependent on seventeen physical and orbital parameters. Prime among these are the moon's mass, semi-major axis, orbital eccentricity, regolith cover, ammonia fraction and tidal efficiency factor; the planet's mass and semi-major axis; and the star's luminosity (see section 3.4.2 for the full list). This means that given some set of parameters for some hypothetical moon, we can now directly compute at what depth thermal conditions allow for liquid water.

Based on this expression, we developed criteria for where a subsurface ocean can exist (Equations 35 and 36). Using Enceladus and Rhea by Saturn, and Titania and Oberon by Uranus as fiducial models, we have explored the range of model parameters (see section 3.4.2 for these ranges). Figures 12 through 15 show that subsurface oceans only nominally rely on stellar illumination: our fiducial moons' melting depths vary little with distance from the Sun. More important is a source of internal heat, which serves to keep the ocean liquid, and may be tidally induced or radiogenic.

Given a sufficiently thick regolith blanket and a high tidal efficiency factor, it is possible to maintain a subsurface ocean at arbitrary far distances from the host star – see for instance Titania (Figure 14) and Oberon (Figure 15), which are at around 30 AU from the Sun yet still maintain subsurface oceans. With their dark surfaces, Titania and Oberon radiate only small amounts of heat and may retain their internal energy on large timescales; Enceladus and Rhea both receive tidal heat from Saturn. Despite this, Rhea is frozen, yet if we change the (poorly constrained) tidal efficiency factor appropriately, it may sustain a subsurface ocean as well or even be fully desiccated – see Figure 17. An ammonia mass fraction of several percents also contributes by lowering the melting point of ice, but may end up rendering the ocean saturated with ammonia and thus toxic to most known life. We must note that our models provide only a snapshot of exomoons at a certain point in time: in no way can we claim that exomoons may retain such habitable environments forever.

Since exogenic heating processes contribute only little, eclipses by the host planet, even when frequent, do not present a fundamental threat to subsurface habitability. While the amount of flux lost in such eclipses may harm surface habitability conditions, as long as sufficient endogenic heat is supplied to the ocean, it will remain liquid.

This leads us to conclude that habitable exomoons (surface *and* subsurface) may be found scattered throughout exoplanetary systems. The circumstellar *subsurface* habitable zone for moons extends arbitrarily further out than that for planets, if the moon's physical characteristics do so allow. Hence, the primary limit on icy moon habitability is their growth from the preceding planetesimal disk. We should not find subsurface habitable moons closer to the star than the snow line: stellar illumination would render them desiccated through sublimation of the ice crust once they trespass this boundary. Hence, the snow line can be regarded as a circumstellar subsurface habitable edge. Like Heller and Barnes (2013), we also found a circumplanetary habitable "edge", although we believe (at least when it concerns subsurface habitability) it better classified as a maximum melting criterion (again, Equation 35), since it is dependent on multiple parameters. Regardless, we speculate that subsurface habitable exomoons may populate the parameter space from the least massive round moons (Mimas/Enceladus), to at least Titania, and probably well beyond.

6.2 Prospects

Future exomoon hunters may use Equation 32 to determine whether their newly discovered worlds are capable of sustaining a subsurface ocean. It can be improved upon by better study of ice thermal conductivity behaviour under vacuum circumstances; by better constraints on regolith thickness, composition and crustal ammonia mass fraction; by improved determination of tidal coefficients Q and μ and their coupling to observable qualities of exomoons, and viscoelastic modelling of their interiors; and by physical exploration of our fiducial moons, so that we may compare our predictions with empirical data. The author would like to express his hope that this research in some way contributes to finding the first exo-Enceladus.

Appendices

A Geometry

In the following treatment, S or the subscript $*$ denote *source* (i.e. the star), P denotes *parent* (the planet), C denotes *child* (the moon) and q stands for the arbitrary landing site on the moon's surface. Furthermore, the superscript $'$ indicates a (base) vector in the moon's frame; and finally, composite vectors (e.g. $\vec{CP}$) indicate the vector from the point described by the first letter to the point described by the second, i.e. $\vec{CP} = \vec{P} - \vec{C}$. If a second letter is omitted, we mean the vector from the rest frame's origin to that point. *Rebound* directly supplies us with the vectors $\vec{S}$, $\vec{P}$ and $\vec{C}$ and their associated velocities; all other vectors are computed using Python's numpy package.

A.1 Surface landing coordinates

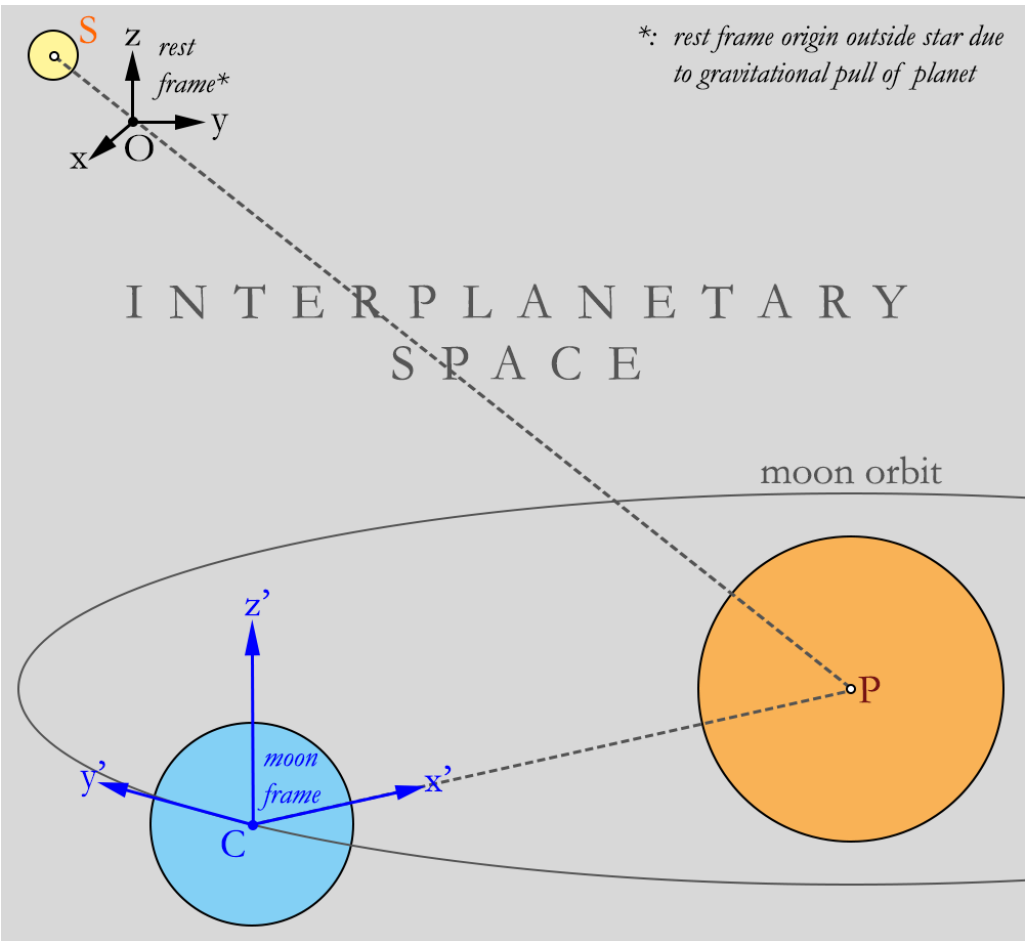

Figure 19: The geometry of our system, showing the static rest frame and the comoving moon frame.

To compute the illumination to a certain surface point, we require a moon-centric coordinate system. In our new moon system, we define its first base vector as

$$\hat{x}' = \frac{\vec{CP}}{|\vec{CP}|} \tag{37}$$

Since we assume our moon to be tidally locked to its host planet and the orbit to be close to circular (eccentricities typically do not exceed 0.01 for major Solar System moons), this assumption is sound: the

same point on the moon's surface will always have the host planet directly overhead, and $\vec{CP}$ will always (approximately, since libration and precession introduce a slight wobble) pass through this subplanetary point.

We want our second base vector to be perpendicular to the plane subtended by the moon's orbit around the planet. Such a vector can be constructed by taking the cross product of the moon's orbital velocity with $\hat{x}'$. We label it z since it is pointed out of the orbital plane. Hence, this means

$$\hat{z}' = \frac{\vec{v}_{C,orb} \times \hat{x}'}{|\vec{v}_{C,orb} \times \hat{x}'|}$$

wherein

$$\vec{v}_{C,orb} = \vec{v}_C - \vec{v}_P$$

And since the orbit is close to circular, the velocity will be close to perpendicular to $\hat{x}'$ (which has length unity), hence

$$\begin{aligned} \vec{v}_{C,orb} \times \hat{x}' &= |\vec{v}_{C,orb}||\hat{x}'| \cdot \sin\theta \cdot \hat{z}' \\ &\approx |\vec{v}_{C,orb}| \cdot \hat{z}' \end{aligned}$$

Therefore,

$$\hat{z}' \approx \frac{\vec{v}_{C,orb} \times \hat{x}'}{|\vec{v}_{C,orb}|} \tag{38}$$

The final base vector can then be constructed perpendicular to $\hat{x}'$ and $\hat{z}'$:

$$\hat{y}' = \hat{x}' \times \hat{z}' \tag{39}$$

To now find our landing coordinates given some longitude ϑ and latitude φ relative to the subplanetary point, we first compute the position of the subplanetary point r in the moon frame:

$$\vec{Cr} = R_C \cdot \hat{x}'$$

wherein R_C is the moon's radius, ignoring possible oblateness. We use a rotation matrix given by:

$$\bar{\mathbf{R}}_u(\alpha) = \begin{bmatrix} u_1^2(1-\cos\alpha)+\cos\alpha & u_1u_2(1-\cos\alpha)-u_3\sin\alpha) & u_1u_3(1-\cos\alpha)+u_2\sin\alpha) \\ u_2u_1(1-\cos\alpha)+u_3\sin\alpha) & u_2^2(1-\cos\alpha)+\cos\alpha & u_2u_3(1-\cos\alpha)-u_1\sin\alpha) \\ u_3u_1(1-\cos\alpha)-u_2\sin\alpha) & u_3u_2(1-\cos\alpha)+u_1\sin\alpha) & u_3^2(1-\cos\alpha)+\cos\alpha \end{bmatrix} \tag{40}$$

In which α is the rotation angle and u the vector serving as the rotation axis. First, we rotate in longitude, i.e. around $\hat{z}'$, to find the point l on the moon's equator:

$$\vec{Cl} = \bar{\mathbf{R}}_{\hat{z}'}(\vartheta) \cdot \vec{Cr}$$

Subsequently, we rotate in latitude around a fictitious axis $\hat{a}'$, which is obtained by rotating another 90 degrees around $\hat{z}'$ and normalising:

$$\vec{a}' = \frac{\bar{\mathbf{R}}_{\hat{z}'}(\pi/2) \cdot \vec{Cl}}{|\bar{\mathbf{R}}_{\hat{z}'}(\pi/2) \cdot \vec{Cl}|}$$

And then, to obtain $\vec{Cq}$:

$$\vec{Cq} = \bar{\mathbf{R}}_{\hat{a}'}(\varphi) \cdot \vec{Cr}$$

Finally, to obtain the coordinates of q in the rest frame, we simply add the moon's position:

$$\vec{q} = \vec{Cq} + \vec{C}$$

Now that we know our coordinates on the surface, we can compute the flux of the incident stellar or planetary illumination. We know that the radiation flux from any point source S is mitigated by its incident angle via

$$F_{xi,q} = \begin{cases} F_{x,d} \sin \delta_x, & \delta_x > 0 \\ 0, & \delta_x < 0 \end{cases} \tag{41}$$

wherein $F_{xi,q}$ is the incident flux on the surface at q, $F_{x,d}$ is the flux at some distance d from the luminous source X and δ_x denotes X's elevation above the horizon at q – therefore, δ_x must be larger than 0. The elevation angle δ_x is computed by first taking the dot product of the normal vector at q, $\vec{Cq}$, and the vector pointing to the arbitrary source:

$$\gamma_x = \arccos\left(\frac{q\vec{X} \cdot \vec{Cq}}{|q\vec{X}|R_C}\right)$$

wherein γ_x is the angle measuring how far off the normal X is in the sky, and R_C is the moon's radius, and thus the magnitude (in reality, within some margin due to uneven terrain and/or an oblate shape) of $\vec{Cq}$. δ_x is subsequently found by realising that

$$\begin{aligned} \delta_x &= \frac{\pi}{2} - \gamma_x \\ &= \frac{\pi}{2} - \arccos\left(\frac{q\vec{X} \cdot \vec{Cq}}{|q\vec{X}|R_C}\right) \end{aligned}$$

However, since $\frac{\pi}{2} - \arccos a = \arcsin a$, we may write

$$\delta_x = \arcsin\left(\frac{q\vec{X} \cdot \vec{Cq}}{|q\vec{X}|R_C}\right) \tag{42}$$

And subsequently, we can rewrite Equation 41 to read:

$$F_{xi,q} = \begin{cases} F_{x,d} \dfrac{q\vec{X} \cdot \vec{Cq}}{|q\vec{X}|R_C}, & \gamma_x < \dfrac{\pi}{2} \\ 0, & \gamma_x > \dfrac{\pi}{2} \end{cases} \tag{43}$$

This treatment is valid for point sources; however, our sources are extended. We adopt this method nonetheless as a simplification: if we assume the sources emit homogeneously over their surfaces, we can assume that the average mitigation suffered by their emission is equal to the mitigation suffered by their centres, i.e. the points S and P. Although this is not entirely physically correct, we thus adopt the elevations of these points as the incident angles in our further treatment. An exception occurs during dusk, dawn and on the moon's poles (as well as during eclipses, but assuming the star is small enough on the sky this difference is negligible); this is discussed in the following sections.

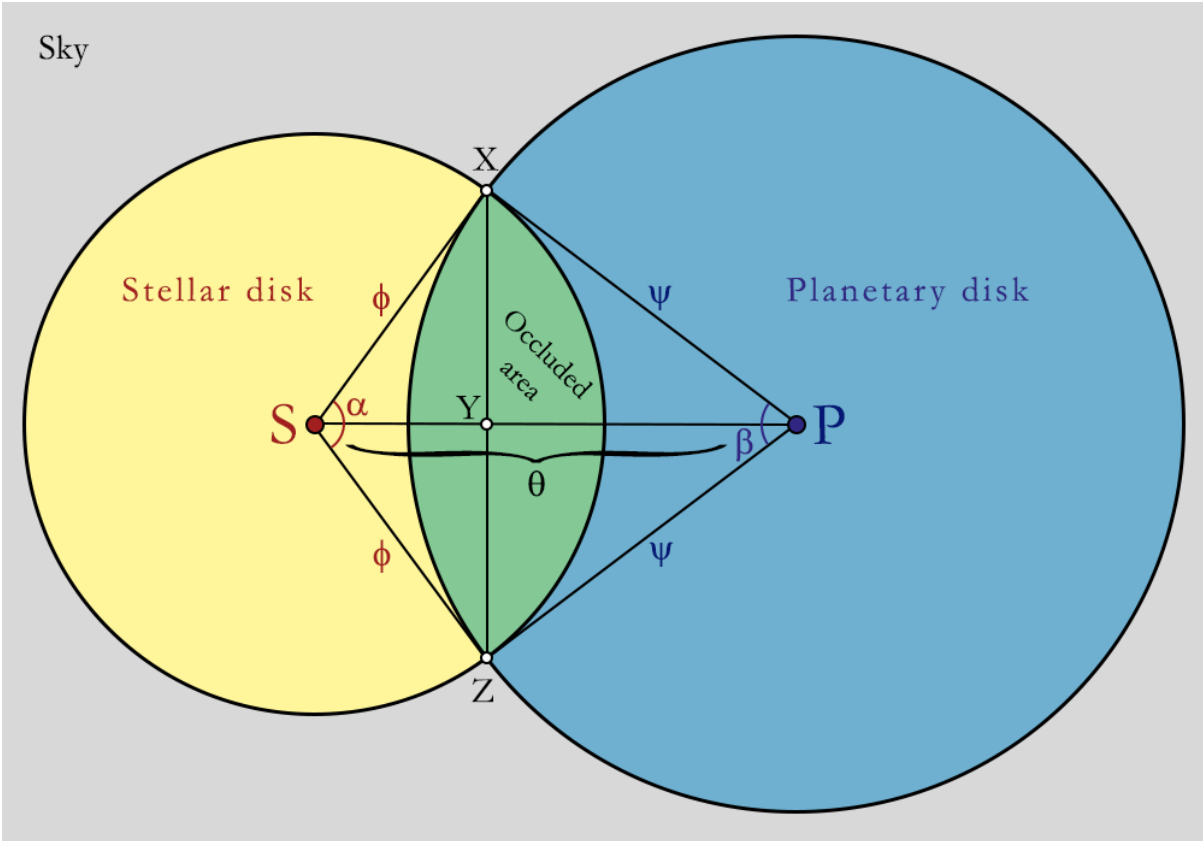

Figure 20: The geometry of an eclipse: overlapping circular patches.

A.2 Planetary eclipses

To adjust for planetary eclipses, we went with an analytic approach: since both star and planet are assumed to be extended objects in the moon's sky, we consider the projected overlapping circles and calculate the solid angle of said overlap. We then check how large a fraction of the star is still visible – say, 70% – and subsequently multiply the stellar flux to that point on the surface by this modifier – in this case, 0.7.

Consider two disks around points P (the planet) and S (the star) on the celestial sphere. The solid angle subtended by the to be eclipsed object, i.e. S, is

$$\Omega_S = \pi\phi^2 \tag{44}$$

With ϕ the projected angle of the radius of S. If the patches S and P overlap (their circumferences touching at points X and Z), the solid angles subtended by the arcs between X and Z α (as measured from the centre of S) and β (as measured from the centre of P) are given by

$$\Omega_{S,\alpha} = \frac{1}{2}\alpha\phi^2 \tag{45}$$

$$\Omega_{P,\beta} = \frac{1}{2}\beta\psi^2 \tag{46}$$

Where ϕ and ψ are the projected angles of the radii of S and P, respectively. As can be deduced from Figure 20, the total overlapping solid angle is the sum of these two arcs, minus the irregular polygon $SXPZ$, which compensates for the double counting of the overlapping section and the non-overlapping portions of both arcs. Due to symmetry, the solid angle of $SXPZ$ can be described by two triangles via

$$\Omega_{SXPZ} = 2\Omega_{SXP} = 2\Omega_{SZP}$$

We arbitrarily pick SXP to find

$$\begin{aligned} 2\Omega_{SXP} &= 2 \cdot \frac{1}{2}\theta \cdot XY \\ &= \theta \cdot XY \end{aligned}$$

wherein Y is the sagittal point of the chord XZ, and θ is the angle of the projected separation of the centres of S and P. XY (or ZY) can be found by taking the sine of half of α (or β):

$$XY = \phi \sin \frac{1}{2}\alpha$$

Hence

$$\Omega_{SXPZ} = \theta\phi \sin \frac{1}{2}\alpha \tag{47}$$

And

$$\begin{aligned} \Omega_{over} &= \Omega_{S,\alpha} + \Omega_{P,\beta} - \Omega_{SXPZ} \\ \Omega_{over} &= \frac{1}{2}\alpha\phi^2 + \frac{1}{2}\beta\psi^2 - \theta\phi \sin \frac{1}{2}\alpha \end{aligned}$$

ϕ And ψ can both be computed by

$$\begin{aligned} \phi &= \arctan \frac{R_S}{|\vec{Sq}|} \\ \psi &= \arctan \frac{R_P}{|\vec{Pq}|} \end{aligned}$$

While θ is computed via the dot product:

$$\theta = \arccos \left(\frac{\vec{Sq} \cdot \vec{Pq}}{|\vec{Sq}||\vec{Pq}|} \right)$$

α And β both require inverse application of the cosine rule for triangles:

$$c^2 = a^2 + b^2 - 2ab \cdot \cos\gamma$$

With γ the angle opposite side c. Following this, we obtain

$$\begin{aligned} \alpha &= 2 \arccos \left(\frac{\theta^2 + \phi^2 - \psi^2}{2\theta\phi} \right) \\ \beta &= 2 \arccos \left(\frac{\theta^2 + \psi^2 - \phi^2}{2\theta\psi} \right) \end{aligned}$$

So in terms of only the separation (θ) and the angular radii of S (ϕ) and P (ψ), we finally obtain

$$\Omega_{over} = \phi^2 \arccos\left(\frac{\theta^2+\phi^2-\psi^2}{2\theta\phi}\right) + \psi^2 \arccos\left(\frac{\theta^2+\psi^2-\phi^2}{2\theta\psi}\right) - \theta\phi\sqrt{1-\frac{\theta^2+\phi^2-\psi^2}{2\theta\phi}} \tag{48}$$

Which means that the visibility fraction of the star during eclipsing, $f_{*,ecl}$, becomes

$$f_{*,ecl} = \frac{\Omega_S - \Omega_{over}}{\Omega_S} \tag{49}$$

In case of no overlap, this reduces to 1; in case there is partial overlap, it takes a value between 1 and 0; and if there is total overlap (registered by the algorithm as that the point P is closer than $\psi - \phi$ to the point S), $f_{*,ecl}$ is simply set to 0.

A.3 Dusk, dawn & polar illumination

Due to the way our algorithm computes the angle of incidence of radiation from both S and P, we require a treatment for situations where, at some point q, part of the star or planet is occluded by the moon's own surface. This occurs during dusk, dawn and at angles close to 90 degrees to either the planetary or the moon's own orbital plane. Illumination is simplified by assuming all light from the extended source emanates from the object's visible surface's centroid (the point V): since our source objects are (roughly) spherical, this coincides with their physical centres of mass (CM). Hence, all the light suffers the same mitigation: $\sin\delta$, where δ is the elevation of the object's CM above the horizon. This simplification is no longer valid when part of the source is occluded, since then V no longer coincides with the source's CM; we must then compute the new elevation of the object's point V, to determine the mitigation suffered by the light still above the horizon.

Consider the stellar disk around a point S partially occluded behind the horizon (see Figure 21). Its elevation δ_S is computed using Equation 42 from the vectors supplied by *Rebound*; its radius ϕ is computed the same way as in the previous section. The disk's circumference touches the horizon at the points X and Z: in this fashion, both the visible and invisible surfaces' solid angles can be computed through the summation or subtraction of a sector (subtending from X to Y from S) and a triangle (SXZ). The surface of this triangle is given by

$$\Omega_{SXZ} = \delta_S\sqrt{\phi^2 - \delta_S^2}$$

The angles below and above S are, respectively

$$\zeta = 2\arccos\frac{\delta_S}{\phi}$$
$$\xi = 2\pi - \zeta = 2\pi - 2\arccos\frac{\delta_S}{\phi} = 2\arccos\frac{-\delta_S}{\phi}$$

And the surfaces of the sectors below and above S are, respectively

$$\Omega_{lower} = \frac{1}{2}\phi^2\zeta = \phi^2\arccos\frac{\delta_S}{\phi}$$
$$\Omega_{upper} = \frac{1}{2}\phi^2\xi = \phi^2\arccos\frac{-\delta_S}{\phi}$$

Hence, the solid angles of both surfaces are

$$\Omega_V = \Omega_{upper} + \Omega_{SXZ} = \phi^2\arccos\frac{-\delta_S}{\phi} + \delta_S\sqrt{\phi^2-\delta_S^2} \tag{50}$$

$$\Omega_O = \Omega_{lower} - \Omega_{SXZ} = \phi^2\arccos\frac{\delta_S}{\phi} - \delta_S\sqrt{\phi^2-\delta_S^2} \tag{51}$$

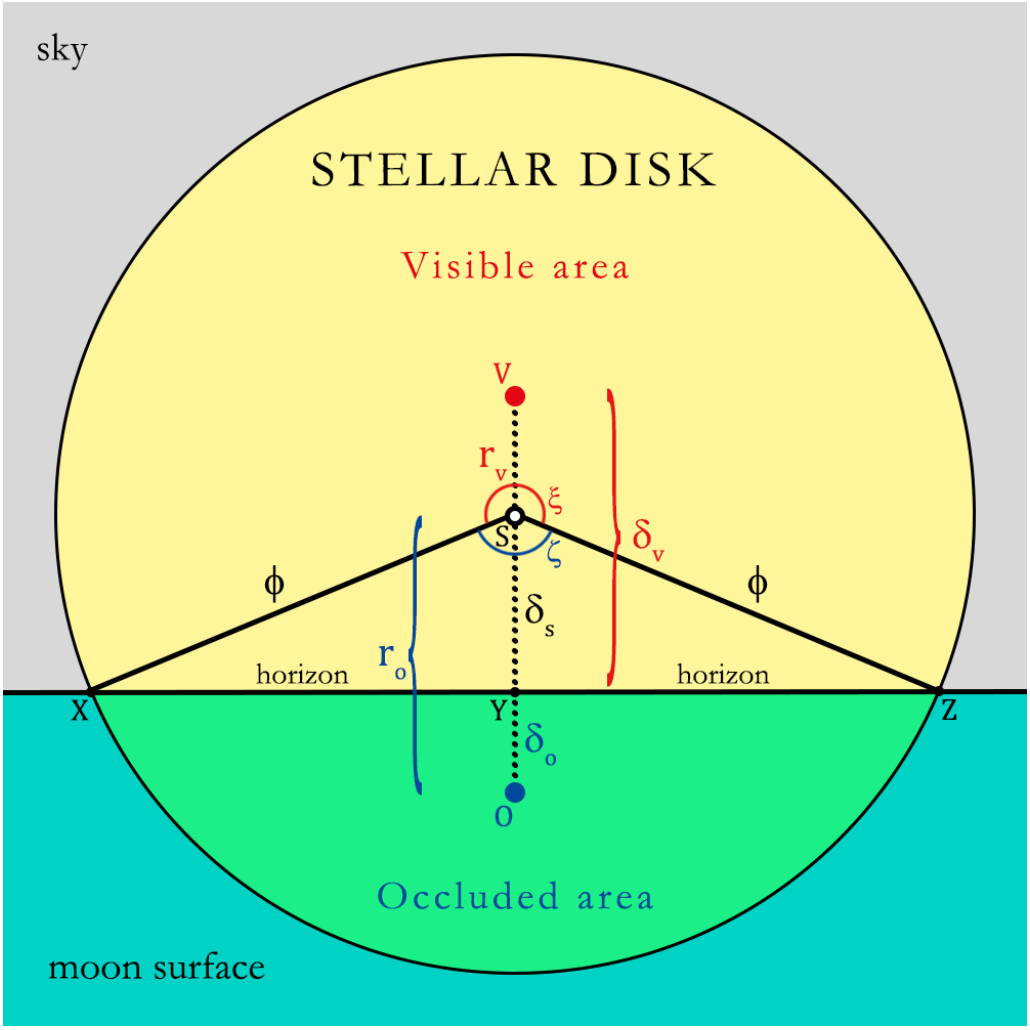

Figure 21: The geometry of dawn or dusk: a partially occluded disk. Elevation of centroids is *not* accurate, and exaggerated for clarity.

Since elevation is negative below the horizon, this formula holds there too: flipping the signs of δ_S returns the equations flipped also. Assuming the simplification that the entire disk radiates uniformly (not truly the case because of limb darkening), taking the average of the weighted elevations of V and the occluded surface's centroid (the point O) should yield the elevation of the disk's CM – the point S itself – i.e.:

$$\delta_S = \frac{\delta_V \Omega_V + \delta_O \Omega_O}{\Omega_S}$$

wherein the subscript V denotes a quantity in the visible and O in the occluded area, and where all the other parameters take their usual meanings. Since we wish to solve for δ_V, this can be rewritten to

$$\delta_V = \frac{\delta_S \Omega_S - \delta_O \Omega_O}{\Omega_V} \tag{52}$$

While the point S is above the horizon, the occluded area takes the shape of a circular segment, of which the centroid's distance to the circle's centre is known to be

$$\bar{r}_O = \frac{4\phi \sin^3 \zeta}{3\,(2\zeta - \sin 2\zeta)}$$

wherein ϕ is S's radius and ζ is the occluded segment's associated arc. Since we wish not to know the angle from S to O, but O's elevation, we subtract $\bar{r}_O$ from δ_S to find

$$\delta_O = \delta_S - \bar{r}_O = \delta_S - \frac{4\phi \sin^3 \zeta}{3\left(2\zeta - \sin 2\zeta\right)}$$

We also know that

$$\Omega_O = \Omega_S - \Omega_V$$

So substituting into Equation 52, we obtain

$$\begin{aligned}
\delta_V &= \frac{\delta_S \Omega_S - \left(\delta_S - \bar{r}_O\right)\left(\Omega_S - \Omega_V\right)}{\Omega_V} \\
&= \frac{\delta_S \Omega_S - \delta_S \Omega_S + \bar{r}_O \Omega_S + \delta_S \Omega_V - \bar{r}_O \Omega_V}{\Omega_V} \\
&= \bar{r}_O \frac{\Omega_S}{\Omega_V} + \delta_S - \bar{r}_O = \delta_S - \bar{r}_O \left(1 - \frac{\Omega_S}{\Omega_V}\right)
\end{aligned}$$

Inverting and substituting the relation between the surfaces again, we finally find that

$$\delta_V = \delta_S - \bar{r}_O \left(1 - \frac{\Omega_V + \Omega_O}{\Omega_V}\right) = \delta_S - \bar{r}_O \frac{\Omega_O}{\Omega_V} \tag{53}$$

When the point S dives below the horizon, the visible area takes the shape of a circular segment and the equation for the V's elevation simply becomes that of a circular segment's centroid, namely:

$$\delta_V = \delta_S + \bar{r}_V = \delta_S + \frac{4\phi \sin^3 2\xi}{3\left(2\xi - \sin 2\xi\right)} \tag{54}$$

Similar to the eclipse scenario, we must also take into consideration how large a fraction of the setting/rising object is in fact visible. Hence, we find that, for the visibility fraction during horizon occlusion $f_{*,hor}$ (or similarly, in the case of the planet, $f_{p,hor}$):

$$f_{*,hor} = \frac{\Omega_V}{\Omega_S} \tag{55}$$

In case of no horizon occlusion, this reduces to 1; in case there is partial overlap, it takes a value between 1 and 0; and if there is total horizon occlusion (registered by the algorithm as that the elevation of the point S is lower than $-\phi$), $f_{*,hor}$ is simply set to 0.

A.4 Planetary phase

Similar to how Earth's moon displays phases over the course of a month, so does the host planet of our hypothetical exomoon turn from new to full and back again. This is described by the phase angle ε_c of the moon's orbit (see section 2.4.2), which is the angle between the vector from planet to star ($\vec{PS}$) and between planet and moon ($\vec{PC}$) – or more precisely, for some point q, between planet and q ($\vec{Pq}$). Hence, this angle is found via the dot product:

$$\vec{PS} \cdot \vec{Pq} = |\vec{PS}||\vec{Pq}| \cos \varepsilon_c$$

So for ε_c, we find

$$\varepsilon_c = \arccos\left(\frac{\vec{PS} \cdot \vec{Pq}}{|\vec{PS}||\vec{Pq}|}\right) \tag{56}$$

References

Andersson, O. and Inaba, A. (2005). Thermal conductivity of crystalline and amorphous ices and its implications on amorphization and glassy water. *PCCP*, 7:1441.

Armitage, P. J., Eisner, J. A., and Simon, J. B. (2016). Prompt Planetesimal Formation beyond the Snow Line. *ApJ Letters*, 828:L2.

Bland, M. T., Singer, K. N., McKinnon, W. B., and Schenk, P. M. (2012). Enceladus' extreme heat flux as revealed by its relaxed craters. *GRL*, 39:L17204.

Chen, J. and Kipping, D. (2017). Probabilistic Forecasting of the Masses and Radii of Other Worlds. *ApJ*, 834:17.

Ćuk, M., Dones, L., and Nesvorný, D. (2016). Dynamical Evidence for a Late Formation of Saturns Moons. *ApJ*, 820:97.

Czechowski, L. (2004). Parameterized model of convection driven by tidal and radiogenic heating. In Paillé, J.-P., editor, *35th COSPAR Scientific Assembly*, volume 35 of *COSPAR Meeting*, page 797.

Desch, S. J., Cook, J. C., Hawley, W., and Doggett, T. C. (2007). Cryovolcanism on Charon and Other Kuiper Belt Objects. In *Lunar and Planetary Science Conference*, volume 38 of *Lunar and Planetary Science Conference*, page 1901.

Dobos, V., Barr, A. C., and Kiss, L. L. (2019). Tidal heating and the habitability of the TRAPPIST-1 exoplanets. *A&A*, 624:A2.

Dobos, V., Heller, R., and Turner, E. L. (2017). The effect of multiple heat sources on exomoon habitable zones. *A&A*, 601:A91.

Dobos, V. and Turner, E. L. (2015). Viscoelastic Models of Tidally Heated Exomoons. *ApJ*, 804:41.

Dodd, M. S., Papineau, D., Grenne, T., Slack, J. F., Rittner, M., Pirajno, F., O'Neil, J., and Little, C. T. S. (2017). Evidence for early life in earth's oldest hydrothermal vent precipitates. *Nature*, 543(7643):60–64.

Dodson-Robinson, S. E., Willacy, K., Bodenheimer, P., Turner, N. J., and Beichman, C. A. (2009). Ice lines, planetesimal composition and solid surface density in the solar nebula. *Icarus*, 200:672–693.

Driscoll, P. E. and Barnes, R. (2015). Tidal Heating of Earth-like Exoplanets around M Stars: Thermal, Magnetic, and Orbital Evolutions. *Astrobiology*, 15(9):739–760.

Forgan, D. and Dobos, V. (2016). Exomoon climate models with the carbonate-silicate cycle and viscoelastic tidal heating. *MNRAS*, 457:1233–1241.

Forgan, D. and Yotov, V. (2014). The effect of planetary illumination on climate modelling of Earth-like exomoons. *MNRAS*, 441(4):3513–3523.

Galilei, G. (1610). *Sidereus Nuncius (Starry Messenger)*. Thomas Baglioni.

Glein, C. R., Postberg, F., and Vance, S. D. (2018). *The Geochemistry of Enceladus: Composition and Controls*, pages 39–56.

Hammond, N. P., Parmenteir, E. M., and Barr, A. C. (2018). Compaction and melt transport in ammonia-rich ice shells: Implications for the evolution of triton. *Journal of Geophysical Research: Planets*, 123(12):3105–3118.

Heller, R. (2012). Exomoon habitability constrained by energy flux and orbital stability. *A&A*, 545:L8.

Heller, R. and Barnes, R. (2013). Exomoon Habitability Constrained by Illumination and Tidal Heating. *Astrobiology*, 13:18–46.

Heller, R., Marleau, G. D., and Pudritz, R. E. (2015). The formation of the Galilean moons and Titan in the Grand Tack scenario. *A&A*, 579:L4.

Henning, W. G., O'Connell, R. J., and Sasselov, D. D. (2009). Tidally Heated Terrestrial Exoplanets: Viscoelastic Response Models. *ApJ*, 707(2):1000–1015.

Holland, H. D. (2002). Volcanic gases, black smokers, and the great oxidation event. *GCA*, 66:3811–3826.

Hussmann, H., Sohl, F., and Spohn, T. (2006). Subsurface oceans and deep interiors of medium-sized outer planet satellites and large trans-neptunian objects. *Icarus*, 185:258–273.

Hussmann, H. and Spohn, T. (2004). Thermal-orbital evolution of Io and Europa. *Icarus*, 171:391–410.

Huygens, C. (1656). *De Saturni Luna Observatio Nova (Observation of Saturn's New Moon)*. Adriaan Vlacq.

Ip, Y., Chew, S., and Randall, D. (2001). Ammonia toxicity, tolerance, and excretion. In *Nitrogen Excretion*, volume 20 of *Fish Physiology*, pages 109 – 148. Academic Press.

Jackson, B., Greenberg, R., and Barnes, R. (2008). Tidal Evolution of Close-in Extrasolar Planets. *ApJ*, 678:1396–1406.

Jellinek, A. M. and Jackson, M. G. (2015). Connections between the bulk composition, geodynamics and habitability of Earth. *Nature Geoscience*, 8:587–593.

Kaltenegger, L., Fridlund, M., and Kasting, J. (2002). Review on habitability and biomarkers. In Foing, B. H. and Battrick, B., editors, *Earth-like Planets and Moons*, volume 514 of *ESA Special Publication*, pages 277–282.

Kempf, S., Horányi, M., Hsu, H. W., Hill, T. W., Juhász, A., and Smith, H. T. (2018). *Saturn's Diffuse E Ring and Its Connection with Enceladus*, page 195.

Khurana, K. K., Jia, X., Kivelson, M. G., Nimmo, F., Schubert, G., and Russell, C. T. (2011). Evidence of a Global Magma Ocean in Ios Interior. *Science*, 332:1186.

Kipping, D. M. (2009). Transit timing effects due to an exomoon. *MNRAS*, 392:181–189.

Kollmeier, J. A. and Raymond, S. N. (2019). Can moons have moons? *MNRAS*, 483(1):L80–L84.

Kreidberg, L., Luger, R., and Bedell, M. (2019). No Evidence for Lunar Transit in New Analysis of HST Observations of the Kepler-1625 System. *arXiv e-prints*, page arXiv:1904.10618.

Lainey, V. (2016). Quantification of tidal parameters from Solar System data. *Celestial Mechanics and Dynamical Astronomy*, 126(1-3):145–156.

Lammer, H., Schiefer, S.-C., Juvan, I., Odert, P., Erkaev, N. V., Weber, C., Kislyakova, K. G., Güdel, M., Kirchengast, G., and Hanslmeier, A. (2014). Origin and Stability of Exomoon Atmospheres: Implications for Habitability. *Origins of Life and Evolution of the Biosphere*, 44:239–260.

Leliwa-Kopystyński, J., Maruyama, M., and Nakajima, T. (2002). The Water-Ammonia Phase Diagram up to 300 MPa: Application to Icy Satellites. *Icarus*, 159:518–528.

Li, S., Lucey, P. G., Milliken, R. E., Hayne, P. O., Fisher, E., Williams, J.-P., Hurley, D. M., and Elphic, R. C. (2018). Direct evidence of surface exposed water ice in the lunar polar regions. *Proceedings of the National Academy of Science*, 115:8907–8912.

Lunine, J. I. and Stevenson, D. J. (1985). Thermodynamics of clathrate hydrate at low and high pressures with application to the outer solar system. *ApJ Supplements*, 58:493–531.

Markellos, V. V. and Roy, A. E. (1981). Hill stability of satellite orbits. *Celestial mechanics*, 23(3):269–275.

Martin, W., Baross, J., Kelley, D., and Russell, M. (2008). Hydrothermal vents and the origin of life. *Nature Rev. Microbiol.*, 29:1–10.

Mayor, M. and Queloz, D. (1995). A Jupiter-mass companion to a solar-type star. *Nature*, 378:355–359.

McKinnon, W. B. (1997). Galileo at Jupiter meetings with remarkable moons. *Nature*, 390:23–26.

Meyer, J. and Wisdom, J. (2007). Tidal heating in Enceladus. *Icarus*, 188:535–539.

Moore, W. B. (2003). Tidal heating and convection in Io. *Journal of Geophysical Research (Planets)*, 108:5096.

Morabito, L. A., Synnott, S. P., Kupferman, P. N., and Collins, S. A. (1979). Discovery of currently active extraterrestrial volcanism. *Science*, 204:972.

Mousis, O., Drouard, A., Vernazza, P., Lunine, J. I., Monnereau, M., Maggiolo, R., Altwegg, K., Balsiger, H., Berthelier, J. J., Cessateur, G., De Keyser, J., Fuselier, S. A., Gasc, S., Korth, A., Le Deun, T., Mall, U., Marty, B., Rème, H., Rubin, M., Tzou, C. Y., Waite, J. H., and Wurz, P. (2017). Impact of Radiogenic Heating on the Formation Conditions of Comet 67P/Churyumov-Gerasimenko. *ApJ*, 839(1):L4.

Nimmo, F., Barr, A. C., Běhounková, M., and McKinnon, W. B. (2018). *The Thermal and Orbital Evolution of Enceladus: Observational Constraints and Models*, page 79.

Porco, C. C., Helfenstein, P., Thomas, P. C., Ingersoll, A. P., Wisdom, J., West, R., Neukum, G., Denk, T., Wagner, R., Roatsch, T., Kieffer, S., Turtle, E., McEwen, A., Johnson, T. V., Rathbun, J., Veverka, J., Wilson, D., Perry, J., Spitale, J., Brahic, A., Burns, J. A., Del Genio, A. D., Dones, L., Murray, C. D., and Squyres, S. (2006). Cassini Observes the Active South Pole of Enceladus. *Science*, 311:1393–1401.

Rein, H. and Liu, S.-F. (2012). REBOUND: an open-source multi-purpose N-body code for collisional dynamics. *A&A*, 537:A128.

Renaud, J. P. and Henning, W. G. (2018). Increased Tidal Dissipation Using Advanced Rheological Models: Implications for Io and Tidally Active Exoplanets. *ApJ*, 857(2):98.

Rufu, R. and Canup, R. M. (2017). Triton's Evolution with a Primordial Neptunian Satellite System. *AJ*, 154:208.

Sahijpal, S. and Bhatia, G. K. (2015). The role of impact and radiogenic heating in the early thermal evolution of Mars. *Journal of Earth System Science*, 124(1):241–260.

Sartoretti, P. and Schneider, J. (1999). On the detection of satellites of extrasolar planets with the method of transits. *A&A Supplement*, 134:553–560.

Schidlowski, M. (2001). Carbon isotopes as biogeochemical recorders of life over 3.8 Ga of Earth history: evolution of a concept. *Precambrian Research*, 106:117–134.

Schwieterman, E. W., Reinhard, C. T., Olson, S. L., Harman, C. E., and Lyons, T. W. (2019). A Limited Habitable Zone for Complex Life. *arXiv e-prints*.

Segatz, M., Spohn, T., Ross, M. N., and Schubert, G. (1988). Tidal dissipation, surface heat flow, and figure of viscoelastic models of Io. *Icarus*, 75:187–206.

Soderblom, L. A., Kieffer, S. W., Becker, T. L., Brown, R. H., Cook, II, A. F., Hansen, C. J., Johnson, T. V., Kirk, R. L., and Shoemaker, E. M. (1990). Triton's geyser-like plumes - Discovery and basic characterization. *Science*, 250:410–415.

Spencer, J. R., Barr, A. C., Esposito, L. W., Helfenstein, P., Ingersoll, A. P., Jaumann, R., McKay, C. P., Nimmo, F., and Waite, J. H. (2009). *Enceladus: An Active Cryovolcanic Satellite*, page 683.

Spiegel, D. S., Burrows, A., and Milsom, J. A. (2011). The Deuterium-burning Mass Limit for Brown Dwarfs and Giant Planets. *ApJ*, 727(1):57.

Stofan, E. R., Elachi, C., Lunine, J. I., Lorenz, R. D., Stiles, B., Mitchell, K. L., Ostro, S., Soderblom, L., Wood, C., Zebker, H., Wall, S., Janssen, M., Kirk, R., Lopes, R., Paganelli, F., Radebaugh, J., Wye, L., Anderson, Y., Allison, M., Boehmer, R., Callahan, P., Encrenaz, P., Flamini, E., Francescetti, G., Gim, Y., Hamilton, G., Hensley, S., Johnson, W. T. K., Kelleher, K., Muhleman, D., Paillou, P., Picardi, G., Posa, F., Roth, L., Seu, R., Shaffer, S., Vetrella, S., and West, R. (2007). The lakes of Titan. *Nature*, 445:61–64.

Taubner, R.-S., Pappenreiter, P., Zwicker, J., Smrzka, D., Pruckner, C., Kolar, P., Bernacchi, S., Seifert, A. H., Krajete, A., Bach, W., Peckmann, J., Paulik, C., Firneis, M. G., Schleper, C., and Rittmann, S. K.-M. R. (2018). Biological methane production under putative Enceladus-like conditions. *Nature Communications*, 9:748.

Teachey, A. and Kipping, D. M. (2018). Evidence for a large exomoon orbiting Kepler-1625b. *Science Advances*, 4:eaav1784.

Tittemore, W. C. and Wisdom, J. (1990). Tidal evolution of the Uranian satellites. III - Evolution through the Miranda-Umbriel 3:1, Miranda-Ariel 5:3, and Ariel-Umbriel 2:1 mean-motion commensurabilities. *Icarus*, 85:394–443.

Truong, N., Monroe, A. A., Glein, C. R., Anbar, A. D., and Lunine, J. I. (2019). Decomposition of amino acids in water with application to in-situ measurements of Enceladus, Europa and other hydrothermally active icy ocean worlds. *Icarus*, 329:140–147.

Tyler, R. H. (2009). Ocean tides heat Enceladus. *GRL*, 36(15):L15205.

Waite, J. H., Glein, C. R., Perryman, R. S., Teolis, B. D., Magee, B. A., Miller, G., Grimes, J., Perry, M. E., Miller, K. E., Bouquet, A., Lunine, J. I., Brockwell, T., and Bolton, S. J. (2017). Cassini finds molecular hydrogen in the Enceladus plume: Evidence for hydrothermal processes. *Science*, 356:155–159.

Yoder, C. F. (1995). Astrometric and Geodetic Properties of Earth and the Solar System. In Ahrens, T. J., editor, *Global Earth Physics: A Handbook of Physical Constants*, page 1.

Yu, S. and Fa, W. (2016). Thermal conductivity of surficial lunar regolith estimated from Lunar Reconnaissance Orbiter Diviner Radiometer data. *PlanSS*, 124:48–61.

Zollinger, R. R., Armstrong, J. C., and Heller, R. (2017). Exomoon habitability and tidal evolution in low-mass star systems. *MNRAS*, 472:8–25.